[American Journal of Science, Vol. 319, May, 2019, P. 381-429, DOI 10.2475/05.2019.02]

ALTERNATING CONTRACTION AND EXTENSION IN THE SOUTHERN CENTRAL ANDES (35°–37°S)

LUCAS M. FENNELL*,†, SOFIA B. IANNELLI*, ALFONSO ENCINAS**, MAXIMILIANO NAIPAUER*, VICTOR VALENCIA***, and ANDRÉS FOLGUERA*

ABSTRACT. The Andes are thought to be formed through discrete contractional stages separated by periods of little to no orogenic construction. This paper analyzes the intervals between the main contractional phases that built the Southern Central Andes between 35° and 37°S in order to determine whether they were characterized by neutral, contractional or extensional conditions. During an interruption in orogenesis between the Late Cretaceous and the Miocene shortening phases, two extensional stages are recorded through the opening of a series of intra- and retro-arc basins. U-Pb dating of detrital zircons in a sample collected from the Los Ángeles unit, a syn-extensional volcano-sedimentary succession located at ~35°40'S along the Chile and Argentina international border, provided a maximum depositional age of 67.1 +2.4/−0.9 Ma. This age, in association with evidence of regional crustal thinning, suggests a previously unrecognized extensional phase during latest Cretaceous times. Limited shortening succeeded this extensional event and was followed by a second extensional episode during late Oligocene and earliest Miocene times. While the first extensional event was restricted to the core of the Late Cretaceous orogen, the second episode affected a wide area ranging between the present forearc and retroarc areas. A structural section across the Malargüe fold-thrust belt at ~36°S indicates inversion of normal faults where extension was focused and new thrust generation in areas not affected by extensional deformation. Our data reveal that the growth of the Southern Central Andes is the product of a complex alternation of contractional and extensional phases, with inherited structures playing a role in their tectonic evolution. A comparison with other Cordilleran orogenic systems such as the Puna-Altiplano plateau, the northern Peruvian Andes and the North American Sevier-Laramide orogenic belt, suggests that extensional deformation in the Southern Central Andes responds better to changes in plate kinematics, rather than to localized events within a continuous contractional setting.

Key words: fold-thrust belt, intra-arc basin, retroarc basin, inheritance, geodynamics, tectonic regime

INTRODUCTION

The growth of orogenic systems can be characterized as a succession of contractional phases, whose onset tends to correlate with changes in subduction parameters, collision of oceanic or continental features and even climatic events (Lamb and Davis, 2003; Heuret and Lallemand, 2005; Lallemand and others, 2005; Sobolev and Babeyko, 2005; Oncken and others, 2006; Espurt and others, 2008; Martinod and others, 2010; van Dinther and others, 2010, Capitanio and others, 2011). However, in orogenic systems developed along active subduction settings such as the Andes, changes at the plate margins affect and may even interrupt their growth (Ramos, 2010; Horton, 2018). The interruptions in the growth of these subduction-type orogenic systems can be characterized by extensional or neutral conditions, which are mainly driven by: 1) changes in relative convergence rates or absolute rate of the upper-plate

* CONICET – Universidad de Buenos Aires, Instituto de Estudios Andinos Don Pablo Groeber (IDEAN), Buenos Aires 1428, Argentina
** Departamento de Ciencias de la Tierra, Facultad de Ciencias Químicas, Universidad de Concepción, Concepción 4030000, Chile
*** School of the Environment, Washington State University, Pullman, Washington 99164, USA.
† Corresponding author: lucasfennell90@gmail.com

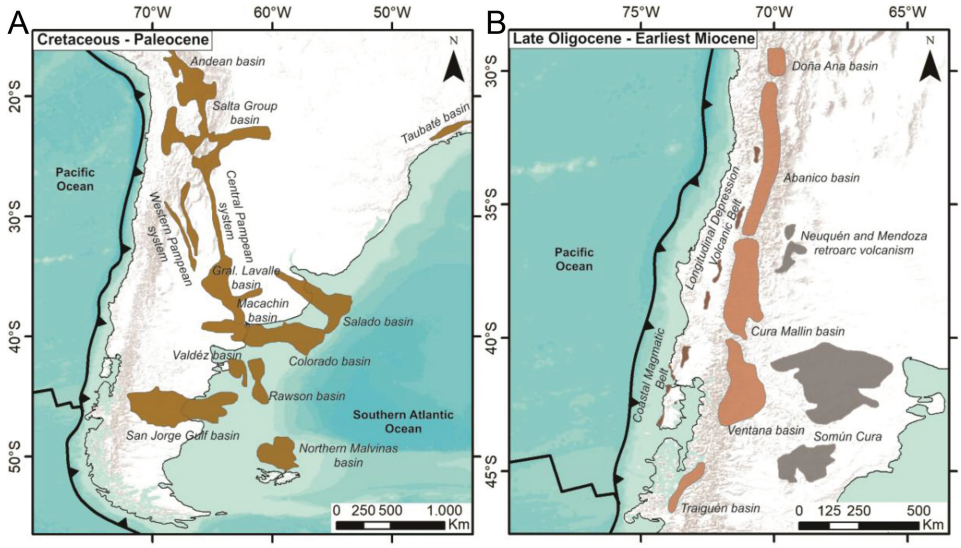

Fig. 1. (A) Cretaceous to Paleocene rift and transtensional basins in southern South America, related to the opening of the Southern Atlantic Ocean and extensional reactivations linked to the initial rise of the Andes, respectively (based on Ramos, 2009 and Gianni and others, 2015). (B) Late Oligocene to earliest Miocene intra-arc extensional basins (light brown), magmatic belts (dark brown) and volcanic plateaus in the Southern Central Andes (based on Fennell and others, 2018).

(Heuret and Lallemand, 2005; Lallemand and others, 2005; Schellart, 2008; Schellart and Moresi, 2013; Horton, 2018; Muñoz and others, 2018); 2) steepening and rollback of the subducted slab (Muñoz and others, 2000; Ramos, 2009; Ramos and Folguera, 2009; Encinas and others, 2016; Horton, 2018; Fennell and others, 2018); 3) extreme crustal thickening leading to gravitational spreading (Coney and Harms, 1984; Dewey, 1988; Schoenbohm and Strecker, 2009; Giovanni and others, 2010; Wells and others, 2012; Giambiagi and others, 2016). As a consequence, the tectonic evolution of some sectors of the Andes has been characterized by shortening with alternating periods of neutral to extensional conditions (Ramos and Folguera, 2005; Charrier and others, 2015; Folguera and others, 2016; Horton and Fuentes, 2016; Echaurren and others, 2016; Horton, 2018). Through the study of the fold-thrust belt's structure and associated syntectonic strata, we are able to define areas that were affected by crustal shortening or extension, which can be used to identify changes in the tectonic regime through time.

After a Neoproterozoic to late Paleozoic complex evolution that alternates compressional and extensional tectonic regimes including accretion of several allochtonous terranes, the Early Jurassic marked the beginning of the Andean Cycle in South America (for a review, see Ramos, 2009). The first stages of this cycle were closely linked to the breakup of Pangea, when a major extensional regime resulted in the development of several rift systems that were responsible for the opening of important hydrocarbon-bearing basins in Argentina (Uliana and others, 1989). Extension in southern South America continued until the Early Cretaceous, resulting in the development of a series of rift basins related to the opening of the southern Atlantic Ocean, such as the Salta rift system in northwestern Argentina and western Bolivia (fig. 1A) (Ramos, 2009). This was followed by the onset of contractional deformation on South America's western margin during the mid-Cretaceous, when the Andes experienced their first constructional phase (fig. 1A) (Somoza and Zaffarana, 2008).

Consequently, a series of pre-existing rifts basins and basement heterogeneities trending parallel to the E-W contractional stress field suffered an extensional reactivation between the latest Cretaceous and the Paleocene (fig. 1A) (Gianni and others, 2015).

The growth of the Andes between 35° and 37°S initiated in the Late Cretaceous, with the onset of the first phase of contractional deformation and synorogenic deposition within the adjacent foreland basin (Ramos and Folguera, 2005; Tunik and others, 2010; Orts and others, 2012; Mescua and others, 2013; Balgord and Carrapa, 2016; Horton and Fuentes, 2016; Fennell and others, 2017). Reduced sedimentation and unconformity development in the foreland during the Paleogene has led to the proposal of a neutral tectonic regime (Horton and Fuentes, 2016), although some works have suggested the occurrence of a middle to late Eocene contractional phase (Groeber, 1946, 1947; Cobbold and Rossello, 2003; Charrier and others, 2007, 2015; Sagripanti and others, 2012; Álvarez Cerimedo and others, 2013; Mosolf and others, 2018). Furthermore, a number of authors have documented evidence of extensional activity in the Southern Central Andes during the late Paleogene (Hervé and others, 1995; Suárez and Emparán, 1995; Charrier and others, 1996, 2002; López-Escobar and Vergara, 1997; Godoy and others, 1999; Muñoz and others, 2000; Jordan and others, 2001). Following these pioneering works, more recent research constrained this extensional episode between the late Oligocene and the earliest Miocene, characterized by the opening of a series of intra-arc extensional basins and widespread mafic volcanic eruptions between the present forearc and retroarc areas (fig. 1B) (Kay and others, 2005, 2007; Kay and Copeland, 2006; Burns and others, 2006; Radic, 2010; Rojas Vera and others, 2010; Garcia Morabito and Ramos, 2012; Dhyr and others, 2013a, 2013b; Ramos and others, 2014a; Winocur and others, 2015; Encinas and others, 2016). Shortening resumed in the early Miocene (Horton and Fuentes, 2016), when a new phase of orogenic construction began, generating the present structural relief (Silvestro and others, 2005; Giambiagi and others, 2008; Silvestro and Atencio, 2009; Sagripanti and others, 2011, 2012; Turienzo and others, 2012; Álvarez Cerimedo and others, 2013; Tapia and others, 2015; Fuentes and others, 2016; Horton and others, 2016).

The main objective of this contribution is to analyze the intervals between the main contractional phases that built the Southern Central Andes, with the aim of determining whether they were characterized by neutral, contractional or extensional conditions. In order to do this, structural and geochronological analyses were performed in volcaniclastic units deposited between the Late Cretaceous and Miocene in the arc and retroarc regions. Field work was carried out in the Malargüe fold-thrust belt located in west-central Argentina, analyzing exposures of these volcaniclastic units and aiming to determine their depositional framework and their significance to the evolution of the Andean orogenic system between 35° and 37°S.

GEOLOGICAL AND TECTONIC SETTING

The Andes constitute a more than 7000 km-long subduction-type orogen, which has been divided into the Northern, Central and Southern Andes based on great differences in their geological history along strike (Gansser, 1973; Ramos, 1999). The study area is part of the Southern Central Andes (27°-46°30'S), which are located between the Juan Fernández aseismic ridge and the Chile mid-ocean ridge (fig. 2) (Gansser, 1973; Ramos, 1999). In this sector, the South American plate is moving westwards over the subducting Nazca plate, resulting in a N78°E oriented convergence at a rate of ~8 cm/yr (Gripp and Gordon, 2002). The Southern Central Andes at the latitudes of the study area (35°-37°S) are segmented into five morphostructural units, which correspond, from west to east, to the Coastal Cordillera, the Central Depression, the Principal Cordillera, the San Rafael Block and the present foreland zone (fig. 2).

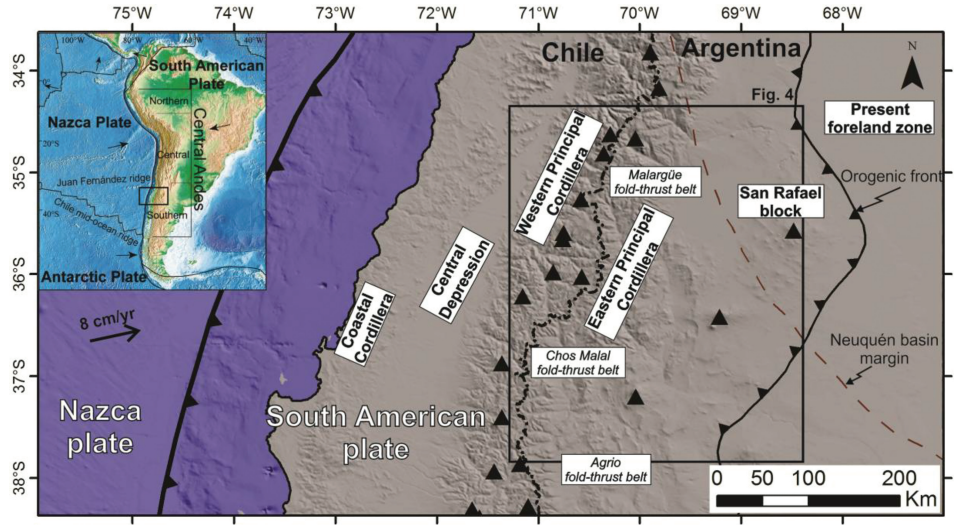

Fig. 2. Main morphostructural units of the Southern Central Andes and location of the study area in west-central Argentina. The Southern Central Andes, following the subdivision of the Andes of Gansser (1973) and Ramos (1999), are located between the Juan Fernández aseismic ridge and the Chile mid-ocean ridge (see inset in the upper-left corner). Black triangles represent the present magmatic arc, product of the ongoing convergence between the Nazca and South American plates at a rate of 8 cm/yr (Gripp and Gordon, 2002). The Andean orogenic front and the eastern border of the Neuquén basin are based on Sagripanti and others (2011).

Moreover, the Principal Cordillera can be subdivided into the western and eastern Principal Cordilleras (compare Muñoz and others, 2018), the latter being constituted by a series of east-verging fold-thrust belts located in Argentine territory (fig. 2). In particular, the Meso-Cenozoic history of the study area, located in the Argentinean Andean flank between 35° and 37°S, is recorded in rocks presently exposed in the Malargüe fold-thrust belt, a hybrid thick- and thin-skinned system formed through tectonic inversion of normal faults and new thrust generation (fig. 2) (Kozlowski and others, 1993; Manceda and Figueroa, 1995; Mescua and Giambiagi, 2012; Turienzo and others, 2012; Branellec and others, 2016; Fuentes and others, 2016).

The Malargüe fold-thrust belt is developed over a Grenville-aged basement corresponding to the Chilenia terrane, which was accreted to Western Gondwana in the Middle Devonian (Ramos, 2009). After the collision, the emplacement of a new magmatic arc associated with synorogenic deposits marks the beginning of a new tectonic cycle during the final assembly of Gondwana in Carboniferous time (Cingolani and Ramos, 2017). This phase of orogenic building was followed by a Late Permian to Early Triassic orogenic collapse, which favored the eruption of rhyolitic intraplate volcanic rocks known as the Choiyoi Group (Ramos and Folguera, 2009). The oldest rocks that crop out in the Malargüe fold-thrust belt include Upper Permian to Lower Triassic igneous rocks of the Choiyoi Group (fig. 3) (Sato and others, 2015), which form the basement of a retroarc extensional basin developed between Late Triassic and Early Cretaceous times, known as the Neuquén basin (fig. 3) (Uliana and others, 1989; Legarreta and Gulisano, 1989). The Neuquén basin opened in the Late Triassic as a series of unconnected depocenters controlled by mechanical subsidence, which were filled with marine, nonmarine and volcanic deposits grouped within the Precuyano cycle (fig. 3) (Carbone and others, 2011; Bechis and others, 2014). In the Early Jurassic, these depocenters started to connect, being gradually filled by marine and

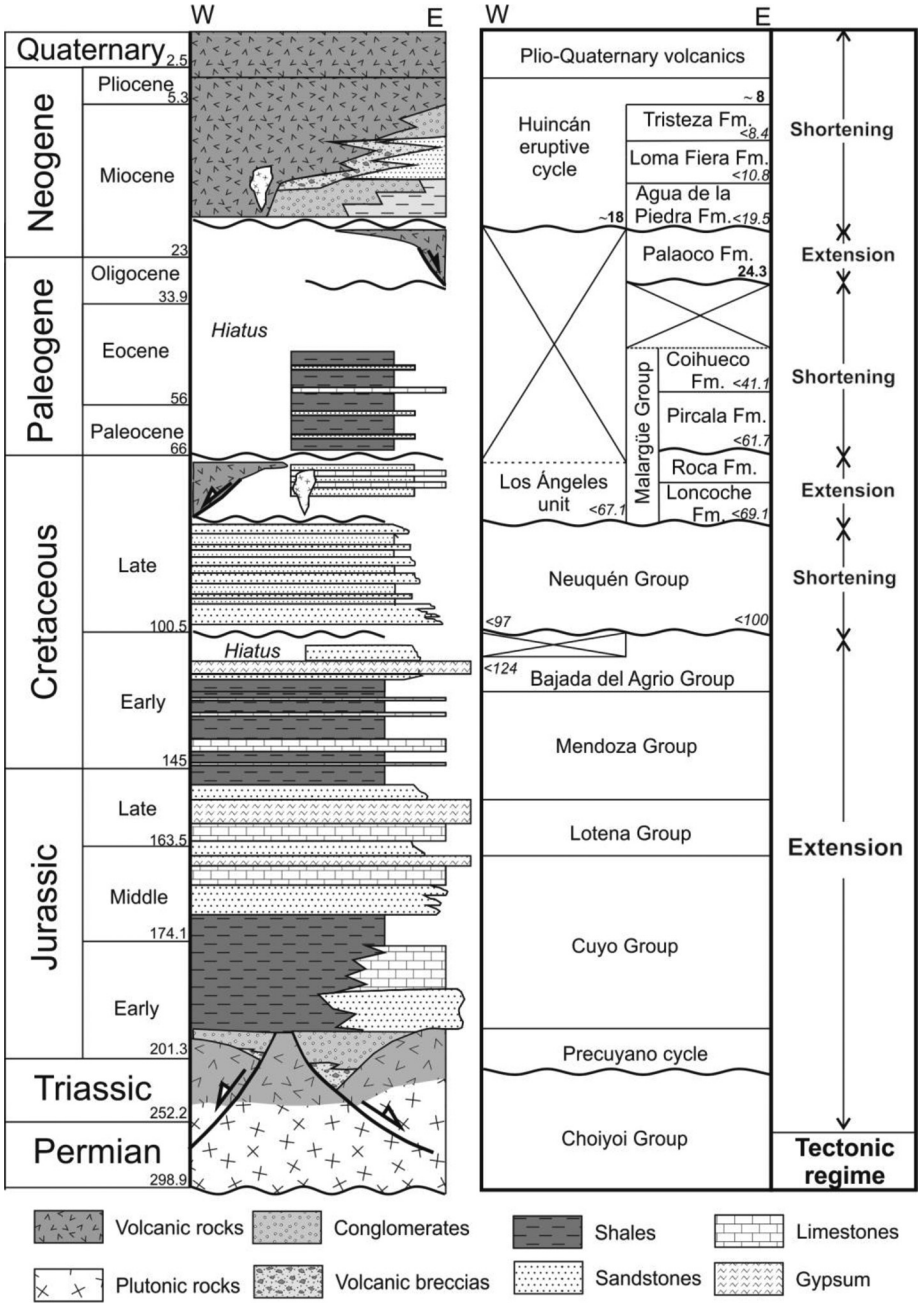

Fig. 3. Stratigraphic chart for the western and eastern sectors of the Malargüe fold-thrust belt (~36°S) modified from Orts and others (2012). Maximum depositional ages are given in italics for sedimentary successions that form part of the foreland basin, and are based on Balgord and Carrapa (2016), Horton and others (2016), Fennell and others (2017), and data from this work. Ar/Ar ages are given in bold for volcanic rocks, based on Dhyr and others (2013b) and Litvak and others (2015).

nonmarine deposits during a series of transgressive-regressive cycles that lasted until Early Cretaceous times (Legarreta and Uliana, 1991, 1996). These marine transgressions and regressions were controlled by regional thermal subsidence and eustatic sea level fluctuations, and are recorded in the study area by the Cuyo, Lotena, Mendoza and Bajada del Agrio Groups (fig. 3) (Gulisano and Gutiérrez Pliemling, 1994; Vergani and others, 1995). These sequences are unconformably overlain by the nonmarine foreland basin deposits of the Neuquén Group and equivalent Diamante Formation (fig. 3), related to the initial shortening in the Malargüe fold-thrust belt in Late Cretaceous time (Orts and others, 2012; Mescua and others, 2013; Balgord and Carrapa, 2016; Fennell and others, 2017).

A 25 to 30 Myr hiatus detected in the western sector of the Malargüe fold-thrust belt represents the transition between post-rift thermal subsidence and initial flexural loading, related to the beginning of a crustal shortening event (fig. 3). The foreland basin deposits of the Neuquén Group can be up to 1.5 to 2 km thick in the central sector, thinning out against the San Rafael block to the east and the Late Cretaceous topographic front to the west, which was likely located along the international border between Chile and Argentina (fig. 2) (Mescua and others, 2013; Muñoz and others, 2018). An initial west-directed paleoflow of sediments coming from the cratonic area was later reversed towards the east, due to the approximation of the thrust belt (Balgord and Carrapa, 2016). Foredeep and wedge top depozones, including both piggyback and thrust top basins, were defined based on the recognition of syncontractional growth strata and differences in detrital zircon age patterns, although a migration of the thrust front and forebulge cannot be resolved with the present data (Orts and others, 2012; Fennell and others, 2017; Muñoz and others, 2018).

The onset of volcanism in the arc in the study area occurred in latest Cretaceous time, after an eastward migration of the locus of magmatic activity during the Late Cretaceous contractional phase (Ramos and Folguera, 2005; Spagnuolo and others, 2012a; Fennell and others, 2017; Muñoz and others, 2018) (figs. 3 and 4). Recent field observations in the western Principal Cordillera at 35°S identified a 2200 m thick volcaniclastic succession composed of andesites, volcanic breccias and tuffs with interbedded sandstones and conglomerates, whose thickness varies due to normal faulting (Muñoz and others, 2018). These rocks correspond to the Plan de los Yeuques Formation (González and Vergara, 1962), whose age has been constrained by a series of Ar/Ar and U-Pb dates between 80 and 65 Ma, implying that it was deposited within an extensional intra-arc basin during latest Cretaceous time (fig. 4) (Muñoz and others, 2018; Mosolf and others, 2018). Additionally, a series of subvolcanic bodies and lava domes constrained between 69 and 67 Ma by Ar/Ar dating intruded the Neuquén Group in the retroarc area, along the present Río Grande valley (figs. 3 and 4) (Spagnuolo and others, 2012a), while their pyroclastic facies became interbedded with the shallow marine deposits of the Loncoche and Roca Formations of the lower Malargüe Group (fig. 3) (Barrio, 1990; Aguirre Urreta and others, 2011; Parras and Griffin, 2013; Balgord and Carrapa, 2016).

Towards the beginning of the Paleogene, volcanic rocks continued their emplacement to the south of the study area (fig. 4) (Llambías and Rapela, 1989; Kay and others, 2006; Llambías and Aragón, 2011), while shallow marine sedimentation in the retroarc area was replaced by distal fluvial deposition represented by the Pircala and Coihueco Formations, constituting the upper Malargüe Group (fig. 3) (Parras and others, 1998; Balgord and Carrapa, 2016; Horton and others, 2016). This event marked the beginning of a stage of reduced sediment accumulation in the retroarc region (Horton and Fuentes, 2016) and a hiatus in magmatic arc activity (figs. 3 and 4) (Gana and Wall, 1997; Balgord, 2017; Muñoz and others, 2018). However, a recent seismic survey performed in the present foreland zone has detected the presence of

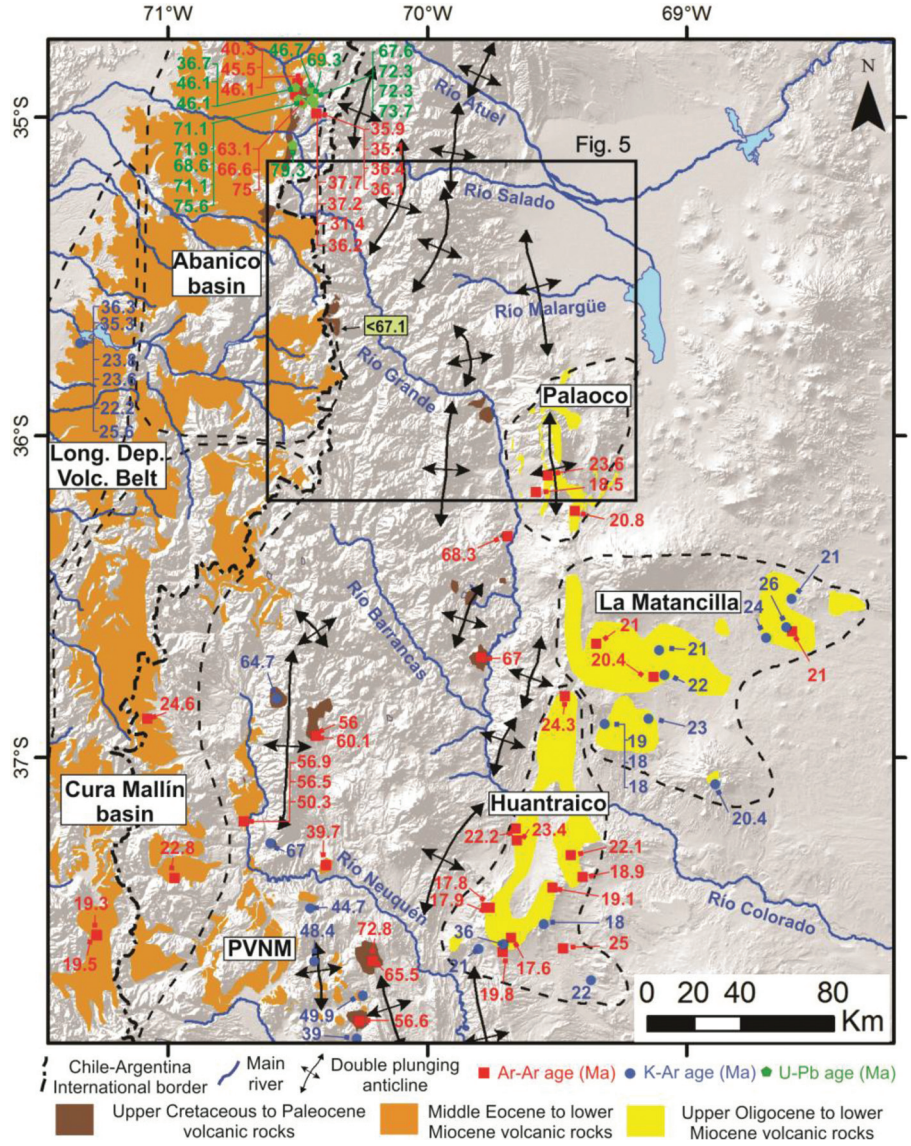

Fig. 4. Map showing the location of outcrops and radiometric ages of volcanic rocks emplaced between the Late Cretaceous and the Miocene contractional phases in the study area (main anticlines and rivers are given as a reference). Upper Cretaceous to Paleocene volcanic rocks based on Llambías and Aragón (2011), Spagnuolo and others (2012), Muñoz and others (2018), Mosolf and others (2018), and data from this work (indicated as a maximum depositional age in the green box). Middle Eocene to lower Miocene volcanic rocks based on López-Escobar and Vergara (1997) for the Longitudinal Depression Volcanic Belt; Jordan and others (2001) and Shockey and others (2012) for the Cura Mallín basin; Charrier and others (1996), SERNAGEOMIN (2003) and Mosolf and others (2018) for the Abanico basin; Llambías and Rapela (1989) for Provincia Volcánica Neuquino Mendocina (PVNM). Upper Oligocene to lower Miocene volcanic rocks are based on Silvestro and Atencio (2009) and Dhyr and others (2013a) for the Palaoco area; Kay and Copeland (2006) and Dhyr and others (2013b) for the Huantraico and La Matancilla areas.

thick sequences corresponding to the Pircala and Coihueco Formations deposited over an erosive surface at the top of Roca Formation, representing a regional unconformity at the latitudes of the study area (fig. 3) (Onnis and others, 2018).

An Eocene contractional event has been suggested as being responsible for the uplift of the Upper Cretaceous to lower Paleogene volcanic arc in the western Principal Cordillera (Charrier and others, 2007, 2015; Muñoz and others, 2018; Mosolf and others, 2018) and, more speculatively, for the growth of a series of anticlines located in the eastern Principal Cordillera (Groeber, 1946, 1947; Cobbold and Rossello, 2003; Sagripanti and others, 2012; Álvarez Cerimedo and others, 2013). Moreover, after a *ca.* 15 Myr hiatus in volcanic activity (Gana and Wall, 1997; Balgord, 2017; Muñoz and others, 2018), volcano-sedimentary sequences of the Abanico Formation were deposited unconformably on top of the Mesozoic units in the western Principal Cordillera between the Middle Eocene and the early Miocene (figs. 1B and 4) (Wyss and others, 1994; Charrier and others, 1996, 2002; Piquer and others, 2010; Mescua and others, 2013; Muñoz and others, 2018; Mosolf and others, 2018). Although the Abanico Formation has been interpreted as deposited in a basin developed under extensional conditions (Charrier and others, 1996, 2002; Godoy and others, 1999), recent proposals suggested that the deposition of its upper members took place during a transpressive crustal shortening event (Mosolf and others, 2018). Due to the ambiguity about the deformational setting, Horton and Fuentes (2016) interpreted this period as dominated by a neutral tectonic regime, which concluded at *ca.* 40 Ma, followed by a ~20 Myr hiatus in foreland sedimentation.

Despite the apparent ~40 to 20 Ma hiatus in the foreland basin record (Horton and Fuentes, 2016), volcanic sequences of the Abanico Formation continued their deposition in the western Principal Cordillera until the early Miocene (fig. 4) (Charrier and others, 1996, 2002; Godoy and others, 1999; Kay and others, 2005; Piquer and others, 2010; Mosolf and others, 2018). Although the Abanico Formation is not recorded in Argentina at the latitudes of the study area, similar deposits can be found along the international border between 36° and 39°S in the Cura Mallín basin (figs. 1B and 4) (Niemeyer and Muñoz, 1983; Muñoz and Niemeyer, 1984; Suárez and Emparán, 1995; Jordan and others, 2001). The age of the Cura Mallin basin strata are constrained between 25 and 19 Ma by Ar/Ar dating (fig. 4) (Jordan and others, 2001; Burns and others, 2006; Flynn and others, 2008; Shockey and others, 2012), while important thickness variations due to high-angle normal faulting are observed in seismic records (Jordan and others, 2001; Utgé and others, 2009; Radic, 2010; Folguera and others, 2010; Rojas Vera and others, 2010). The volcanic rocks in both the Cura Mallín and Abanico basins correlate with the Longitudinal Depression Volcanic Belt in the Central Depression, which is temporally constrained between 36 and 20 Ma by K-Ar ages (figs. 1B and 4) (López-Escobar and Vergara, 1997).

Important magmatic activity is also recorded in the Neuquén and Mendoza retroarc between the late Oligocene and early Miocene, where thick volcaniclastic deposits of this age can be found in the Palaoco, Matancilla and Huantraico areas (figs. 1B and 4). Although these volcanic deposits have been characterized geochronologically and geochemically (Kay and Copeland, 2006; Dhyr and others, 2013a, 2013b), their tectonic setting and stratigraphic relations remain unclear. The only evidence pointing towards syn-extensional emplacement can be found in the Palaoco area (fig. 4), where Álvarez Cerimedo and others (2013) described progressive unconformities in volcano-sedimentary strata of the Palaoco Formation. The Palaoco Formation corresponds to a stratified thick sequence of basalts, conglomerates, sandstones and andesitic to basaltic breccias with Ar/Ar ages ranging between 24 and 18 Ma, which sits on top of deformed deposits of the Malargüe Group (figs. 3 and 4) (Groeber, 1946, 1947; Silvestro and Atencio, 2009; Galarza and others, 2009; Sagripanti and others, 2012; Orts and others, 2012; Álvarez Cerimedo and others, 2013; Dhyr and others, 2013a). This volcanism extends to the south in the Matancilla and Huantraico areas (González Díaz, 1979; Ramos and Barbieri, 1988), where mafic volcanic rocks with ages

between 26 and 17 Ma are common (fig. 3) (Cobbold and Rossello, 2003; Kay and Copeland, 2006; Dhyr and others, 2013b).

The last shortening phase in the Malargüe fold-thrust belt began at ~20 Ma, evidenced by a shift in exhumation and accumulation compatible with magmatic-arc and thrust-belt sources, as revealed by detrital zircon U-Pb ages obtained from the Neogene foreland basin (Horton and Fuentes, 2016). The base of this 2 to 3 km thick foreland basin is defined by a regional unconformity, which marks a prominent change in the depositional environment from distal fluvial and lacustrine in the Paleogene, towards proximal fluvial and alluvial in the Neogene (Horton and others, 2016). Surface and subsurface analyses detected growth strata associated with growing structures within this foreland basin, composed by the early to middle Miocene conglomerates and sandstones of the Agua de la Piedra Formation and the late Miocene cobble to boulder conglomerates of the Loma Fiera and Tristeza Formations (fig. 3) (Silvestro and others, 2005; Silvestro and Atencio, 2009; Sagripanti and others, 2011, 2012; Álvarez Cerimedo and others, 2013; Horton and others, 2016).

The shift towards a contractional regime was coeval with an eastward migration of the magmatic arc during the Miocene (Kay and others, 2006; Folguera and Ramos, 2011), whose deposits in the study area, grouped within the Huincán eruptive cycle (fig. 3), can be found intruding and unconformably covering Neogene structures (Nullo and others, 2002, 2005; Spagnuolo and others, 2012b; Turienzo and others, 2012; Ramos and others, 2014b; Litvak and others, 2015). Finally, between the Pliocene and the Quaternary, a mafic intraplate volcanic event took place in the retroarc area while a series of silicic and ignimbritic flows were erupted along the international boundary between Chile and Argentina (fig. 3) (Ramos and others, 2014b).

METHODOLOGY

The southern sector of the Malargüe fold-thrust belt is characterized by the presence of Mesozoic rocks in a central position, which currently crop out in the cores of several thick-skinned, N-S trending anticlines (fig. 5). Cenozoic rocks crop out in the western and eastern sectors, which are dominantly composed of thick piles of volcanic rocks and synorogenic deposits (fig. 5).

In this paper, we describe extensional basins that are recognized by some or all of the following criteria: 1) normal faulting at a wide range of scales; 2) syn-extensional deposits that present wedge shaped stratal patterns thickening against fault planes; 3) the presence of progressive unconformities in syn-extensional deposits, with dips decreasing up section and diverging towards the fault plane; 4) vertical volcanic dikes and tension fractures trending parallel to normal faults; 5) volcanic rocks with intraplate chemical signatures and mantelic sources, indicative of crustal thinning. Conversely, periods of contraction are supported by some or all of the following observable features: 1) reverse faulting and folding of strata at various scales; 2) syncontractional deposits thinning against anticline hinges and thickening towards syncline axis; 3) the presence of progressive unconformities within syncontractional deposits, with dips decreasing up section and converging towards the growing structure; 4) angular unconformities, often associated with onlap and offlap basal relations; 5) volcanic rocks with calc-alkaline signatures and evidence of crustal contamination due to crustal thickening.

Therefore, in order to reconstruct the intervals between the main contractional phases responsible for the present configuration of the Malargüe fold-thrust belt, the volcaniclastic sequences deposited between the Late Cretaceous and Miocene syncontractional strata were inspected. The study of these volcaniclastic sequences was approached through the analysis of a structural transect developed between the western and eastern sectors of the Malargüe fold-thrust belt (fig. 5). Both sectors were

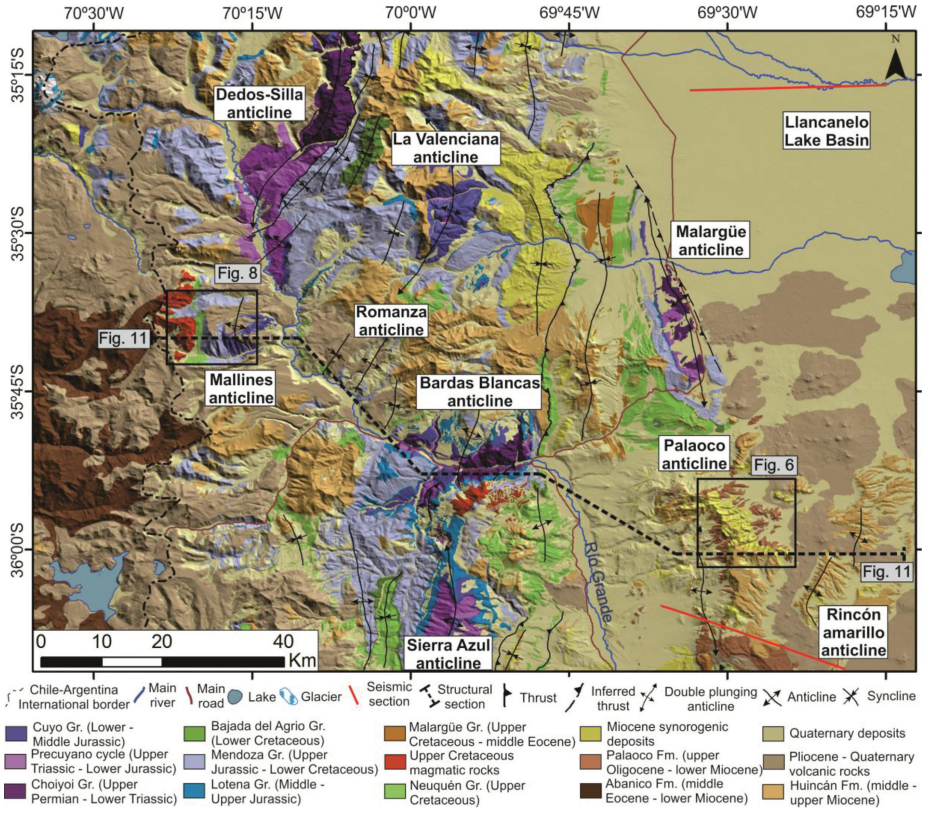

Fig 5. Geological map of the study area showing the location of the structural transect, the analyzed areas mentioned in the text and the seismic sections from Alvarez Cerimedo and others (2013) across the Palaoco anticline and Onnis and others (2018) in the Llancanelo Lake basin. Geology and structure are modified from SERNAGEOMIN (2003), Nullo and others (2005), Silvestro and others (2005), Giambiagi and others (2009), Silvestro and Atencio (2009), Orts and others (2012), Álvarez Cerimedo and others (2013), Naipauer and others (2015), Tapia and others (2015) and data from this work.

inspected with the aim of identifying syntectonic strata which, constrained by previous geochronological analyses (Silvestro and Atencio, 2009) and a new U-Pb age presented herein, allow us to propose a new tectonic evolution model for the Malargüe fold-thrust belt.

Field Work

Field work took place along a structural transect at ~36°S, focusing in two areas located in the western and eastern sectors of the Malargüe fold-thrust belt, represented by the Mallines and Palaoco anticlines respectively (fig. 5). The stratigraphy of the Palaoco anticline was assessed through the compilation of the stratigraphic sections of Silvestro and Atencio (2009), while the stratigraphy of the Mallines anticline was determined via field observations of stratigraphic relationships between different units, and their correlation with better known neighboring areas (Nullo and others, 2005; Naipauer and others, 2015). Mapping along the Mallines anticline allowed the identification of previously unrecognized volcaniclastic deposits informally called the Los Ángeles unit, which was characterized in several stratigraphic sections shown in Iannelli and others (2018). The stratigraphic sections in both areas provided the

framework for our structural analyses, which consisted in the identification of structures, unconformities and syntectonic strata. The identification of growth geometries was made through systematic measurement of strata attitude and thicknesses both in the Palaoco Formation and in the Los Ángeles unit.

Detrital Zircon U-Pb Geochronology

In order to obtain the maximum depositional age of the Los Ángeles unit, analysis of the U-Pb age of detrital zircons was performed on a sample of coarse-grained sandstone interbedded in this volcaniclastic succession. The rock samples were disaggregated using Electro Pulse Disaggregator (EPD) followed by traditional magnetic and heavy liquid techniques at ZirChron LLC. A Detrital zircon non-magnetic fraction was randomly handpicked in alcohol under a binocular microscope and mounted in a 1-inch diameter epoxy puck and polished using standard laboratory procedures.

After cathodoluminiscence and Scanning Electron Microscopy (SEM) imaging, the first 150 LA-ICP-MS U-Pb analyses were conducted at Washington State University using a New Wave Nd:YAG UV 213-nm laser coupled to a ThermoFinnigan Element 2 single collector, double-focusing, magnetic sector ICP-MS. Operating procedures and parameters are similar to those described in detail in Chang and others (2006) and Gaschnig and others (2010). A second session of analyses, obtaining a total of 120 new LA-ICP-MS U-Pb ages, was performed at the University of California Santa Cruz, following the methodology described in Dumitru and others (2015).

Uranium-lead ages were calculated using Isoplot (Ludwig, 2003), and the age probability plots used in this study were constructed using the $^{206}Pb/^{238}U$ age for young (<1.0 Ga) zircons and the $^{206}Pb/^{207}Pb$ age for older (>1.0 Ga) grains. In old grains, ages with >30 percent discordance or >5 percent reverse discordance were considered unreliable and were not used. Also, analyses with error greater than 10 percent were rejected. Sample coordinates, SEM and CL images, detailed analytical methods, concordia plots and U-Pb (LA-ICP-MS) age measurements of zircon grains are available in the Appendix.

Structural Cross Section

In order to integrate the new structural observations in the Palaoco and Mallines anticlines, a structural cross section connecting both sectors was constructed across the Malargüe fold-thrust belt at ~36°S (fig. 5). This section was built using the Midland Valley's software 2D-Move and integrating structural and geological data both from field observations and previous studies (Gulisano and Gutiérrez Pliemling, 1994; Giambiagi and others, 2009; Balgord and Carrapa, 2016). For its construction, the section was divided in two sub-sections: the western one, based on our mapping and structural measurements, encompasses the El Seguro, Mallines, Romanza and Bardas Blancas anticlines (fig. 5); the eastern one, based on sections 9 and 12 of Giambiagi and others (2009), connects the frontal limb of the Bardas Blancas anticline with the Palaoco and Rincón Amarillo anticlines (fig. 5). Due to the lack of deep geophysical constraints, the basal decollement was estimated at a depth of 10 km dipping 2°W, following previous structural sections performed in the area (Giambiagi and others., 2009, 2012; Orts and others, 2012; Mescua and others, 2014).

RESULTS

Eastern Sector of the Malargüe Fold-Thrust Belt: Palaoco Anticline

Part of the Cenozoic stratigraphy of the eastern sector of the Malargüe fold-thrust belt is currently exposed in the core of the Palaoco anticline, where deformed nonmarine deposits of the Malargüe Group of Eocene age are unconformably overlain by the Oligo-Miocene volcaniclastic deposits of the Palaoco Formation (fig. 6). Upper

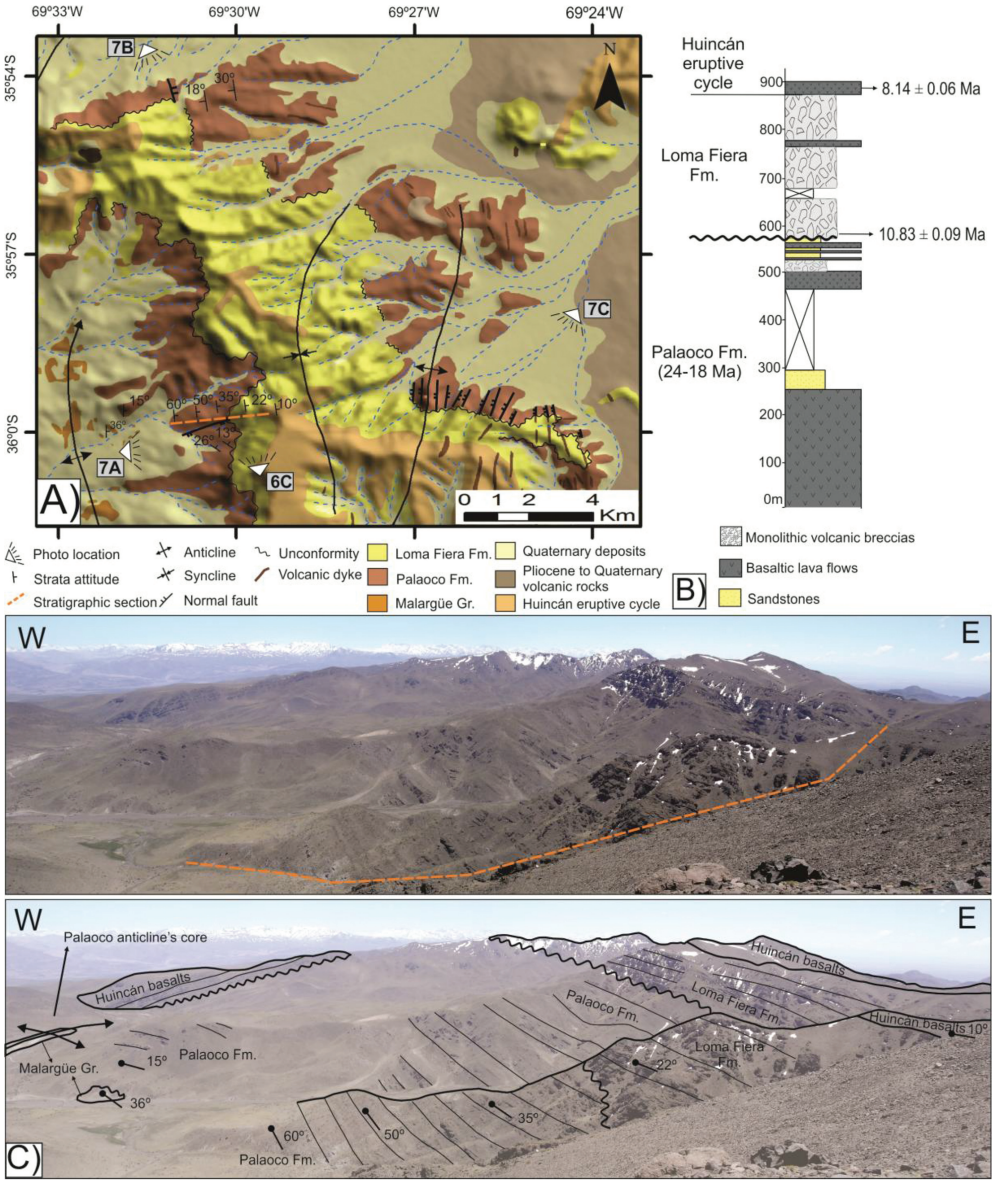

Fig. 6. (A) Detailed geological map showing identified geological units, unconformities and structures in the Palaoco anticline. (B) Stratigraphic section of the eastern limb of the Palaoco anticline showing the unconformable relation between the Palaoco and Loma Fiera Formations, bracketing an ~8 Myr hiatus in this area. Taken and modified from Silvestro and Atencio (2009). (C) View of the eastern limb of the Palaoco anticline, where progressive unconformities identified in the Palaoco Formation are unconformably overlain by the Loma Fiera Formation and the basalts of the Huincán eruptive cycle. Orange dashed line corresponds to the trace of the stratigraphic section.

Miocene andesitic and basaltic breccias of the Loma Fiera Formation rest with angular unconformity over the Palaoco Formation, and the whole sequence is capped by the upper Miocene basalts of the Huincán eruptive cycle (fig 6). While the lower unconformity accounts for a *ca.* 20 to 15 Myr hiatus recorded along the entire eastern

sector of the Malargüe fold-thrust belt, the second unconformity is localized, bracketing a 10 to 5 Myr hiatus identified only in the core of the Palaoco anticline (fig. 6). Although the ages of these formations are based on Ar/Ar datings performed by Silvestro and Atencio (2009), it must be noted that we follow Groeber (1946, 1947)'s initial proposal for the stratigraphy of this area. In this sense, we assigned the basalts, volcanic breccias, tuffaceous sandstones and conglomerates between the Malargüe Group and the Loma Fiera Formation to the Palaoco Formation, instead of the Cerrillos and Ranquil Co denomination used by Silvestro and Atencio (2009) (fig. 6). Therefore, the upper Miocene basalts referred as Palaoco Formation by Silvestro and Atencio (2009) are reassigned to the Huincán eruptive cycle, following Nullo and others (2005) mapping in the study area (fig. 6).

During field work we analyzed the eastern limb of the Palaoco anticline (fig. 6A), where we identified progressive unconformities in the Palaoco Formation, which we interpret are contained within a half-graben bounded by a west dipping, N-S oriented fault located in subsurface east of the anticline's core (fig. 6C). A systematic variation of the dip of the Palaoco Formation is observed along this profile, ranging from 60°E in the base to 35°E towards the top, where the Loma Fiera Formation is found resting on an angular unconformity (fig. 6C). The Loma Fiera Formation also exhibits slight dip variations between 22°E and 10°E and is covered by the basalts of the Huincán eruptive cycle (fig. 6C).

A minor E-W striking normal fault was identified dissecting the eastern limb of the Palaoco anticline (fig. 6A), where the Palaoco Formation contains thickness and dip changes below the angular unconformity with the Loma Fiera Formation, which could be indicating the presence of growth strata associated with the development of this structure (fig. 7A).

In the northern sector of the Palaoco anticline (fig. 6A), growth strata in the Palaoco Formation were found associated with an east dipping, N-S striking normal fault (fig. 7B). Both thickness and dip vary, forming a fan where beds dip 30°W near the base and become subhorizontal towards the top. The Loma Fiera Formation and basalts of the Huincán eruptive cycle are found resting unconformably over the Palaoco Formation and the normal fault that controlled its deposition (fig. 7B).

East of the anticline's core (fig. 6A), its back limb is segmented by a series of N-S normal faults with variable dip orientation controlling thickness variations of the Palaoco Formation (fig. 7C). The timing of activity of these faults is constrained by strata of the Loma Fiera Formation that overlie the Palaoco Formation in angular unconformity (fig. 7C).

Western Sector of the Malargüe Fold-Thrust Belt: Mallines Anticline

The western sector of the Malargüe fold-thrust belt is located along the international border of Chile and Argentina, where the contact between the Mesozoic sedimentary rocks of the Neuquén basin and the overlying volcanic units is exposed (fig. 5). With the objective of analyzing the nature of this stratigraphic contact, field work was performed in the Mallines anticline (fig. 5), a west-verging structure that exposes the Lower to Middle Jurassic marine deposits of the Cuyo Group in its core, with dips of 71°W in its frontal limb (fig. 8A). These deposits are in turn overlain by the Upper Jurassic to Lower Cretaceous marine and nonmarine deposits of the Mendoza Group and the nonmarine foreland basin deposits of the Upper Cretaceous Neuquén Group (fig. 8A).

Along the Los Ángeles Creek and near the international border, the deposits of the Neuquén Group of the frontal limb of the Mallines anticline are unconformably overlain by a sequence of stratified volcano-sedimentary rocks (fig. 8A). This 800 meter-thick volcano-sedimentary sequence, informally referred to as the Los Ángeles unit, is also found unconformably overlying the deformed marine deposits of the Mendoza Group in the headwaters of the El Seguro Creek, which are in turn displaced

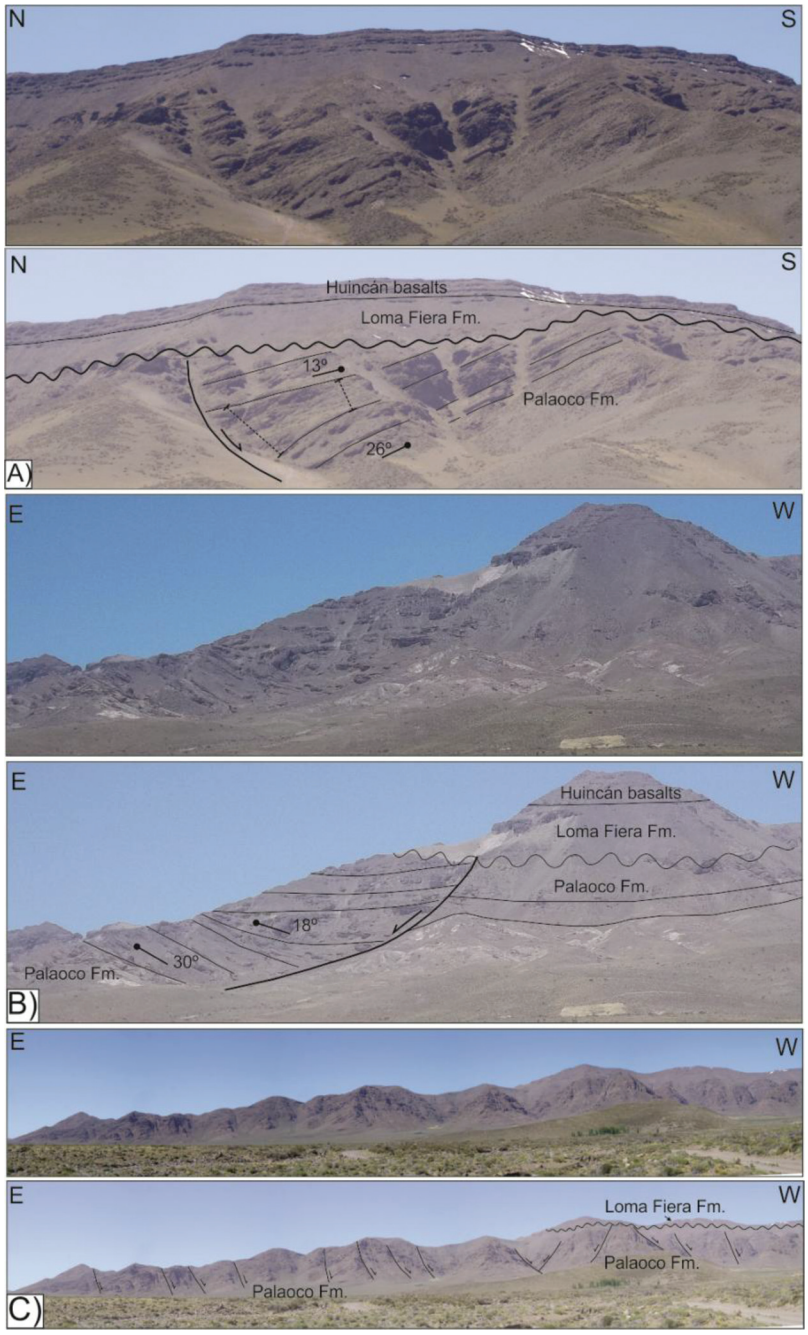

Fig. 7. Normal faults controlling the deposition of the Palaoco Formation in the Palaoco anticline (photo locations indicated in fig. 6A). (A) Progressive unconformities and thickness changes in the Palaoco Formation associated with a minor E-W striking extensional structure, overlain in angular unconformity by the Loma Fiera Formation. (B) Growth strata of the Palaoco Formation controlled by a N-S striking normal fault identified beneath the unconformity with the Loma Fiera Formation. (C) The Palaoco anticline's back-limb is dissected by a series of N-S striking normal faults affecting thickness of the Palaoco Formation.

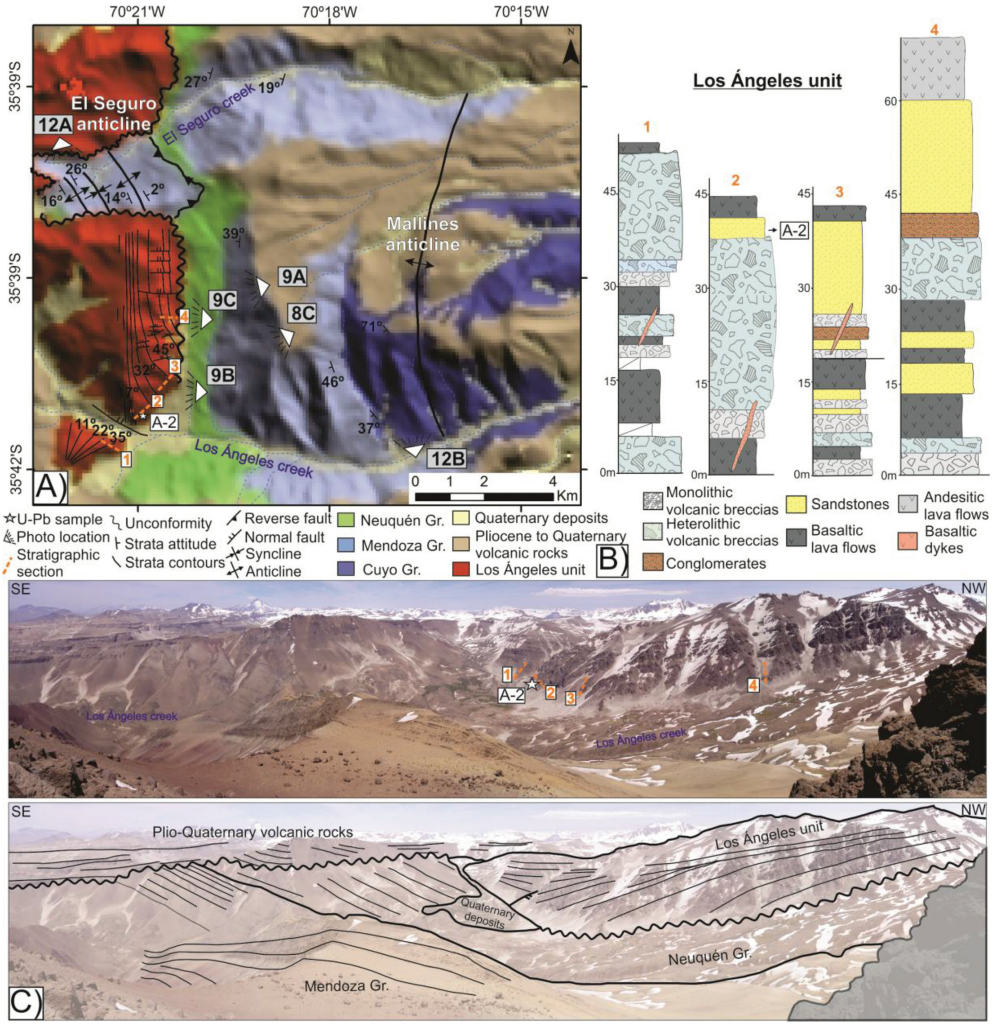

Fig. 8. (A) Detailed geological map showing identified geological units, unconformities, structures, location of the sample A-2 and strata contours of the Los Ángeles unit. (B) Stratigraphic sections of the Los Ángeles unit, a volcaniclastic succession composed of basaltic and andesitic lava flows interbedded with volcanic breccias, conglomerates and sandstones intruded by subvertical basaltic dikes. Location of the sample A-2 is indicated in stratigraphic section 2. Taken and modified from Iannelli and others (2018). (C) Volcano-sedimentary sequences of the Los Ángeles unit unconformably overlying the Neuquén Group deposits in the frontal limb of the Los Mallines anticline. Orange dashed lines correspond to the trace of the 4 stratigraphic sections and the star to the location of sample A-2.

over Neuquén Group deposits by a high angle reverse fault forming the El Seguro anticline (fig. 8A).

The Los Ángeles unit is composed of andesitic and basaltic lavas, volcanic breccias, stratified sandstones and massive conglomerates, which are in turn intruded by subvertical basaltic dikes (fig. 8B). These deposits show dip and thickness variations along strike, displaying two internal sets of strata containing progressive unconformities within the succession, converging into an E-W striking normal fault (fig. 8C). The southern set contains basal strata dipping 35°NW and its overlying strata dipping 11°NW, while it thickens towards the north (fig. 9A). The northern set of strata is

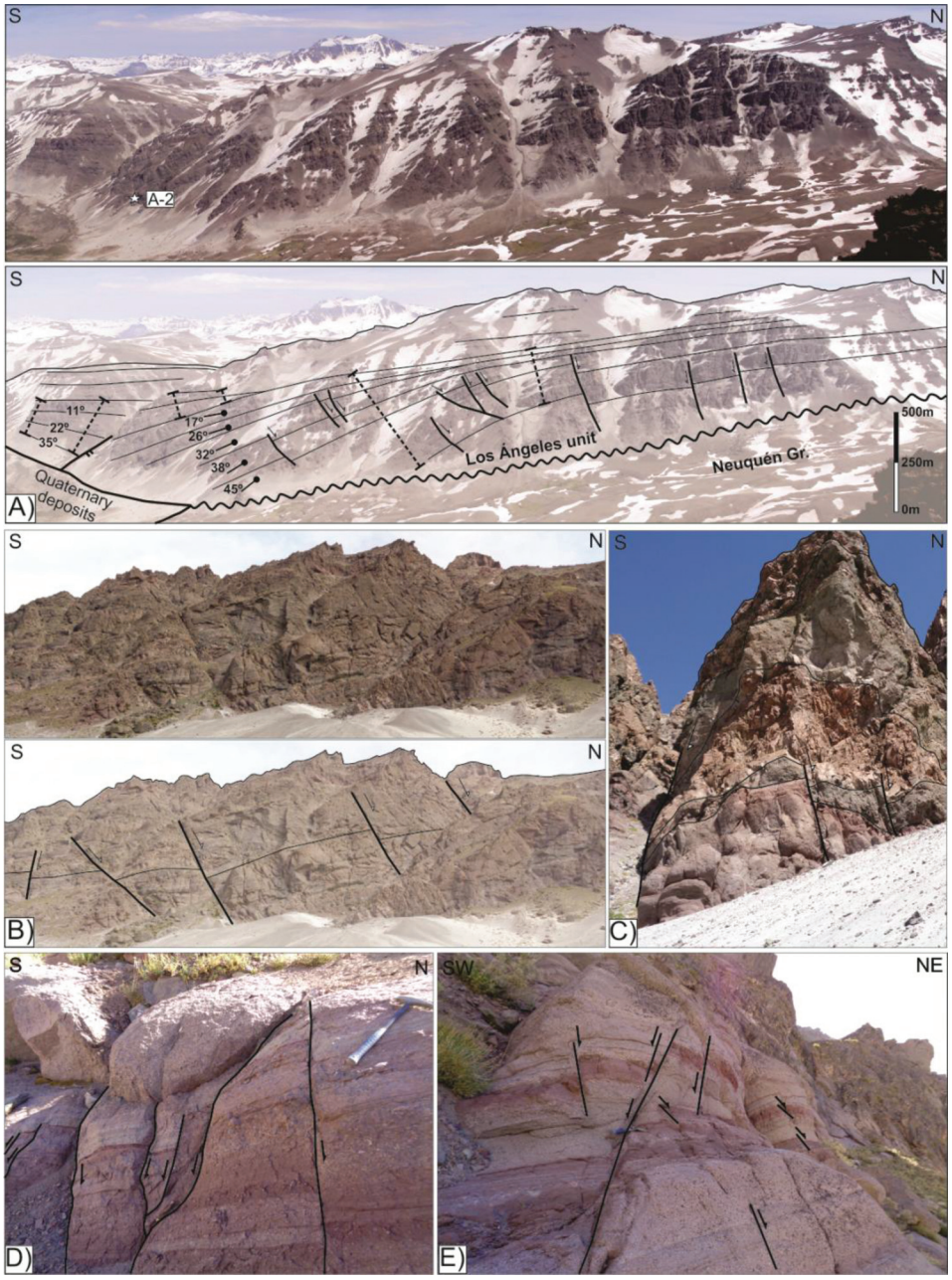

Fig. 9. Normal faults affecting the deposits of the Los Ángeles unit west of the Mallines anticline (photo locations indicated in fig. 8A). (A) The deposits of the Los Ángeles unit show dip and thickness variations along strike controlled by a series of E-W striking normal faults. (B) Medium-scale normal faults affecting deposits of the Los Ángeles unit. (C) Lava flows, volcanic breccias, sandstones and conglomerates presenting evidence of syn-extensional deposition controlled by normal faulting. (D) and (E) Syn-extensional sedimentary deposits of the Los Ángeles unit controlled by small-scale faulting, hammer for scale.

dissected by a series of E-W striking normal faults, displaying 45°SW dips at the base varying to 17°SW at the top, while it thickens towards the south (fig. 9A). A series of E-W striking normal faults have also been identified affecting the Los Ángeles unit over a wide range of scales, controlling thickness and dip of both volcanic and sedimentary rocks (fig. 9).

U-Pb Detrital Zircon Ages of the Los Ángeles Unit

While the syn-extensional deposition of the Los Ángeles unit and the control exerted by the normal faults are evident, the timing of this extensional episode remains poorly constrained. Nullo and others (2002, 2005) mapped these outcrops as lower Miocene volcanic rocks of the Huincán eruptive cycle, but this determination was based on map relations and outcrop patterns, with no geochronological analysis to support their interpretations. Motivated by the implications of this undocumented syn-extensional unit, it becomes necessary to obtain a temporal constraint for these rocks. Therefore, a sample of coarse-grained sandstone (A-2, location in fig. 8) was obtained from the Los Ángeles unit to constrain its age by U-Pb detrital zircon geochronology.

A total of 270 detrital zircons were analyzed from sample A-2, which shows a multimodal distribution of U-Pb ages, including zircon populations with ages between *ca.* 67 and 1972 Ma (fig. 10). The frequency histogram shows peaks in the age distribution at *ca.* 67 (66–71 Ma, 3%), 96 (91–103 Ma, 4%), 182 (174–192 Ma, 7%), 250 (242–263 Ma, 11%), 274 (266–277 Ma, 6%), 300 (294–305 Ma, 6%), 360 (349–368 Ma, 9%), 382 (373–400 Ma, 7%), 459 (453–467 Ma, 4%) and 1100 Ma (1069–1136 Ma, 2%), with isolated ages observed between them (fig. 10A). This heterogeneity of ages is also reflected in zircon morphology, characterized by euhedral and bipyramidal forms of volcanic origin, while some present rounded to subrounded edges (fig. 10B). In particular, all the youngest grains are pristine and elongated with a length-to-width ratio of 6 (fig. 10B). The age of the youngest peak was calculated from a coherent group of 6 zircons using the Tuff-Zirc algorithm (Ludwig, 2003), obtaining a mean age at 67.1 $+2.4/-0.9$ Ma (fig. 10C).

Structural Cross Section Across the Malargüe Fold-Thrust Belt at ~36°S

The structural cross section built across the Malargüe fold-thrust belt is 126.65 kilometers long. A restored length of 139.28 kilometers was calculated using the flexural slip algorithm (Kane and others, 1997; Egan and others, 1997). This yeilds a minimum shortening of 12.72 kilometers, representing a 9.13 percent of the initial length (fig. 11).

Beginning in the western sector of the Malargüe fold-thrust belt, the west dipping reverse fault that displaces the Mendoza Group over the Neuquén Group in the El Seguro creek also corresponds to the eastern limit of the syn-extensional Los Ángeles unit outcrops (figs. 11 and 12A). Therefore, this limit could be interpreted as a tectonically inverted normal fault responsible for the generation of the El Seguro anticline, evidenced by its high angle and a hanging-wall bypass thrust deforming the incompetent Mesozoic strata observed in the headwaters of the El Seguro Creek (figs. 11 and 12A) (Hayward and Graham, 1989; McClay and Buchanan, 1992). This fault also spatially coincides at depth with a west-dipping normal fault that controlled the border of a Late Triassic to Early Jurassic depocenter (figs. 11 and 12A), both presently exposed in the western limb of the Dedos-Silla anticline, located 10 kilometers to the north along the same structural trend (fig. 5) (Villar and others, 2014; Branellec and others, 2016). This anticline, also known as the Las Leñas high, exposes a Late Triassic to Early Jurassic horst in its core, which is bounded to the east by another tectonically inverted east-dipping normal fault (Villar and others, 2014; Branellec and others, 2016). The inversion of this fault is responsible for the Mallines anticline's uplift along

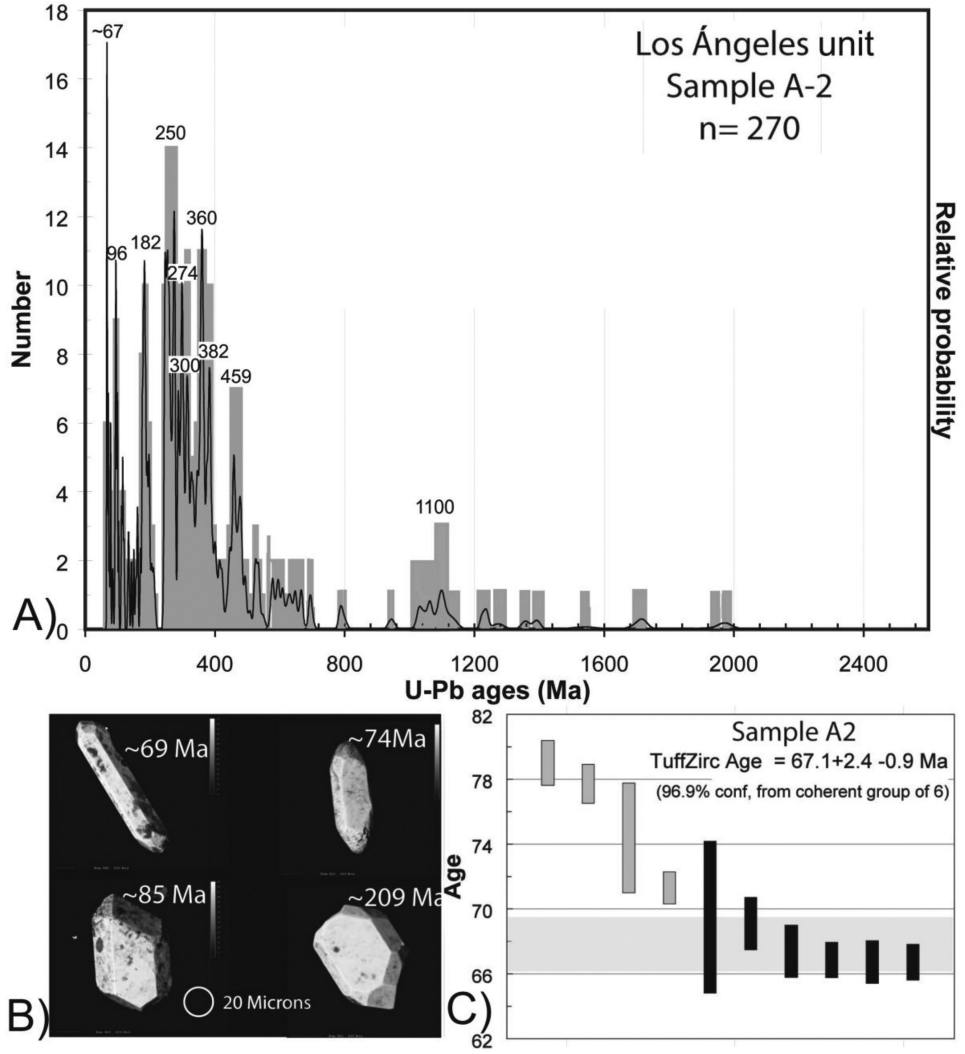

Fig. 10. (A) Frequency histogram and relative probability plots of U-Pb (LA-ICP-MS) ages of detrital zircons from a sample of the Los Ángeles unit (A-2, location in fig. 8). (B) SEM images show that, although morphology of zircons is heterogeneous, all the youngest grains that compose the 67 Ma peak are pristine and have a length-to-width ratio of 6 (see zircon of ~69 Ma). (C) A maximum depositional age of 67.1 +2.4/−0.9 Ma was calculated from a coherent group of 6 zircons using the Tuff-Zirc algorithm (Ludwig, 2003).

our structural transect, indicated by its steeply dipping frontal limb and harpoon geometry (figs. 11 and 12B) (McClay and Buchanan, 1992). To the east, the Romanza anticline corresponds to a long wavelength anticline whose uplift mechanisms are unclear, although its northern continuation through the La Valenciana anticline indicates that it is likely controlled by deep-seated basement thrusting (figs. 5 and 11) (Branellec and others, 2016).

The oldest rocks along the structural transect crop out in the center of the section, where a series of basement blocks are uplifted through low angle thrust faults, constituting the Bardas Blancas anticline (figs. 5 and 11). This area acted as a structural high during the generation of the Late Triassic to Early Jurassic depocenters (Manceda

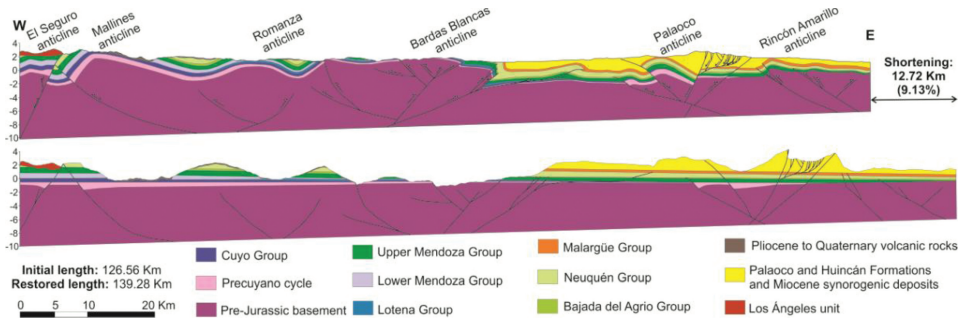

Fig. 11. Structural section built across the study area, connecting the western and eastern sectors of the Malargüe fold-thrust belt (location in fig. 5). The oldest rocks along the structural transect crop out in the center of the section, where a series of basement blocks are uplifted through low angle reverse faults. The youngest rocks crop out both in the western and eastern sectors of the belt, where tectonic inversion mechanisms are predominant due to the presence of inherited extensional structures.

and Figueroa, 1995), leaving no extensional structures available to be inverted (fig. 11). This arrangement has led previous authors to propose that this anticline is formed entirely by major basement thrusts and backthrusts, in absence of tectonic inversion mechanisms (fig. 11) (Manceda and others, 1992; Kozlowski and others, 1993; Manceda and Figueroa, 1995; Dimieri, 1997; Dicarlo and Cristallini, 2007).

In the eastern sector of the Malargüe fold-thrust belt, the section crosses the Palaoco anticline, a thick-skinned structure formed by the tectonic inversion of a series of Late Triassic to Early Jurassic half-grabens, and terminates in the Rincón Amarillo anticline, a west-verging thick-skinned anticline with little surface expression (fig. 11). Since this area is covered almost entirely by late Cenozoic volcanic and sedimentary

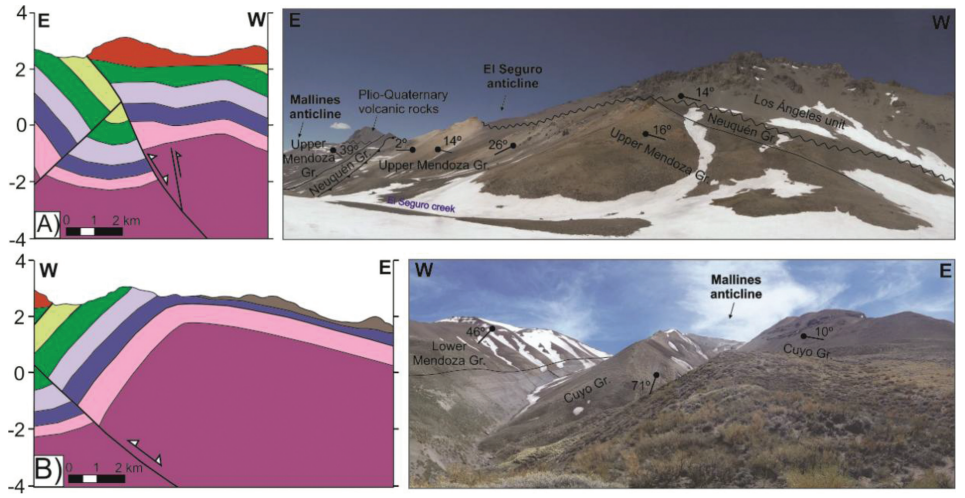

Fig. 12. Structural diagrams and field photos of tectonically inverted structures in the western sector of the Malargüe fold-thrust belt (see figs. 5 and 8 for location and fig. 11 for position along the structural section and diagram color references). (A) Tectonic inversion generating the El Seguro anticline is evidenced by the high angle reverse fault displacing the Upper Mendoza Group over the Neuquén Group and the hanging-wall bypass thrust affecting this structure internally. (B) The west-vergent Mallines anticline presents harpoon geometry and a high-dipping frontal limb, both as a result of the tectonic inversion in depth of a Late Triassic-Early Jurassic normal fault.

rocks, the direct observation of structures in the field is difficult (fig. 5). Therefore, the structure of this area is based on Giambiagi and others (2009)'s interpretation of seismic and borehole information. However, normal faults were observed in the eastern limb of the Palaoco anticline during field observations (figs. 6 and 7), which we interpret to be associated in subsurface with a west dipping master fault marking the eastern border of a late Oligocene to early Miocene half-graben (fig. 11).

A general analysis of the present structure shows that a series of thick-skinned anticlines form part of a basement high in the central sector of the Malargüe fold-thrust belt, while in the western and eastern sectors the structural basement is depressed. As a consequence, while tectonic inversion mechanisms were responsible for the uplift of the western and eastern sectors of the Malargüe fold-thrust belt, the generation of new thrusts uplifted the central sector (fig. 11).

DISCUSSION

Maximum Depositional Age and Provenance of the Los Ángeles Unit

Geochronological data presented in this work reveal that the youngest peak of U-Pb detrital zircon ages in the Los Ángeles unit is 67 Ma (fig. 10A). SEM images show that the zircons composing the 67 Ma peak are pristine and present an elongated morphology (fig. 10B), suggesting a primary syn-depositional volcanic origin (Corfu and others, 2003). This age is consistent with 3 Ar-Ar ages and 11 U-Pb crystallization ages obtained in volcaniclastic rocks of very similar characteristics located 50 to 75 km to the north in the western Principal Cordillera (fig. 4) (Mosolf and others, 2018; Muñoz and others, 2018). Therefore, we interpret that the Los Ángeles unit was deposited in latest Cretaceous times.

The multimodal distribution of detrital zircon ages in the sample A-2 of the Los Ángeles unit reveals that the source area was composed mainly of Mesozoic and Paleozoic rocks, with a minor contribution from Precambrian rocks (fig. 10A). This pattern is indicative of exhumation and contribution from western Andean sources (see Naipauer and Ramos, 2016 for a discussion regarding source regions in the Neuquén basin), showing no significant changes in source areas compared to the Upper Cretaceous deposits of the Neuquén Group (Tunik and others, 2010; Di Giulio and others, 2012) or the equivalent Diamante Formation (Balgord and Carrapa, 2016) (fig. 13). The cratonic sources in the sample A-2 are subordinate and can be interpreted as the recycling from older sedimentary units (fig. 13). However, given the unconformity on the base of the Los Ángeles unit and the missing thickness of the Neuquén Group along the headwaters of the El Seguro Creek (figs. 8 and 12A), recycling of material representing the western Andean sources emerges as another possibility (fig. 13).

A comparison with the relative probability plot of the sample 15EAB12 obtained from the Diamante Formation located 15 km to the east of the Los Ángeles unit (fig. 14A) (Balgord and Carrapa, 2016) shows a great resemblance to the age pattern of sample A-2, with the exception of the 67 Ma peak (fig. 13). These ~67 Ma volcanic zircons have also been detected in tuffs, pyroclastic rocks and dikes interbedded in the Plan de los Yeuques Formation located 50 to 75 km to the north (Mosolf and others, 2018; Muñoz and others, 2018) and in shallow marine deposits of the Malargüe Group located in the retroarc area (fig. 14B) (Aguirre Urreta and others, 2011; Balgord and Carrapa, 2016). This suggests that the volcanic arc was active during latest Cretaceous time and that the Los Ángeles unit was receiving volcanic input from it.

Although a younger age for the Los Ángeles unit remains as a possibility, it is unlikely, since it would imply the absence of syndepositional volcanism and the recycling of a latest Cretaceous unit. In this scenario, the Los Ángeles unit could be an equivalent of the Abanico Formation located in the western Principal Cordillera, or correspond to the

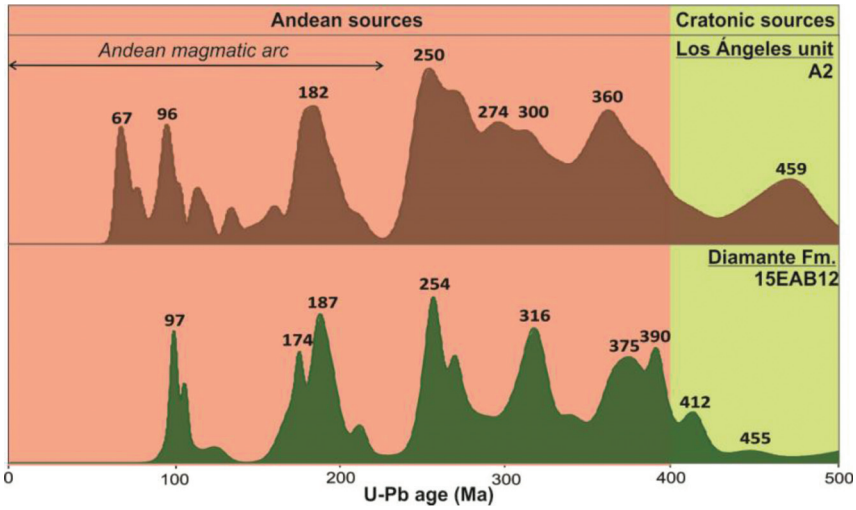

Fig. 13. A comparison of the relative probability plots of U-Pb ages (<500 Ma) of detrital zircons shows the similarity of zircon signatures between the Los Ángeles unit and the Diamante Formation, an equivalent to the Neuquén Group (Balgord and Carrapa, 2016). These data could suggest that both units were receiving sediments from the same western Andean sources, or that the recycling of the Neuquén Group could have been the main source of detrital zircons of sample A-2, with the exception of the 67 Ma peak. The source of this peak would be the coeval magmatic arc and, therefore, 67 Ma is interpreted as the most probable age of sedimentation of sample A-2. The subdivision between Andean sources and cratonic sources is based on Naipauer and Ramos (2016).

Huincán eruptive cycle, as originally mapped by Nullo and others (2002, 2005). However, the presence of normal faults affecting the deposits of the Los Ángeles unit would undermine its correspondence with the Huincán eruptive cycle, emplaced under a contractional regime. The only remaining possibility would be that the Los Ángeles unit is an equivalent of the Abanico Formation but without syndepositional zircons, although this would contrast with what has been reported for this formation (Mosolf and others, 2018) and coeval sedimentary units in the retroarc area (Horton and others, 2016). Moreover, this possibility implies recycling of the lower Malargüe Group, not reported in the vicinity of the Mallines anticline (figs. 5 and 8). However, if this still were the case, the normal faults documented in this study would constitute the first direct evidences of normal faulting in the Abanico Formation at these latitudes.

Cretaceous Tectonic Setting

The opening of the Southern Atlantic Ocean in the Cretaceous had a huge impact in the South American continent, where a series of intracontinental rifts developed, reaching almost as far as the western Pacific margin (fig. 1A). The Salta Group basin is one of the best studied basins of this age, presenting a long-lasting synrift phase bracketed between 128 and 80 Ma (for a recent review, see Gianni and others, 2015 and references therein). However, the final stages of the synrift phase were coeval to the early rise of the Andes at these latitudes, followed by a latest Cretaceous to Paleocene extensional reactivation in the Salta Rift northeastern arm (Lomas de Olmedo sub-basin) (Comínguez and Ramos, 1995). This late extensional event occurred during an important eastward expansion of the orogenic wedge (Bascuñán and others, 2015), suggesting a causal relation between both events. This apparent paradox was addressed by Gianni and others (2015), who suggested a synorogenic foreland rifting reactivation due to the favorable NE trend of the Lomas de Olmedo sub-basin

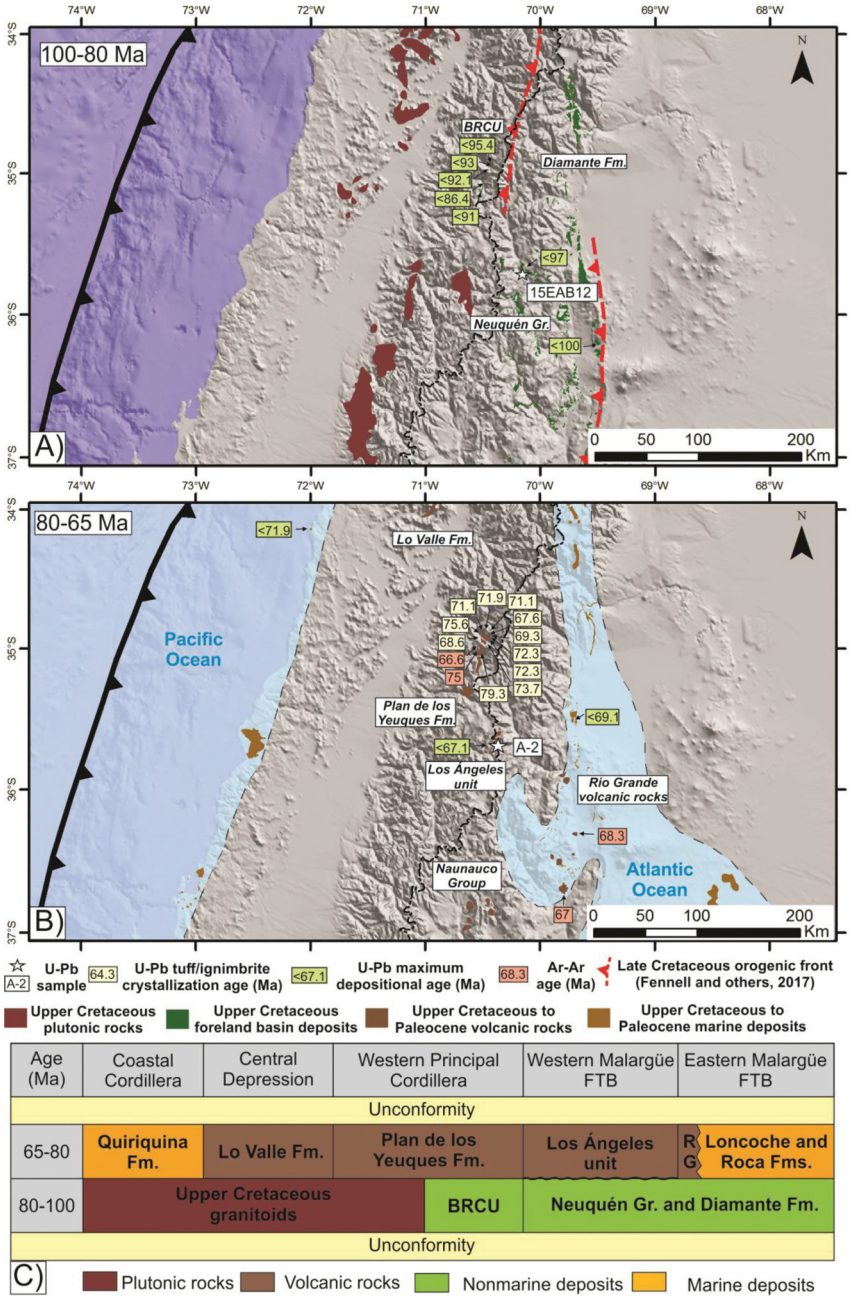

Fig. 14. (A) The 100-80 Ma stage is represented by a Late Cretaceous orogen and associated foreland basin deposits during a magmatic arc migration (Balgord and Carrapa, 2016; Fennell and others, 2017; Muñoz and others, 2018). (B) The 80-65 Ma paleogeographic setting was characterized by a broad volcanic arc associated with intra-arc extensional volcaniclastic basins (Charrier and others, 2007; Llambías and Aragón, 2011; Spagnuolo and others, 2012a; Mosolf and others, 2018; Muñoz and others, 2018 and data of this work) and both Atlantic (Tunik, 2003; Aguirre Urreta and others, 2011; Orts and others, 2012; Balgord and Carrapa, 2016) and Pacific derived marine ingressions (Encinas and others, 2014). (C) Chronostratigraphic relations between Late Cretaceous units at the latitudes of the study area. BRCU stands for Brownish-red Clastic Unit and RG for Río Grande Volcanic rocks.

and the influence of the NE-directed compressional stress field between the latest Cretaceous and the Paleocene. Other examples in the South American continent are constituted by the San Jorge Gulf and Taubaté basins (fig. 1A), whose parallel orientations respect to Andean far-field stresses resulted in the reactivation of pre-existing normal faults and basement fabrics, respectively (Gianni and others, 2015). Therefore, the early to mid Cretaceous and the latest Cretaceous to Paleocene extensional events in southern South America seem to be linked to different geodynamic scenarios. While the first extensional stage was related to the opening of the southern Atlantic Ocean, the second one appears to be a consequence of the interaction between Andean far-field compressional stresses and similarly oriented heterogeneities in the crust.

Studies of the past decades have demonstrated that Upper Cretaceous nonmarine deposits constitute the earliest synorogenic sediments of the Andean foreland basin in the study area (fig. 14A) (Tunik and others, 2010; Di Giulio and others, 2012; Orts and others, 2012; Balgord and Carrapa, 2016; Fennell and others, 2017). In particular, a 25 to 30 Myr unconformity between the Bajada del Agrio Group and the Diamante Formation has been reported in the western sector of the Malargüe fold-thrust belt, possibly representing the passage of the forebulge through this area during initial flexural loading, related to crustal shortening and uplift to the west (fig. 3) (Balgord and Carrapa, 2016). The absence of the Bajada del Agrio Group between the Neuquén and Mendoza Groups in the El Seguro anticline supports this interpretation, indicating that the hiatus could be even longer (figs. 8 and 11A). Although a magmatic lull has been proposed due to the lack of zircons between 100 and 70 Ma preserved in foreland strata (Fennell and others, 2017; Balgord, 2017), plutonic rocks have been reported during this stage between the Coastal Cordillera and the westernmost Principal Cordillera (figs. 14A and 14C) (Ramos and Folguera, 2005; Charrier and others, 2007; Muñoz and others, 2018). Moreover, recent studies have reported detrital zircons of this age in proximal nonmarine foreland strata of the Brownish-Red Clastic Unit (BRCU) in the western Principal Cordillera (Muñoz and others, 2018), indicating the activity of a magmatic arc during foreland basin deposition (fig. 14). This contractional tectonic regime has been linked to the accelerated westward drift of South America after its separation from the rest of Gondwana due to the opening of the southern Atlantic Ocean (Fennell and others, 2017; Horton, 2018). However, synorogenic deposition ended in the foreland at *ca.* 80 Ma, representing the end of the Late Cretaceous contractional stage and associated flexural accommodation (fig. 14) (Muñoz and others, 2018).

The magmatic arc arrived at the core of the Principal Cordillera at 80 Ma (Muñoz and others, 2018), representing an eastern migration of the magmatic loci during the Late Cretaceous contractional stage and reaching the western sector of the Malargüe fold-thrust belt at ~67 Ma (fig. 14). During the analysis of the western sector of the Malargüe fold-thrust belt, we identified growth strata associated with normal fault activity in the uppermost Cretaceous volcaniclastic Los Ángeles unit, suggesting an extensional subsidence mechanism controlling its deposition (figs. 14B and 14C). Given that syn-extensional deposition of the Los Ángeles unit postdates both the opening of the southern Atlantic Ocean and the termination of the Late Cretaceous contractional stage, its interpretation as an intraplate or synorogenic rift basin linked to either processes is discarded. Moreover, the extensional reactivation of inherited heterogeneities during contractional tectonic regimes is unlikely in this area, given the prevalence of N-trending pre-Andean structures, which are orthogonal to the regional stress field during Andean growth (Vergani and others, 1995; Bechis and others, 2014).

However, evidence for extension during this period is not restricted to the western sector of the Malargüe fold-thrust belt. To the north, Muñoz and others (2018) described a 300 meter offset across a normal fault associated with thickness variations

and minor normal faulting in the volcaniclastic sequences of the coeval Plan de los Yeuques Formation (figs. 14B and 14C). Moreover, cropping out in the Central Depression to the northwest, pyroclastic deposits with intercalations of lavas and nonmarine sediments of the uppermost Cretaceous Lo Valle Formation have also been inferred as deposited during extensional conditions (figs. 14B and 14C) (Charrier and others, 2007). Llambías and Aragón (2011) described intrusive facies cutting syncline flanks and anticline cores 100 km to the south (Naunauco Group), suggesting that magmatic activity in this area was favored by a post-orogenic relaxation stage during latest Cretaceous time (fig. 14B). All these volcanic and volcaniclastic sequences are aligned along the present Andean axis, separated 50 to 100 km from the latest Cretaceous magmatic arc that was proposed by Spagnuolo and others (2012a) to the east, based in the position of the Río Grande volcanic rocks (fig. 14B). Thus, it would appear that a broad magmatic arc existed in the study area during latest Cretaceous times, associated with a volcaniclastic intra-arc extensional basin represented by the Los Ángeles unit and the Plan de los Yeuques Formation (fig. 14B).

On a more regional scale, thickness variations in shallow marine deposits (González, 1989; Radic and others, 2005, 2009) support an extensional event that occurred during latest Cretaceous times. These deposits crop out along South America's western coast between 33° and 37°S and are considered Maastrichtian in age and Pacific Ocean derived based on their fossil content (fig. 14B) (Salazar and others, 2010; Buatois and Encinas, 2011). A U-Pb maximum depositional age of 71.9 ±0.9 Ma obtained in the Quiriquina Formation confirms previous biostratigraphic data (Encinas and others, 2014) and allows their correlation with the marine deposits of the Roca and Loncoche Formations over the retroarc region (figs. 14B and 14C) (Barrio, 1990; Parras and Griffin, 2013). This eastern marine incursion, constrained to the Campanian-Danian by its fossil biota and confirmed by its U-Pb detrital zircon age signature (Aguirre Urreta and others, 2011; Balgord and Carrapa, 2016), reached the wedge top area of the Late Cretaceous foreland basin through a series of pathways (14B) (Tunik, 2003; Aguirre Urreta and others, 2011; Orts and others, 2012; Parras and Griffin, 2013; Balgord and Carrapa, 2016) surpassing the position of the Late Cretaceous orogenic front (fig. 14A) (Fennell and others, 2017). This Atlantic marine ingression has been traditionally related to a regional tilting of the basin as a consequence of successive thrust loading during the Late Cretaceous deformational phase (Barrio, 1990; Aguirre Urreta and others, 2011). Although this interpretation has been recently challenged by models showing that dynamic subsidence could explain this sudden marine ingression (Gianni and others, 2018a), evidence for extensional tectonism during these times must be also taken into account.

Tectonic Evolution of the Malargüe Fold-Thrust Belt

The description of syn-extensional growth strata along the structural transect adds some complexity to the tectonic evolution of the Malargüe fold-thrust belt, indicating an alternation of contractional and extensional deformation events during the growth of the Southern Central Andes between 35° and 37°S (fig. 15).

The initial uplift of the Malargüe fold-thrust belt took place in Late Cretaceous time (*ca.* 100 Ma), associated with the passage from an extensional retroarc stage (fig. 15A) to a contractional regime (fig. 15B). This passage is reflected by the presence of growing structures between *ca.* 100 and 80 Ma and a change in the accumulation dynamics towards flexural subsidence within a foreland basin (fig. 15B) (Manceda and Figueroa, 1995; Horton and Fuentes, 2016; Balgord and Carrapa, 2016; Fennell and others, 2017; Muñoz and others, 2018). Based on the analysis of synorogenic strata of the Neuquén Group associated with the growth of structures located in the western sector of the Malargüe fold-thrust belt (Fennell and others, 2017), the El Seguro, Mallines, Romanza and Bardas Blancas anticlines would have also been uplifted at that time (figs. 14A and 15B). Moreover, the observation of an angular unconformity

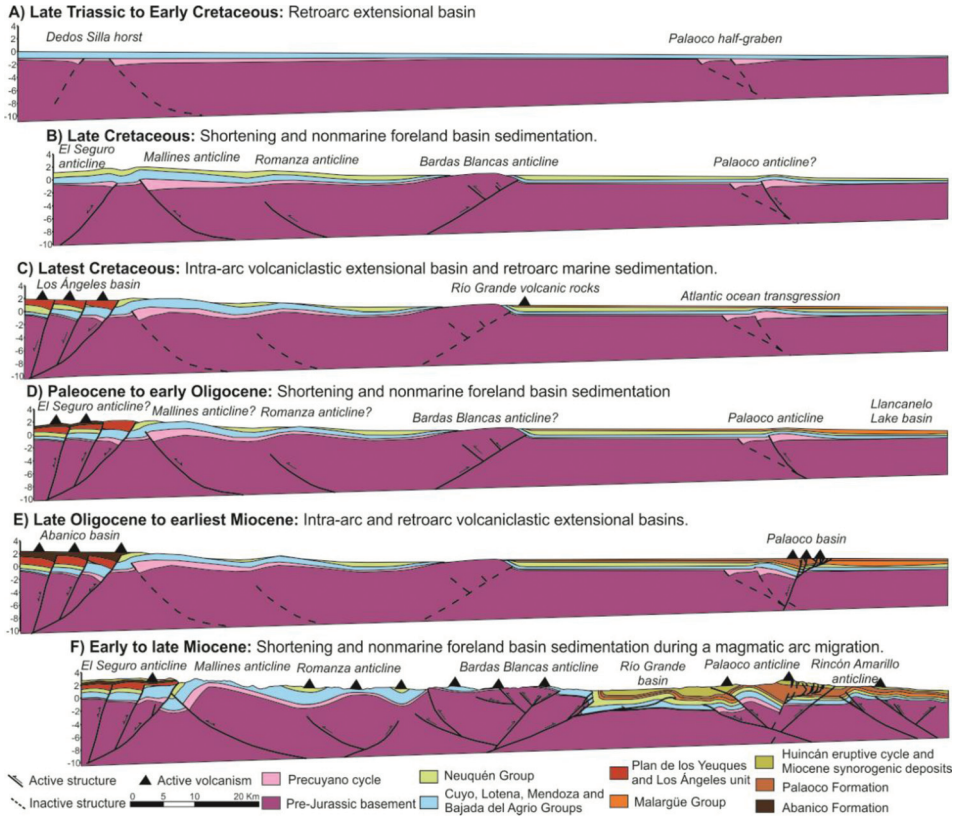

Fig. 15. Schematic tectonic evolution of the Malargüe fold-thrust belt along the analyzed structural section, taking into account active volcanism, sedimentation and deformation through time.

between the Lower Cretaceous deposits of the Mendoza Group and the latest Cretaceous volcaniclastic deposits of the Los Ángeles unit in the El Seguro Creek supports an important non depositional or erosive event during Late Cretaceous times in the western sector (fig. 12A). While the location of the Late Cretaceous orogenic front in the study area has yet to be accurately determined, some evidence indicates that contractional deformation could have reached the eastern sector of the belt, represented by the Palaoco anticline in the analyzed section (figs. 14A and 15B) (Boll and others, 2014; Folguera and others, 2015a; Fennell and others, 2017).

Later, we interpret that an extensional event interrupted the development of the belt in latest Cretaceous times (*ca.* 80–65 Ma) (fig. 15C). The presence of volcanic arc rocks both in the present arc and retroarc areas at 36°S suggests two separate magmatic fronts associated with the opening of an extensional intra-arc basin in the western sector of the belt, where the volcaniclastic Los Ángeles unit was deposited (figs. 14B and 15C). At the same time, the Atlantic Ocean transgressed into the retroarc area, advancing through narrow mountain corridors into the previous deformational front area (figs. 14B and 15C).

The Paleogene constitutes the least studied period of the geological record in the study area, mostly due to poor geochronological constraints and the lack of hydrocarbon interest in Paleocene to Oligocene sequences. However, the recent identification of the Plan de los Yeuques Formation along with the *ca.* 15 Myr angular unconformity

separating it from the overlying Abanico Formation could record an episode of mild contractional deformation in the western Principal Cordillera between Paleocene and middle Eocene time (Charrier and others, 2007, 2015; Muñoz and others, 2018). Furthermore, an erosive surface with toplap reflections between the Roca and Pircala Formations has been detected in a seismic section performed in the Llancanelo Lake basin (see fig. 5 for location), suggesting that the hiatus identified in the arc area could be representing an unconformity of regional significance (fig. 3) (Onnis and others, 2018). Wells along this section reported up to 1200 meters of sediments assigned to the Pircala and Coihueco Formations, demonstrating an important depocenter located in the subsurface east of the Palaoco anticline (fig. 15D) (Onnis and others, 2018). The presence of this depocenter had already been hinted by Alvarez Cerimedo and others (2013), who present a series of seismic sections showing a ~2 km thick Paleogene record that thins onto the crest of the Palaoco anticline (see fig. 5 for location). This geometry would suggest that the Palaoco anticline constituted a growing structure during the Paleogene (fig. 15D).

Paleogene growth of the Palaoco anticline is supported by the description of an angular unconformity between the Malargüe Group and the Palaoco Formation (Álvarez Cerimedo and others, 2013), also reported in other anticlines of the Malargüe fold-thrust belt (Sagripanti and others, 2012; Orts and others, 2012). This notion coincides with Groeber (1946, 1947)'s initial proposal of a contractional event occurred during the Eocene in the eastern Principal Cordillera, which had already been confirmed by Cobbold and Rossello (2003), who interpreted the Paleogene as a period of transpression with a component of right-lateral slip, based on structural, stratigraphical and geochronological evidence collected in the retroarc area. This transpressive crustal shortening event is also recorded in the upper members of the Abanico Formation in the arc area, where well-dated growth strata and a system of dextral-reverse faults active during the late Eocene have been recently recognized (fig. 15D) (Mosolf and others, 2018).

An analysis of the foreland basin deposits carried out by Horton and others (2016) reported slow accumulation rates followed by a sustained 20 Myr period of nondeposition during the Paleogene, which they argue are incompatible with significant topographic loading, leading to their proposal of a neutral tectonic regime (Horton and Fuentes, 2016). However, sedimentation rates would become considerably higher if the 1200 m thick deposits of the Pircala and Coihueco Formations in the Llancanelo Lake basin and the volcaniclastic rocks of the Palaoco Formation were taken into account, marking the end of this slow accumulation stage at *ca.* 25 Ma (fig. 3). Although more evidence and better time constraints are needed, recent proposals of Eocene deformation affecting the Southern Central Andes both to the north and south of the study area (Gianni and others, 2017; Lossada and others, 2017; Fosdick and others, 2017; Rodriguez and others, 2018) indicate this contractional event should be better assessed in the Malargüe fold-thrust belt.

Although the deposition of volcaniclastic strata of the Abanico Formation began in the middle Eocene (Charrier and others, 1996; Mosolf and others, 2018), regional evidence of syn-extensional accumulation is only recorded during late Oligocene and earliest Miocene times (fig. 15E) (Charrier and others, 2002; Kay and others, 2005; Piquer and others, 2010), synchronous with syn-extensional deposition within the Cura Mallin basin to the south (figs. 1B and 4) (Jordan and others, 2001; Burns and others, 2006; Utgé and others, 2009; Radic, 2010; Folguera and others, 2010; Rojas Vera and others, 2010). Extension is also recorded in the retroarc area between the late Oligocene and the earliest Miocene, evidenced by the presence of growth strata in the Palaoco Formation controlled by normal faulting, exposed in the Palaoco anticline (fig. 15E). These volcaniclastic sequences, along with the upper Oligocene to lower Miocene volcaniclastic rocks described in the La Matancilla and Huantraico areas to

the south (fig. 4), would represent the second extensional interruption to the growth of the Malargüe fold-thrust belt (fig. 15E). In this sense, these volcaniclastic rocks would constitute the infill of a retroarc extensional basin between 36° and 38°S (Kay and Copeland, 2006; Dhyr and others, 2013a, 2013b), sharing similar mechanics of deposition and geochemical signatures with a series of basins and volcanic eruptions of the same age, indicative of regional crustal thinning in the Southern Central Andes between the late Oligocene and the earliest Miocene (fig. 1B) (see Fennell and others, 2018 for a recent review).

Finally, the early Miocene marks the beginning of the last deformational phase in the Malargüe fold-thrust belt, recorded by the inversion of previous extensional basins, the reactivation of Late Cretaceous and Eocene thrusts and the generation of new ones along the belt, such as the hanging-wall bypass thrust observed in the El Seguro anticline (fig. 15F). The shift between extensional and contractional deformation is evidenced by the synorogenic deposition of sediments within the Rio Grande basin and the presence of an angular unconformity between the Palaoco and the Loma Fiera Formations in the Palaoco anticline (fig. 15F). Moreover, the localized ~8 Myr hiatus identified in the Palaoco anticline indicates that deformation had already reached the eastern sector of the Malargüe fold-thrust belt in middle Miocene times (fig. 15F). Although deformation in the Malargüe fold-thrust belt was accompanied by the emplacement of the volcanic rocks of the Huincán eruptive cycle during the Miocene eastern magmatic arc migration (Ramos and others, 2014b; Litvak and others, 2015), out-of-sequence thrusting and emplacement of plutonic rocks during the late Miocene in the arc area would indicate both ongoing magmatism and shortening in the western sector of the Malargüe fold-thrust belt towards the end of this contractional stage (fig. 15F) (Tapia and others, 2015).

Hiatus in the Stratigraphic Record of the Malargüe Fold-Thrust Belt

A series of enigmatic regional hiatus have been recorded in the stratigraphic record of the Malargüe fold-thrust belt (fig. 3), although there is no unique interpretation behind their occurrence. In the case of the 25 to 30 Myr hiatus identified in the western sector of the Malargüe fold-thrust belt, the passage of a foreland bulge due to the advance of the Late Cretaceous thrust front is among the most common interpretations (Di Giulio and others, 2012; Balgord and Carrapa, 2016). However, evidence for large topographic loads to the west is meager, and this unconformity is also recorded in structures among the eastern sector of the belt (Ramos and Folguera, 2005; Boll and others, 2014; Fennell and others, 2017). Furthermore, eastward migration of the different depozones that characterize flexural and contiguous foreland basins (DeCelles and Giles, 1996) are not supported by current ages and descriptions of the foreland basin infill (fig. 14A) (Tunik and others, 2010; Di Giulio and others, 2012; Balgord and Carrapa, 2016; Fennell and others, 2017).

A second enigmatic hiatus that occurred during the Paleogene has been detected since the early work's of Groeber (1946, 1947), even though it has been recently temporally constrained between 40 and 20 Ma (Horton and others, 2016; Horton and Fuentes, 2016). These authors argue against the assignation of this late Eocene to earliest Miocene stratigraphic hiatus to the passage of a forebulge, given the lack of evidence for late Paleogene shortening. Moreover, since extensional basins would by definition act to reduce any topographic loading, the synchronicity of this hiatus with extensional deformation reported in the Andes at these latitudes would definitely rule out the foreland bulge passage interpretation. An alternative hypothesis to this hiatus is given by Horton and Fuentes (2016), who propose it might be the product of diminished plate coupling during a neutral tectonic regime, resulting in no thrust loading and slow, limited flexural subsidence in the foreland at these latitudes (Horton, 2018).

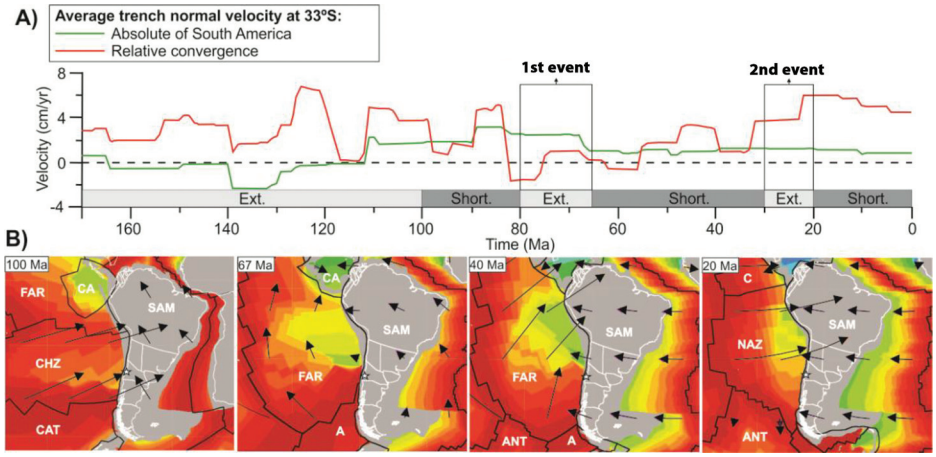

Fig. 16. (A) Proposed shifts between extension and shortening in the study area show good correlation with changes in subduction parameters, with the first extensional event coinciding with a drop in the absolute velocity of South America, and the second with a sudden rise on relative convergence velocity (both curves are taken and modified from Maloney and others, 2013). (B) Plate reconstructions taken and modified from Müller and others (2016) using a hot-spot reference frame for the last 70 Myrs, which is paired with a True Polar Wander-corrected paleomagnetic model for older times allowing for a 35 Myr long transition period between 105 and 70 Ma. These paleoreconstructions show that after an almost orthogonal subduction during Late Cretaceous times, the oblique subduction of the Farallón-Aluk mid-ocean ridge occurred beneath the study area (marked with a white star) during latest Cretaceous times. This event marked the beginning of oblique subduction along the Southern Central Andes, which became orthogonal again towards the end of the Paleogene, situation that has remained unaltered until present. Noteworthy, both extensional stages coincide with these major obliquity changes along the margin. Abbreviations: A, Aluk Plate; ANT, Antarctic Plate; C, Cocos Plate; CA, Caribbean Plate; CAT, Catequil Plate; CHZ, Chasca Plate; FAR, Farallon Plate; NAZ, Nazca Plate; SAM, South American Plate.

In the present, the Andean forebulge has been interpreted to be located in the La Pampa High, 300 km east of the San Rafael block frontal thrust, based on geophysical and geomorphological analyses (Chase and others, 2009; Niviere and others, 2013). However, their interpretation has been challenged by Folguera and others (2015b), who show that the La Pampa High corresponds to a block uplift reactivated towards the end of the Miocene, and that the geometry, thickness and facial distribution of Neogene basins far east of the Andean orogenic front must be related to dynamic forces rather than flexural. Therefore, it seems that the configuration in and around of the Malargüe fold-thrust belt, where extensional faults and inherited basement fabrics would potentially reactivate due to tectonic loading, may preclude the formation of foreland bulges, since foreland crust would have likely behaved as a broken beam, inhibiting the migration of flexural waves.

Possible Causes of Extensional Events

Current data presented in our tectonic evolution model indicate that after a long extensional regime, a strongly convergent retroarc system was established in the study area in Late Cretaceous times (fig. 16A) (Orts and others, 2012; Mescua and others, 2013; Horton and Fuentes, 2016; Balgord and Carrapa, 2016; Fennell and others, 2017; Muñoz and others, 2018). Afterwards, the deformational history of the belt fluctuated, including three contractional stages (~100–80 Ma, ~65–25 Ma and ~20–0 Ma) and two extensional events (~80–65 Ma and ~25–20 Ma) (fig. 16A). However, when attempting to link these extensional episodes with models of extension along convergent margins, numerous hypotheses arise.

A widely cited model for extensional deformation is the extensional collapse and lithospheric foundering as a consequence of thick crustal roots (Coney and Harms, 1984; Dewey, 1988; Kay and others, 1994; Giovanni and others, 2010; Giambiagi and others, 2016). However, due to the lack of paleoelevation estimations and geochemical indicators of crustal thickening in our study area, we cannot either support or rule out this process. Nevertheless, the low shortening estimates (typically 25–10 km) of the Malargüe fold-thrust belt obtained in this and in previous studies (Giambiagi and others, 2012; Orts and others, 2012; Rojas Vera and others, 2014; Mescua and others, 2014; Fuentes and others, 2016) would suggest that crust never reached threshold values necessary to generate the orogenic collapse. Therefore, extension associated with delamination and gravitational spreading seems unlikely.

A slab shallowing event has been proposed between Late Cretaceous and earliest Paleocene times, based on the spatio-temporal evolution of the magmatic arc and the onset of Andean orogenic building in the study area (fig. 16A) (Ramos and Folguera, 2005; Folguera and Ramos, 2011; Spagnuolo and others, 2012a; Fennell and others, 2017; Gianni and others, 2018a). Although kinematic linkages to flat-slab subduction have also been proposed as a potential extensional mechanism (McNulty and Farber, 2002), no evidence of active thrusting and a great amount of volcanic rocks deposited within a broad volcanic arc between 80 and 65 Ma suggest that a shallow subduction angle during the latest Cretaceous-Paleocene below the study area was unlikely, or that a slab tear was formed at 35°30'S, as proposed by Gianni and others (2018a). However, a closer look into the geodynamic context reveals that the subduction of the Farallón-Aluk mid-ocean ridge beneath the study area coincides with the latest Cretaceous extensional stage (fig. 16B) (Cande and Leslie, 1986; Somoza and Ghidella, 2012; Maloney and others, 2013; Müller and others, 2016).

An analysis of Muller and others (2016)'s global plate reconstruction model through the free-access GPlates software (www.gplates.org) shows that a southward migration of this triple junction was coeval with reported extensional deformation along South America's western margin, starting in northern Chile during the Late Cretaceous and reaching central Patagonia in Eocene times, where it opened a series of slab windows beneath the retroarc area (fig. 16B) (Ramos and Kay, 1992; Mpodozis and Allmendinger, 1993; Arévalo and others, 1994; Espinoza and others, 2005; Aragón and others, 2011; Gianni and others, 2018b). Moreover, recent geochemical analyses performed in the Los Ángeles unit show that after an initial arc-like signature, a more alkaline-tendency is observed towards the younger volcanic levels, suggesting a more enriched mantle source and the subduction of anhydrous oceanic crust, which is compatible with the passage of a mid-ocean ridge (Iannelli and others, 2018). Although the subduction of mid-ocean ridges is not a very popular extensional mechanism, weakening of the upper-plate's lithosphere in response to the presence of hot mantle at depth constitutes another process capable of generating a shift towards an extensional regime causing local to regional collapse (Garrett and Storey, 1987; Thorkelson, 1996; Bradley and others, 2003; Lagabrielle and others, 2004, 2007; Scalabrino and others, 2009; Breitsprecher and Thorkelson, 2009; Georgieva and others, 2016).

Another potential cause of upper plate extension in the Southern Central Andes is a change in subduction parameters, such as upper plate absolute velocity and relative convergence velocity (Heuret and Lallemand, 2005; Lallemand and others, 2005; Sobolev and Babeyko, 2005; Schellart, 2008; Schellart and Moresi, 2013; Horton, 2018). While a good correspondence has been observed between the onset of contractional deformation in the study area and the westward accelerated displacement of the South American plate (Fennell and others, 2017; Horton, 2018), the latest Cretaceous extensional phase coincides with a decrease in South America's absolute westward velocity (fig. 16A) (Maloney and others, 2013; Müller and others, 2016; Muñoz and others, 2018). Afterwards, the

westward motion of South America stabilized and convergence velocity seems to have played a major role, since coincidences have been recognized between high average convergence rates and both Eocene and Miocene phases of deformation (fig. 16A) (Pardo-Casas and Molnar, 1987; Lossada and others, 2017).

However, the sudden increase towards fast convergence rates during the Paleogene to Neogene transition overlaps with the second extensional interruption in the study area, showing an inconsistency with models linking high rates of convergence to strong compressional coupling (fig. 16A). The regional event of crustal thinning and widespread volcanism recorded during the late Oligocene and the earliest Miocene has been related to another possible cause of extensional deformation in convergent margins: steepening and rollback of the subducted slab (Muñoz and others, 2000; Ramos and Folguera, 2009; Folguera and Ramos, 2011; Encinas and others, 2016; Horton, 2018). It has been recently suggested through numerical modeling that after the slow subduction rates recorded during most of the Paleogene (fig. 16A), the influence exerted by the slab pull force over the subducting plate resulted in an abrupt increase in the convergence rate, steepening of the slab and the retreat of the trench hinge away from the upper plate between late Oligocene and earliest Miocene times, resulting in the formation of a series of intra-arc basins and in an influx of hot material beneath the continental plate (Fennell and others, 2018).

Although none of the aforementioned models can be discarded, the most plausible explanation for the latest Cretaceous extensional event would involve a decrease in the absolute trenchward motion of the South American plate during a shift towards oblique subduction after the proposed Late Cretaceous slab shallowing event (fig. 16). This would have led to the generation of tensile stresses, increasing magmatic production and crustal thinning, allowing both Atlantic and Pacific derived marine transgressions (fig. 16). Afterwards, a period of slow and oblique subduction took place, associated with sparse evidence of transpressive crustal shortening and slow accumulation rates in the foreland basin (fig. 16). This period came to an end after a sudden change towards almost orthogonal subduction and faster convergence rates associated with the beginning of the second extensional event, which we agree with previous proposals was due to rollback of the subducted slab, explaining overall magmatism, extension and high convergence rates between late Oligocene and earliest Miocene time (fig. 16).

Comparison to Other Cordilleran Orogenic Systems

Considering all the preceding evidence, extensional deformation in the study area does not seem to respond to processes related to the activity of the fold-thrust belt, in contrast to what has been proposed for better known Cordilleran orogenic systems such as the Puna-Altiplano plateau (DeCelles and others, 2009), the northern Peruvian Andes (Giovanni and others, 2010) or the North American Cordillera (DeCelles, 2004).

In the Puna-Altiplano plateau of southern Peru, Bolivia, northern Chile and northwestern Argentina (Allmendinger, 1986), extension is evidenced by the presence of normal and strike-slip faults affecting Quaternary sediments (Sébrier and others, 1985; Schoenbohm and Strecker, 2009; Zhou and others, 2013), as well as by the stress state inferred from analyses of fault kinematics (Allmendinger and others, 1989; Cladouhos and others, 1994; Marrett and others, 1994; Giambiagi and others, 2016) and the age and geochemistry of mafic intraplate volcanism (Kay and others, 1994). The current interpretation is that crustal thinning would have been dominated by extensional collapse and lithospheric foundering due to the presence of extremely thick crust (DeCelles and others, 2009, and references therein), while extension in the Southern Central Andes (35°–37°S) seems to correlate better with changes in the plate kinematic framework.

An exceptional example of active extension within convergent orogenic systems is represented by the Cordillera Blanca in northern Peru, located above the modern Peruvian flat slab (Dalmayrac and Molnar, 1981; Schwartz, 1988; Sébrier and others, 1988). Here, a *ca.* 200 kilometer long active detachment fault has accommodated a minimum of 12 to 15km dip-slip displacement orthogonal to E-W regional compression (McNulty and Farber, 2002; Giovanni and others, 2010). Focused extension along this fault has resulted in the opening of a *ca.* 10 kilometer thick supradetatchment basin in the Peruvian Andes hinterland (Giovanni and others, 2010), where Quaternary fault scarps and seismicity provide evidence of active normal faulting (Sébrier and others, 1988; Mercier and others, 1992). However, active shortening in the frontal Sub-Andean thrust belt has led to the proposal of compressive forces acting on the eastern flank of the Andes, while gravitational forces affected the highest parts of the orogen as the result of overthickenned crust (Dalmayrac and Molnar, 1981; Suárez and others, 1983; Giovanni and others, 2010). Conversely, this contrasting scenario has not been observed in the Southern Central Andes between 35° and 37°S along their geological history, where shortening and extension seem to occur alternately, not synchronously.

A closer analogue can be found in the North American Cordillera, where an alternation between contractional and extensional stages has been identified in the hinterland of the Cretaceous Sevier-Laramide orogenic belt (Wells, 1997; Wells and others, 2012). Numerous evidence such as stratigraphic omissions, ductile shear zones with low-angle normal displacement and rapid cooling ages suggest that an extensional event affected the internal zone of the orogen between the Late Cretaceous and the Paleocene, which was responsible for the unroofing of several metamorphic core complexes in western USA (for example, Wells and others, 1990; Applegate and others, 1992; Wells, 1997). However, the absence of syn-extensional sedimentation would imply that extension, although widespread, had little surface expression (Hodges and Walker, 1992). Moreover, evidence of active shortening in the frontal Sevier thrust belt coeval to extensional deformation in the hinterland would indicate that the Late Cretaceous-Paleocene was a stage of synconvergent extension (Hodges and Walker, 1992; Wells and others, 2012; Long and others, 2015). The prevailing interpretation is that isostatic adjustment and thermal weakening following a regional lithosphere delamination event was responsible for the Late Cretaceous to Paleocene extension in the hinterland of the Sevier-Laramide orogenic system (DeCelles, 2004; Wells and others, 2012; Long and others, 2015). This is in marked contrast with our results, which suggest that extensional events in the Southern Central Andes (35°–37°S) must be associated with major velocity and obliquity changes rather than to localized extension within a continuous contractional setting.

CONCLUSIONS

The geological history of the Malargüe fold-thrust belt is characterized by an alternation of three shortening and two extensional episodes since its initial uplift in Late Cretaceous times. In this work, evidences of both extensional episodes have been described and temporally constrained along the belt. In the western sector, dating of detrital zircons obtained from a syn-extensional volcaniclastic sequence yielded a maximum depositional age of 67.1+2.4/−0.9 Ma. In the eastern sector, the age of growth strata indicates normal faulting and associated deposition of volcaniclastic strata in late Oligocene to earliest Miocene times.

A structural section along the Malargüe fold-thrust belt at 36°S constructed to integrate the new structural observations suggests a link between inherited extensional structures and the present structural style. Structural inversion dominated in both the western and eastern sectors, which had previously been affected by normal faulting. In the central section, the absence of extensional faults encouraged the generation of new thrusts. These new data show that two extensional stages occurred during the intervals

developed between the main contractional phases in the Southern Central Andes (35°–37°S). In particular, the first extensional event occurred immediately after its initial uplift, reflecting an interruption in orogenesis during latest Cretaceous times (*ca.* 80–65 Ma). This stage, not previously recognized, is characterized by the opening of an intra-arc basin associated with a broad magmatic arc. Additional evidence of regional crustal thinning corresponds to the opening of a series of marine-filled extensional forearc basins and a marine transgression in the retroarc area. Afterwards, localized shortening associated with slow accumulation rates occurred in the retroarc area during most of the Paleogene. Finally, syn-extensional accumulation within a series of intra-arc and retroarc volcaniclastic basins occurred between late Oligocene and earliest Miocene times (*ca.* 25–20 Ma), indicating a shift towards an extensional regime.

While the first extensional episode is potentially linked to a decrease in the absolute motion of the South American plate and an increase in subduction obliquity due to the passage of a mid-ocean ridge, we infer that the second extensional stage was driven by steepening and rollback of the subducted slab associated with high convergence rates, in accordance with previous proposals. This history and its comparison with better known Cordilleran orogenic systems would indicate that extensional deformation in the Southern Central Andes (35°–37°S) is controlled by geodynamic events rather than by intrinsic processes within the orogenic wedge.

ACKNOWLEDGMENTS

We acknowledge Bruno Colavitto, Lucia Sagripanti and Emilio Rojas Vera for their assistance in the field, Andrés Echaurren, Guido Gianni, Felipe Tapia and Mark Brandon for fruitful discussions and Midland Valley Ltd. for providing academic licenses of Move Software. The present contribution was benefited by thorough reviews made by Steve Boyer and Mike McGroder, which greatly improved the present work. We are also in debt with Brian Horton, Brian Mahoney, Taylor Schildgen, Lindsay Schoenbohm and two anonymous reviewers for their detailed and constructive reviews in a previous version of this manuscript. Analytical methods, concordia plot, SEM and CL images and U-Pb data can be found in table A1 in the Appendix. This study has been funded by PICT-2012-1490 and FONDECYT Project 1151146. This is the R-292 contribution of the Instituto de Estudios Andinos "Don Pablo Groeber".

APPENDIX

ANALYTICAL METHODS

After cathodoluminiscence and SEM imaging (figs. A1A and A1B), the first 150 LA-ICP-MS U-Pb analyses were conducted at Washington State University using a New Wave Nd:YAG UV 213-nm laser coupled to a ThermoFinnigan Element 2 single collector, double-focusing, magnetic sector ICP-MS. Operating procedures and parameters are similar to those described in detail in Chang and others (2006) and Gaschnig and others (2010). A second session of analyses was performed at the University of California Santa Cruz, following the methodology described in Dumitru and others (2015), obtaining a total of 120 new LA-ICP-MS U-Pb ages (table A1). Laser spot size, fluence and repetition rate were 30 microns, 7 J/Cm2 and 10 Hz, respectively. He and Ar carrier gases delivered the sample aerosol to the plasma. Each analysis consists of a short blank analysis followed by 250 sweeps through masses 202, 204, 206, 207, 208, 232, 235, and 238, taking approximately 30 seconds. Unknowns were run in blocks of 10 analyses bracketed by standards. Time-independent fractionation was corrected by normalizing U/Pb and Pb/Pb ratios of the unknowns to the zircon standards (Chang and others, 2006; Dumitru and others, 2015). U and Th concentration were monitored by comparing to 91500 zircon standard. Two zircon standards were used: Plesovice (Sláma and others, 2008) and FC-1 (Paces and Miller, 1993). Uranium-lead ages were calculated using Isoplot (Ludwig, 2003).

The age probability plots (Ludwig, 2003) used in this study were constructed using the $^{206}Pb/^{238}U$ age for young (<1.0 Ga) zircons and the $^{206}Pb/^{207}Pb$ age for older (>1.0 Ga) grains. In old grains, ages with >30% discordance or >5% reverse discordance are considered unreliable and were not used. Also analyses with error greater than 10% were rejected. Concordia plot is shown in figure A1C, where only the concordant analyses used in the frequency histogram and relative probability plots are plotted.

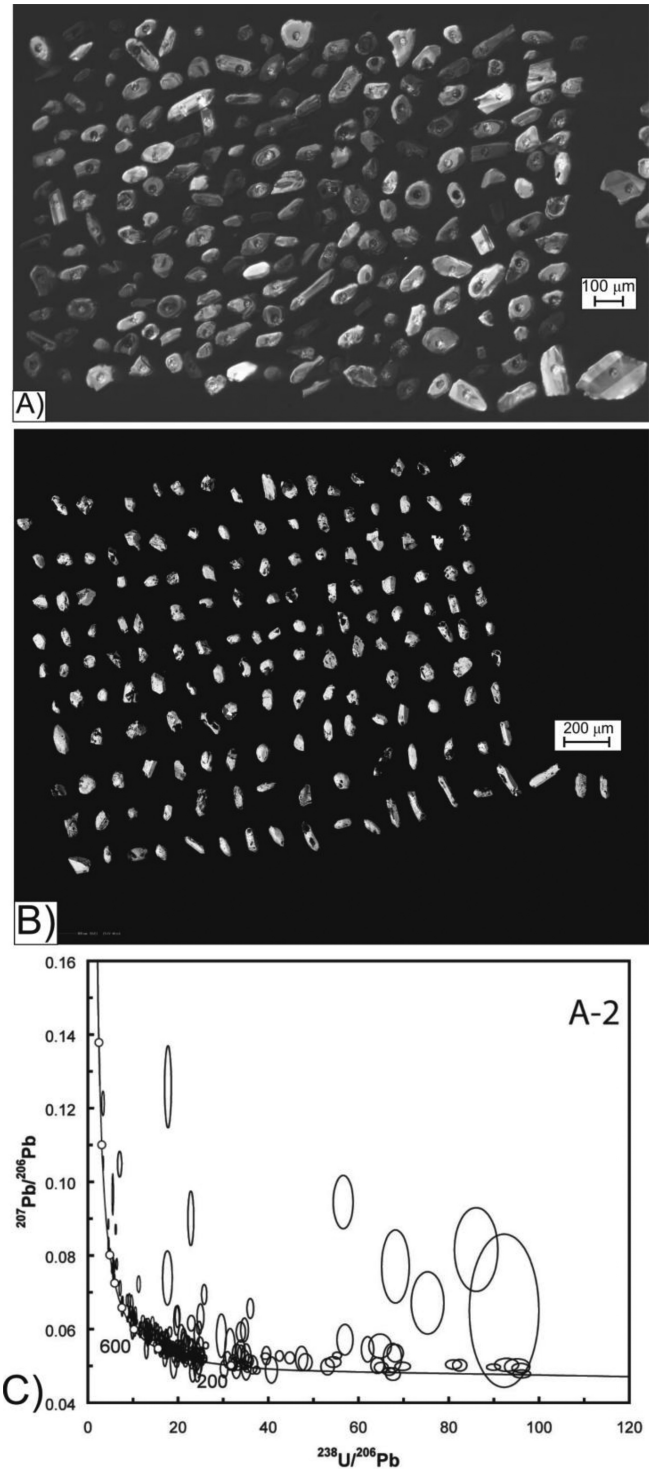

Fig. A1. (A) Cathodoluminescense images of the first 150 analyzed zircons. (B) SEM images of the 120 analyzed zircons during the second session. (C) Concordia plot of U-Pb ages from sample A-2.

TABLE A1

U-Pb Data

Sample Name	U ppm	U/Th	Isotopic Ratios $^{207}Pb/^{235}U$	2 SE	$^{206}Pb/^{238}U$	2SE	Corr. Coef.	$^{238}U/^{206}Pb$	2SE	$^{207}Pb/^{206}Pb$	2SE	Ages $^{207}Pb/^{235}U$ Ma	2 SE Ma	$^{206}Pb/^{238}U$	2SE Ma	$^{207}Pb/^{206}Pb$ Ma	2SE Ma	Best Age Ma	2SE Ma
A-2: Los Angeles unit; n=270 (35°41'12.78"S 70°20'53.58"W)																			
University of California Santa Cruz data																			
A2_1	74	1.07	2.40000	0.12000	0.18110	0.00430	0.3757	5.521811	0.131109	0.0966	0.0046	1235.0	37.0	1074.0	23.0	1540.0	86.0	1540.0	86.0
A2_2	471	1.32	0.22200	0.00980	0.02952	0.00071	0.3751	33.87534	0.814752	0.0543	0.0022	204.7	7.8	187.5	4.5	353.0	89.0	187.5	4.5
A2_3	1055	0.71	0.14550	0.00610	0.02075	0.00053	0.3931	48.19277	1.230948	0.051	0.0019	137.9	5.5	132.4	3.3	212.0	81.0	132.4	3.3
A2_4	614	4.64	0.88700	0.03300	0.08870	0.00240	0.7359	11.27396	0.305045	0.0722	0.0018	643.0	17.0	547.0	14.0	992.0	50.0	547.0	14.0
A2_5	699	2.40	0.59600	0.01700	0.07530	0.00140	0.5884	13.28021	0.24691	0.057	0.0013	473.0	11.0	467.7	8.2	497.0	50.0	467.7	8.2
A2_6	459	0.99	0.54400	0.04100	0.04380	0.00100	0.4898	22.83105	0.521257	0.0901	0.006	429.0	26.0	276.3	6.2	1340.0	140.0	276.3	6.2
A2_7	617	6.60	0.67300	0.01800	0.07960	0.00150	0.5725	12.56281	0.236736	0.0606	0.0014	521.0	11.0	493.7	8.8	624.0	50.0	493.7	8.8
A2_8	472	2.75	0.70900	0.02000	0.08540	0.00160	0.4234	11.7096	0.219384	0.06	0.0015	541.0	12.0	529.8	9.3	622.0	52.0	529.8	9.3
A2_9	372	0.41	0.33700	0.01400	0.04143	0.00080	0.2832	24.1371	0.46608	0.0586	0.0023	295.0	10.0	261.6	4.9	530.0	85.0	261.6	4.9
A2_10	644	1.04	0.10650	0.00690	0.01481	0.00036	0.1941	67.52194	1.641317	0.0522	0.0032	102.6	6.3	94.8	2.3	290.0	120.0	94.8	2.3
A2_11	629	1.81	0.37400	0.02100	0.04710	0.00110	0.5048	21.23142	0.495851	0.057	0.0026	319.0	15.0	296.5	6.7	522.0	98.0	296.5	6.7
A2_12	1099	1.03	0.28370	0.00950	0.03966	0.00088	0.5291	25.21432	0.559471	0.0531	0.0016	253.9	7.4	250.6	5.5	330.0	65.0	250.6	5.5
A2_13	947	0.98	0.18350	0.00730	0.02528	0.00051	0.2821	39.55696	0.798024	0.0528	0.002	171.5	6.2	160.9	3.2	309.0	76.0	160.9	3.2
A2_14	1195	7.63	0.94400	0.03400	0.10580	0.00360	0.8250	9.451796	0.321611	0.0647	0.0014	671.0	18.0	647.0	21.0	760.0	44.0	647.0	21.0
A2_15	527	0.63	0.30800	0.01100	0.04233	0.00082	0.3258	23.62391	0.457633	0.054	0.0019	274.7	8.8	267.2	5.1	348.0	78.0	267.2	5.1
A2_16	744	5.02	0.25010	0.00900	0.02777	0.00046	0.3771	36.01008	0.596494	0.0656	0.0022	226.3	7.4	176.6	2.9	756.0	75.0	176.6	2.9
A2_17	548	1.30	0.60900	0.01800	0.07500	0.00160	0.5461	13.33333	0.284444	0.0581	0.0015	481.0	12.0	466.0	9.5	517.0	59.0	466.0	9.5
A2_18	134.2	0.85	0.44100	0.02600	0.05740	0.00130	0.1832	17.4216	0.394566	0.0558	0.0031	373.0	18.0	360.3	8.0	390.0	120.0	360.3	8.0
A2_19	972	2.01	0.64400	0.01600	0.07620	0.00180	0.6429	13.12336	0.310001	0.0605	0.0013	505.0	10.0	474.0	11.0	625.0	46.0	474.0	11.0
A2_20	88.9	0.52	0.36400	0.03000	0.05260	0.00170	0.2753	19.01141	0.614437	0.0516	0.004	309.0	22.0	330.0	11.0	150.0	150.0	330.0	11.0
A2_21	1131	7.77	0.46900	0.01300	0.06140	0.00120	0.7080	16.28664	0.318306	0.0551	0.0011	390.3	8.9	384.2	7.3	419.0	46.0	384.2	7.3
A2_22	264	1.06	5.10000	0.39000	0.29800	0.02100	0.9400	3.355705	0.236476	0.1213	0.0027	1800.0	69.0	1670.0	100.0	1972.0	39.0	1972.0	39.0
A2_23	398	3.22	2.13000	0.14000	0.14190	0.00770	0.9178	7.047216	0.382407	0.1048	0.0028	1145.0	47.0	852.0	43.0	1703.0	49.0	1703.0	49.0
A2_24	236	1.00	0.19800	0.01500	0.02851	0.00079	0.0456	35.07541	0.971925	0.0511	0.004	184.0	13.0	181.1	4.9	220.0	150.0	181.1	4.9
A2_25	766	2.54	0.21730	0.00870	0.02945	0.00053	0.4830	33.95586	0.61109	0.0534	0.0018	198.7	7.3	187.1	3.3	334.0	75.0	187.1	3.3
A2_26	909	0.95	1.67700	0.04100	0.15600	0.00370	0.8167	6.410256	0.152038	0.0777	0.0012	998.0	16.0	933.0	21.0	1136.0	30.0	1136.0	30.0
A2_27	642	8.42	0.83300	0.02300	0.09610	0.00170	0.5976	10.40583	0.184078	0.0626	0.0015	614.0	13.0	592.0	10.0	697.0	52.0	592.0	10.0
A2_28	143.8	0.55	0.23600	0.02000	0.03172	0.00095	0.1285	31.52585	0.944185	0.0545	0.0046	216.0	16.0	201.2	5.9	330.0	160.0	201.2	5.9
A2_29	522	8.73	0.42700	0.01500	0.05630	0.00120	0.5245	17.76199	0.378586	0.0559	0.0016	360.0	10.0	352.8	7.1	419.0	65.0	352.8	7.1
A2_30	418	2.09	0.43500	0.01700	0.05030	0.00110	0.4506	19.88072	0.434767	0.0634	0.0024	365.0	11.0	316.0	6.9	706.0	79.0	316.0	6.9
A2_31	675	5.45	0.59000	0.02000	0.06980	0.00150	0.6778	14.32665	0.307879	0.0615	0.0015	471.0	12.0	436.0	9.4	638.0	54.0	436.0	9.4
A2_32	475	2.08	1.79500	0.03600	0.17150	0.00290	0.5837	5.830904	0.098598	0.077	0.0013	1045.0	13.0	1019.0	16.0	1112.0	35.0	1112.0	35.0
A2_33	1061	1.20	0.30880	0.00980	0.04023	0.00096	0.5820	24.85707	0.593159	0.056	0.0015	273.1	7.6	254.1	5.9	436.0	58.0	254.1	5.9
A2_34	485	3.63	1.97700	0.03700	0.18770	0.00320	0.6761	5.327651	0.090828	0.0765	0.0011	1106.0	12.0	1110.0	17.0	1104.0	29.0	1104.0	29.0
A2_35	174.4	0.84	0.63000	0.02800	0.07730	0.00160	0.2988	12.93661	0.267769	0.0598	0.0025	494.0	18.0	479.8	9.9	569.0	92.0	479.8	9.9
A2_36	683	2.97	1.20100	0.02700	0.13000	0.00210	0.5437	7.692308	0.12426	0.0672	0.0014	801.0	13.0	787.0	12.0	832.0	42.0	787.0	12.0
A2_37	1291	1.40	0.12810	0.00520	0.01882	0.00043	0.4930	53.13496	1.214029	0.0498	0.0018	122.9	4.6	120.2	2.7	165.0	78.0	120.2	2.7
A2_38	499	1.41	0.37400	0.01300	0.05230	0.00110	0.4400	19.12046	0.402151	0.0528	0.0016	324.0	10.0	328.8	6.5	302.0	69.0	328.8	6.5
A2_39	276	1.01	0.58600	0.02400	0.07700	0.00190	0.4314	12.98701	0.320459	0.0547	0.0022	465.0	15.0	479.0	11.0	383.0	85.0	479.0	11.0

TABLE A1
(continued)

Sample Name	U ppm	U Th	Isotopic Ratios $^{207}Pb/^{235}U$	2 SE	$^{206}Pb/^{238}U$	2SE	Corr. Coef.	$^{238}U/^{206}Pb$	2SE	$^{207}Pb/^{206}Pb$	2SE	Ages $^{207}Pb/^{235}U$ Ma	2 SE Ma	$^{206}Pb/^{238}U$	2SE Ma	$^{207}Pb/^{206}Pb$ Ma	2SE Ma	Best Age Ma	2SE Ma
A-2: Los Angeles unit; n=270 (35°41'12.78"S 70°20'53.58"W)																			
University of California Santa Cruz data																			
A2_40	158	1.12	0.43400	0.02200	0.05080	0.00130	0.2299	19.68504	0.503751	0.0623	0.0032	365.0	16.0	319.1	7.7	640.0	110.0	319.1	7.7
A2_41	632	1.51	0.34800	0.01400	0.04760	0.00110	0.3831	21.0084	0.485488	0.0545	0.002	303.0	11.0	299.8	6.6	347.0	80.0	299.8	6.6
A2_42	720	5.09	1.94600	0.04000	0.16220	0.00300	0.8135	6.165228	0.11403	0.0871	0.0011	1099.0	14.0	968.0	17.0	1357.0	25.0	1357.0	25.0
A2_43	141.7	2.03	0.43400	0.02500	0.05850	0.00140	0.2894	17.09402	0.409088	0.0536	0.003	364.0	18.0	366.4	8.4	320.0	120.0	366.4	8.4
A2_44	462	1.16	0.23600	0.01700	0.01767	0.00056	0.5468	56.5931	1.793556	0.0945	0.0059	212.0	14.0	112.9	3.5	1480.0	120.0	112.9	3.5
A2_45	624	1.19	0.34900	0.01500	0.04580	0.00110	0.3472	21.83406	0.524399	0.0556	0.0021	302.0	11.0	288.8	6.6	377.0	81.0	288.8	6.6
A2_46	712	2.26	0.20790	0.00890	0.03039	0.00070	0.3463	32.90556	0.757943	0.0491	0.002	191.7	7.5	192.9	4.4	147.0	85.0	192.9	4.4
A2_47	543	0.57	0.22210	0.00880	0.03310	0.00073	0.3733	30.21148	0.666296	0.0492	0.0019	205.7	7.4	209.9	4.6	142.0	79.0	209.9	4.6
A2_48	196	1.15	0.08600	0.01900	0.01084	0.00074	0.0002	92.25092	6.297572	0.065	0.017	83.0	18.0	69.5	4.7	200.0	390.0	69.5	4.7
A2_49	1126	0.60	0.21300	0.00770	0.03111	0.00070	0.5257	32.14401	0.723266	0.0511	0.0016	195.3	6.4	197.8	4.4	213.0	66.0	197.8	4.4
A2_50	603	0.92	0.28900	0.01100	0.03980	0.00080	0.4458	25.12563	0.505038	0.0527	0.0017	258.2	8.3	251.5	5.0	288.0	71.0	251.5	5.0
A2_51	394	0.96	0.13590	0.00880	0.01755	0.00045	0.2724	56.98006	1.461027	0.0571	0.0034	129.2	7.7	112.1	2.9	440.0	120.0	112.1	2.9
A2_52	760	0.81	0.23940	0.00980	0.02948	0.00072	0.4503	33.9213	0.828471	0.0592	0.0022	218.9	7.8	187.3	4.5	553.0	82.0	187.3	4.5
A2_53	713	2.26	0.32690	0.00980	0.04619	0.00091	0.4677	21.64971	0.426526	0.0516	0.0015	286.9	7.5	291.0	5.6	244.0	61.0	291.0	5.6
A2_54	393	0.34	2.49600	0.06700	0.21770	0.00480	0.6591	4.593477	0.10128	0.0828	0.0017	1273.0	19.0	1268.0	25.0	1273.0	37.0	1273.0	37.0
A2_55	796	15.44	0.33500	0.01100	0.04562	0.00086	0.4409	21.92021	0.413226	0.0525	0.0015	293.1	8.3	287.5	5.3	299.0	65.0	287.5	5.3
A2_56	1368	23.00	0.87600	0.03100	0.09860	0.00280	0.7439	10.14199	0.288008	0.0635	0.0014	636.0	17.0	606.0	16.0	727.0	49.0	606.0	16.0
A2_57	119.5	0.54	0.28300	0.02300	0.04120	0.00120	0.2246	24.27184	0.706947	0.0511	0.0044	254.0	19.0	260.1	7.4	200.0	160.0	260.1	7.4
A2_58	173.4	1.25	0.82700	0.02900	0.09500	0.00220	0.3777	10.52632	0.243767	0.0633	0.0022	609.0	16.0	584.0	13.0	715.0	73.0	584.0	13.0
A2_59	876	4.35	1.79500	0.04300	0.17580	0.00350	0.7386	5.688282	0.113248	0.0755	0.0012	1041.0	16.0	1043.0	19.0	1069.0	32.0	1069.0	32.0
A2_60	730	1.61	0.37500	0.01100	0.05019	0.00097	0.4639	19.92429	0.385068	0.0531	0.0015	322.4	8.4	315.6	6.0	314.0	62.0	315.6	6.0
A2_61	980	8.19	0.46500	0.01200	0.05764	0.00087	0.4503	17.34906	0.261861	0.0584	0.0013	387.8	8.2	361.2	5.3	533.0	48.0	361.2	5.3
A2_62	342.8	60.00	0.71200	0.02200	0.08600	0.00180	0.5859	11.62791	0.243375	0.0599	0.0017	544.0	14.0	532.0	11.0	611.0	58.0	532.0	11.0
A2_63	1017	0.96	0.37500	0.01300	0.04360	0.00130	0.6440	22.93578	0.683865	0.0616	0.0017	325.0	10.0	274.7	7.8	657.0	60.0	274.7	7.8
A2_64	204.5	3.83	0.91100	0.04000	0.10350	0.00310	0.3666	9.661836	0.289388	0.0659	0.0027	657.0	22.0	634.0	18.0	793.0	89.0	634.0	18.0
A2_65	165.3	1.47	0.12400	0.01400	0.01162	0.00053	0.1741	86.05852	3.925216	0.0816	0.0093	117.0	13.0	74.4	3.4	1020.0	230.0	74.4	3.4
A2_66	467	5.99	1.38400	0.05300	0.14010	0.00360	0.7558	7.137759	0.183411	0.0711	0.0017	881.0	22.0	846.0	20.0	944.0	50.0	944.0	20.0
A2_67	1050	1.66	0.61800	0.01400	0.07730	0.00130	0.5958	12.93661	0.217563	0.0575	0.0011	487.4	8.9	479.8	7.5	506.0	42.0	479.8	7.5
A2_68	974	1.93	0.31310	0.00990	0.04294	0.00083	0.6056	23.28831	0.450147	0.0532	0.0013	277.7	7.8	271.0	5.2	331.0	55.0	271.0	5.2
A2_70	379.1	1.90	0.52500	0.01800	0.06480	0.00130	0.4046	15.4321	0.309595	0.0577	0.0018	429.0	12.0	404.8	7.8	501.0	69.0	404.8	7.8
A2_71	629	0.96	0.15060	0.00760	0.02111	0.00049	0.2770	47.37091	1.099562	0.052	0.0027	142.9	6.6	134.6	3.1	250.0	100.0	134.6	3.1
A2_72	538	15.30	0.59600	0.01900	0.07160	0.00160	0.4778	13.96648	0.3121	0.0594	0.0017	478.0	12.0	445.7	9.6	584.0	61.0	445.7	9.6
A2_73	358	0.66	0.29000	0.01400	0.04300	0.00100	0.3777	23.25581	0.540833	0.0484	0.0022	257.0	11.0	271.3	6.4	151.0	90.0	271.3	6.4
A2_74	230.7	0.82	0.38600	0.01900	0.04830	0.00140	0.3073	20.70393	0.600114	0.0579	0.0027	333.0	13.0	303.8	8.8	518.0	97.0	303.8	8.8
A2_75	871	1.37	0.47200	0.01400	0.06190	0.00130	0.6607	16.15509	0.339283	0.0547	0.0013	392.1	9.3	387.8	7.9	396.0	50.0	387.8	7.9
A2_76	568	3.76	0.59000	0.02000	0.07360	0.00180	0.5487	13.58696	0.33229	0.0579	0.0017	468.0	13.0	457.0	11.0	509.0	63.0	457.0	11.0
A2_78	124.2	2.21	0.85300	0.03800	0.10110	0.00260	0.3738	9.891197	0.254373	0.0606	0.0027	622.0	21.0	620.0	15.0	592.0	96.0	620.0	15.0
A2_79	735	0.87	0.12080	0.00590	0.01613	0.00029	0.2063	61.99628	1.114626	0.0545	0.0028	115.8	5.4	103.1	1.8	340.0	110.0	103.1	1.8
A2_80	880	1.25	0.38100	0.01200	0.04930	0.00110	0.3490	20.28398	0.452584	0.0551	0.0015	326.0	8.7	310.0	6.8	381.0	58.0	310.0	6.8
A2_81	174.6	0.66	0.15100	0.01500	0.01467	0.00054	0.0712	68.16633	2.50919	0.077	0.0081	141.0	13.0	93.9	3.5	950.0	210.0	93.9	3.5
A2_82	190.8	0.74	0.12400	0.01200	0.01328	0.00052	0.0927	75.3012	2.948541	0.0671	0.0069	116.0	11.0	85.0	3.3	620.0	210.0	85.0	3.3

TABLE A1
(continued)

Sample Name	U ppm	U/Th	Isotopic Ratios $^{207}Pb/^{235}U$	2 SE	$^{206}Pb/^{238}U$	2SE	Corr. Coef.	$^{238}U/^{206}Pb$	2SE	$^{207}Pb/^{206}Pb$	2SE	Ages $^{207}Pb/^{235}U$ Ma	2 SE Ma	$^{206}Pb/^{238}U$	2SE Ma	$^{207}Pb/^{206}Pb$ Ma	2SE Ma	Best Age Ma	2SE Ma
A-2: Los Angeles unit; n=270 (35°41'12.78"S 70°20'53.58"W)																			
University of California Santa Cruz data																			
A2_84	170	0.86	0.26900	0.02200	0.03380	0.00100	0.1444	29.5858	0.87532	0.0582	0.0048	243.0	17.0	214.2	6.3	430.0	160.0	214.2	6.3
A2_85	187.8	0.93	0.31700	0.02000	0.04340	0.00140	0.2891	23.04147	0.743273	0.0533	0.0033	277.0	15.0	273.4	8.7	340.0	120.0	273.4	8.7
A2_86	147.8	1.36	1.87000	0.06300	0.17790	0.00410	0.4491	5.621135	0.129548	0.0767	0.0023	1071.0	22.0	1054.0	22.0	1094.0	61.0	1094.0	61.0
A2_88	258.7	2.30	0.29800	0.01500	0.04114	0.00091	0.3623	24.30724	0.537666	0.0521	0.0024	263.0	11.0	259.8	5.6	262.0	97.0	259.8	5.6
A2_90	150.5	0.60	1.20300	0.04400	0.13180	0.00310	0.4775	7.587253	0.178456	0.0662	0.0022	802.0	20.0	797.0	18.0	803.0	68.0	797.0	18.0
A2_91	80.9	1.44	0.59000	0.05400	0.05670	0.00280	0.4551	17.63668	0.870947	0.0739	0.006	454.0	34.0	355.0	17.0	940.0	170.0	355.0	17.0
A2_92	825	0.82	0.28800	0.01000	0.03987	0.00084	0.3869	25.08151	0.528429	0.0524	0.0017	256.1	8.0	251.9	5.2	279.0	70.0	251.9	5.2
A2_93	2030	5.73	0.36300	0.01200	0.04560	0.00130	0.8191	21.92982	0.625192	0.0568	0.0012	313.4	8.8	287.3	8.2	474.0	45.0	287.3	8.2
A2_94	778	1.19	0.45800	0.01600	0.05860	0.00140	0.6616	17.06485	0.407693	0.0562	0.0015	380.0	11.0	366.7	8.5	460.0	55.0	366.7	8.5
A2_95	614	1.19	2.70000	0.05300	0.22000	0.00380	0.8092	4.545455	0.078512	0.0885	0.0011	1328.0	15.0	1283.0	20.0	1392.0	23.0	1392.0	23.0
A2_96	655	1.42	0.18970	0.00840	0.02740	0.00068	0.3629	36.49635	0.905749	0.0503	0.002	178.3	7.2	174.2	4.3	214.0	83.0	174.2	4.3
A2_97	1031	6.45	0.34000	0.01000	0.04716	0.00097	0.5717	21.20441	0.436138	0.0527	0.0013	297.6	7.7	297.0	6.0	297.0	54.0	297.0	6.0
A2_98	1272	11.80	0.60100	0.02800	0.07390	0.00240	0.8829	13.5318	0.439463	0.0588	0.0013	473.0	17.0	459.0	15.0	595.0	49.0	459.0	15.0
A2_99	342	1.18	0.16400	0.01100	0.02458	0.00065	0.3544	40.68348	1.075845	0.0489	0.0029	154.7	9.3	156.5	4.1	130.0	120.0	156.5	4.1
A2_100	497	4.20	4.32000	0.10000	0.29720	0.00600	0.7521	3.364738	0.067929	0.105	0.0016	1699.0	19.0	1678.0	30.0	1718.0	30.0	1718.0	30.0
A2_101	196	2.31	0.87600	0.03100	0.10250	0.00210	0.4119	9.756098	0.199881	0.0626	0.0021	640.0	17.0	630.0	12.0	660.0	72.0	630.0	12.0
A2_102	581	1.21	0.63000	0.01700	0.07720	0.00140	0.6258	12.95337	0.234906	0.0591	0.0013	495.0	10.0	479.4	8.6	554.0	47.0	479.4	8.6
A2_103	827	0.62	0.37500	0.01200	0.03879	0.00071	0.3912	25.77984	0.471866	0.0694	0.0022	322.7	8.9	245.3	4.4	891.0	66.0	245.3	4.4
A2_104	317	3.65	0.54200	0.02200	0.06640	0.00130	0.4119	15.06024	0.294854	0.0591	0.0022	441.0	14.0	414.1	8.1	564.0	76.0	414.1	8.1
A2_105	367	1.29	0.33900	0.01700	0.04005	0.00098	0.3817	24.96879	0.610972	0.0633	0.0029	296.0	13.0	253.0	6.1	663.0	95.0	253.0	6.1
A2_106	67.2	1.00	0.97800	0.07300	0.05630	0.00190	0.3009	17.76199	0.599428	0.1258	0.0091	680.0	37.0	352.0	11.0	1940.0	140.0	1940.0	140.0
A2_107	465	1.13	0.23700	0.01100	0.02880	0.00058	0.2632	34.72222	0.699267	0.0598	0.0026	216.4	8.5	183.0	3.6	594.0	91.0	183.0	3.6
A2_108	1451	1.12	0.36450	0.00810	0.04942	0.00082	0.4686	20.23472	0.335744	0.0541	0.0011	315.5	5.9	310.9	5.1	364.0	46.0	310.9	5.1
A2_109	306.9	1.19	0.63100	0.02400	0.07730	0.00210	0.5602	12.93661	0.351447	0.0594	0.0019	497.0	14.0	479.0	13.0	588.0	69.0	479.0	13.0
A2_110	359	2.30	0.48700	0.02000	0.06210	0.00140	0.4284	16.10306	0.363032	0.0579	0.0022	401.0	14.0	388.1	8.6	487.0	83.0	388.1	8.6
A2_111	440	0.93	0.32500	0.01300	0.04380	0.00090	0.3037	22.83105	0.469131	0.0547	0.0021	284.1	9.6	276.2	5.5	391.0	83.0	276.2	5.5
A2_112	748	1.69	1.06300	0.02500	0.11440	0.00240	0.6699	8.741259	0.183383	0.0678	0.0013	735.0	13.0	697.0	14.0	858.0	39.0	697.0	14.0
A2_113	1278	0.59	0.21350	0.00730	0.03086	0.00057	0.5410	32.40441	0.598526	0.0505	0.0015	196.4	6.2	195.9	3.6	201.0	65.0	195.9	3.6
A2_114	1159	4.37	0.63600	0.02100	0.07490	0.00180	0.8206	13.35113	0.320855	0.0614	0.0012	499.0	13.0	465.0	11.0	652.0	41.0	465.0	11.0
A2_115	201.5	1.99	1.78400	0.05800	0.17500	0.00410	0.5930	5.714286	0.133878	0.0739	0.002	1038.0	21.0	1038.0	22.0	1046.0	52.0	1046.0	52.0
A2_116	291.8	0.90	0.29200	0.01400	0.04210	0.00100	0.2909	23.75297	0.564204	0.0519	0.0025	258.0	11.0	266.0	6.4	270.0	100.0	266.0	6.4
A2_117	695	1.42	0.32080	0.00980	0.04233	0.00087	0.5215	23.62391	0.485537	0.0544	0.0015	282.2	7.6	267.2	5.4	372.0	62.0	267.2	5.4
A2_118	516	0.71	0.28400	0.01000	0.04170	0.00110	0.3862	23.98082	0.632588	0.0508	0.0018	253.1	8.1	263.0	6.9	213.0	77.0	263.0	6.9
A2_119	390	0.78	0.28000	0.01100	0.04063	0.00092	0.2876	24.61236	0.557307	0.0503	0.0021	250.0	8.8	256.7	5.7	211.0	86.0	256.7	5.7
A2_120	208.1	3.42	1.02000	0.03700	0.10880	0.00260	0.5461	9.191176	0.219642	0.0672	0.002	710.0	18.0	665.0	15.0	820.0	62.0	665.0	15.0
A2_121	1014	1.00	0.19790	0.00690	0.02809	0.00068	0.5926	35.59986	0.861798	0.0514	0.0014	183.8	5.7	178.5	4.3	264.0	59.0	178.5	4.3

TABLE A1
(continued)

Sample Name	U ppm	U Th	Isotopic Ratios $^{207}Pb/^{235}U$	2 SE	$^{206}Pb/^{238}U$	2SE	Corr. Coef.	$^{238}U/^{206}Pb$	2SE	$^{207}Pb/^{206}Pb$	2SE	Ages $^{207}Pb/^{235}U$ Ma	2 SE Ma	$^{206}Pb/^{238}U$	2SE Ma	$^{207}Pb/^{206}Pb$ Ma	2SE Ma	Best Age Ma	2SE Ma
Washington State University data																			
A-2_1	1,242	2.42	0.27594	0.00681	0.03882	0.00072	0.8997	25.7616	0.4805	0.0516	0.0006	247.4	5.4	245.5	4.5	266.4	25.8	245.5	4.5
A-2_2	214	3.01	0.41031	0.01270	0.05426	0.00114	0.8319	18.4302	0.3880	0.0549	0.0010	349.1	9.1	340.6	7.0	406.5	39.4	340.6	7.0
A-2_3	157	4.55	0.11787	0.00763	0.01544	0.00049	0.7043	64.7772	2.0358	0.0554	0.0027	113.1	6.9	98.8	3.1	427.9	103.8	98.8	3.1
A-2_4	639	0.19	0.54134	0.01395	0.06797	0.00130	0.8849	14.7114	0.2803	0.0578	0.0007	439.3	9.2	423.9	7.8	521.2	27.4	423.9	7.8
A-2_5	1,090	3.37	0.19697	0.00496	0.02875	0.00053	0.8865	34.7856	0.6448	0.0497	0.0006	182.6	4.2	182.7	3.3	181.2	28.3	182.7	3.3
A-2_6	275	1.03	0.39931	0.01415	0.05351	0.00131	0.8264	18.6870	0.4585	0.0541	0.0011	341.1	10.2	336.1	8.0	376.5	45.5	336.1	8.0
A-2_7	767	2.16	1.74176	0.04086	0.17065	0.00313	0.9220	5.8600	0.1075	0.0740	0.0007	1024.1	15.0	1015.7	17.2	1042.7	19.4	1042.7	19.4
A-2_8	52	2.33	0.36378	0.01887	0.04859	0.00131	0.7233	20.5821	0.5528	0.0543	0.0020	315.0	14.0	305.8	8.0	384.2	81.9	305.8	8.0
A-2_9	466	1.51	0.33007	0.00873	0.04577	0.00087	0.8723	21.8493	0.4171	0.0523	0.0007	289.6	6.6	288.5	5.4	299.3	30.6	288.5	5.4
A-2_10	385	1.25	0.33551	0.00926	0.04713	0.00091	0.8539	21.2198	0.4084	0.0516	0.0008	293.8	7.0	296.9	5.6	269.8	34.0	296.9	5.6
A-2_11	837	0.15	0.56652	0.01423	0.07139	0.00140	0.9100	14.0069	0.2739	0.0576	0.0006	455.8	9.2	444.5	8.4	513.2	23.8	444.5	8.4
A-2_12	974	0.31	0.42704	0.01062	0.05877	0.00115	0.9178	17.0156	0.3341	0.0527	0.0005	361.1	7.5	368.1	7.0	316.5	23.4	368.1	7.0
A-2_13	687	0.29	0.39503	0.00998	0.05361	0.00099	0.8844	18.6533	0.3455	0.0535	0.0007	338.0	7.2	336.6	6.1	348.1	27.8	336.6	6.1
A-2_14	1,030	0.36	0.45328	0.01133	0.06178	0.00120	0.9095	16.1869	0.3141	0.0532	0.0006	379.6	7.9	386.4	7.3	338.5	24.5	386.4	7.3
A-2_15	120	2.71	0.23034	0.01068	0.03233	0.00071	0.7174	30.9325	0.6810	0.0517	0.0018	210.5	8.8	205.1	4.4	271.6	76.6	205.1	4.4
A-2_16	230	1.22	0.44556	0.01260	0.05742	0.00114	0.8541	17.4143	0.3465	0.0563	0.0009	374.2	8.8	359.9	7.0	463.7	33.6	359.9	7.0
A-2_17	581	3.85	0.49861	0.01257	0.06382	0.00118	0.8844	15.6691	0.2892	0.0567	0.0007	410.8	8.5	398.8	7.1	479.0	27.1	398.8	7.1
A-2_18	609	0.44	0.70717	0.02051	0.08188	0.00185	0.8935	12.2127	0.2760	0.0627	0.0008	543.1	12.1	507.3	11.0	696.4	28.4	507.3	11.0
A-2_19	982	3.05	0.09855	0.00302	0.01433	0.00029	0.8220	69.7715	1.4050	0.0499	0.0009	95.4	2.8	91.7	1.8	189.3	41.7	91.7	1.8
A-2_20	354	1.62	0.16079	0.00578	0.02235	0.00044	0.7604	44.7520	0.8879	0.0522	0.0013	151.4	5.0	142.5	2.8	294.2	55.0	142.5	2.8
A-2_21	299	2.27	0.12942	0.00492	0.01838	0.00047	0.8094	54.3927	1.3859	0.0511	0.0012	123.6	4.4	117.4	3.0	243.8	52.0	117.4	3.0
A-2_22	1,138	0.67	1.91235	0.04233	0.18232	0.00309	0.9230	5.4850	0.0930	0.0761	0.0007	1085.4	14.7	1079.6	16.8	1097.5	18.3	1097.5	18.3
A-2_23	817	0.63	0.41660	0.01023	0.05609	0.00103	0.8966	17.8298	0.3276	0.0539	0.0006	353.6	7.3	351.8	6.3	366.2	25.7	351.8	6.3
A-2_24	993	1.78	0.18454	0.00488	0.02543	0.00050	0.8827	39.3308	0.7710	0.0527	0.0007	172.0	4.2	161.9	3.1	313.9	29.2	161.9	3.1
A-2_25	977	3.71	0.29313	0.00746	0.03828	0.00070	0.8780	26.1244	0.4809	0.0556	0.0007	261.0	5.8	242.2	4.4	434.5	28.3	242.2	4.4
A-2_26	444	3.01	0.56647	0.01423	0.07166	0.00132	0.8856	13.9553	0.2572	0.0573	0.0007	455.7	9.2	446.1	7.9	505.0	26.8	446.1	7.9
A-2_27	1,122	3.24	0.28478	0.00687	0.03953	0.00072	0.9008	25.2973	0.4580	0.0523	0.0006	254.4	5.4	249.9	4.4	296.9	25.1	249.9	4.4
A-2_28	215	4.31	0.42357	0.01253	0.05511	0.00106	0.8237	18.1443	0.3505	0.0558	0.0010	358.6	8.9	345.8	6.5	442.5	38.5	345.8	6.5
A-2_29	727	1.60	0.42463	0.01044	0.05690	0.00105	0.8995	17.5752	0.3258	0.0541	0.0006	359.4	7.4	356.7	6.4	376.9	25.3	356.7	6.4
A-2_30	851	1.77	0.48319	0.01152	0.05992	0.00103	0.8874	16.6902	0.2872	0.0585	0.0007	400.3	7.9	375.1	6.3	548.6	25.3	375.1	6.3
A-2_31	155	1.46	0.44525	0.01508	0.05778	0.00116	0.7827	17.3072	0.3482	0.0559	0.0012	374.0	10.5	362.1	7.1	448.5	48.2	362.1	7.1
A-2_32	765	0.53	0.48183	0.01276	0.06091	0.00130	0.9209	16.4189	0.3516	0.0574	0.0006	399.3	8.7	381.1	7.9	506.5	23.5	381.1	7.9
A-2_33	270	1.93	0.57403	0.01521	0.07293	0.00141	0.8763	13.7125	0.2653	0.0571	0.0008	460.6	9.8	453.8	8.5	495.5	29.1	453.8	8.5
A-2_34	1,473	2.15	0.29418	0.00714	0.04121	0.00074	0.8925	24.2674	0.4341	0.0518	0.0006	261.8	5.6	260.3	4.6	276.1	26.3	260.3	4.6
A-2_35	595	4.06	0.10507	0.00357	0.01538	0.00029	0.7700	65.0387	1.2456	0.0496	0.0011	101.4	3.3	98.4	1.9	175.1	52.4	98.4	1.9
A-2_36	447	1.23	0.07469	0.00313	0.01078	0.00025	0.7522	92.7993	2.1889	0.0503	0.0014	73.1	3.0	69.1	1.6	207.9	65.3	69.1	1.6
A-2_37	1,331	0.78	0.35349	0.00855	0.04851	0.00089	0.9065	20.6156	0.3801	0.0529	0.0006	307.3	6.4	305.3	5.5	323.1	24.3	305.3	5.5
A-2_38	410	0.98	0.29893	0.00869	0.04167	0.00080	0.8295	23.9982	0.4614	0.0520	0.0009	265.6	6.8	263.2	5.0	287.2	38.3	263.2	5.0
A-2_39	1,007	2.49	0.33650	0.00823	0.04675	0.00084	0.8917	21.3886	0.3857	0.0522	0.0006	294.5	6.2	294.6	5.2	294.7	26.5	294.6	5.2
A-2_40	482	2.37	0.45889	0.01334	0.05737	0.00133	0.9055	17.4293	0.4052	0.0580	0.0007	383.5	9.2	359.6	8.1	530.6	27.6	359.6	8.1
A-2_41	288	2.44	0.43278	0.01211	0.05787	0.00117	0.8652	17.2793	0.3492	0.0542	0.0008	365.1	8.5	362.7	7.1	381.4	32.5	362.7	7.1

TABLE A1
(continued)

Sample Name	U ppm	U Th	Isotopic Ratios $^{207}Pb/^{235}U$	2 SE	$^{206}Pb/^{238}U$	2SE	Corr. Coef.	$^{238}U/^{206}Pb$	2SE	$^{207}Pb/^{206}Pb$	2SE	Ages $^{207}Pb/^{235}U$ Ma	2 SE Ma	$^{206}Pb/^{238}U$	2SE Ma	$^{207}Pb/^{206}Pb$ Ma	2SE Ma	Best Age Ma	2SE Ma
Washington State University data																			
A-2_42	969	2.41	0.20104	0.00527	0.02886	0.00056	0.8798	34.6514	0.6670	0.0505	0.0007	186.0	4.4	183.4	3.5	219.7	29.9	183.4	3.5
A-2_43	188	3.41	0.41612	0.01261	0.05569	0.00118	0.8454	17.9577	0.3817	0.0542	0.0009	353.3	9.0	349.3	7.2	379.8	37.3	349.3	7.2
A-2_44	221	1.20	0.44946	0.01401	0.05505	0.00112	0.8187	18.1652	0.3710	0.0592	0.0011	376.9	9.8	345.5	6.9	575.5	40.0	345.5	6.9
A-2_45	726	0.58	0.39256	0.01078	0.05167	0.00107	0.8855	19.3537	0.4013	0.0551	0.0007	336.2	7.8	324.8	6.6	416.9	29.3	324.8	6.6
A-2_46	806	1.79	0.37056	0.00777	0.04962	0.00082	0.8630	20.1521	0.3346	0.0539	0.0006	320.1	5.7	312.2	5.1	367.8	23.9	312.2	5.1
A-2_47	554	2.35	0.31777	0.00696	0.04291	0.00065	0.7863	23.3038	0.3529	0.0535	0.0007	280.2	5.3	270.9	4.0	348.9	30.6	270.9	4.0
A-2_48	609	2.41	0.60572	0.01163	0.07632	0.00116	0.8705	13.1019	0.1995	0.0573	0.0005	480.9	7.3	474.1	7.0	503.3	20.9	474.1	7.0
A-2_49	500	1.08	0.64714	0.01368	0.07942	0.00127	0.8378	12.5905	0.2021	0.0588	0.0007	506.7	8.4	492.7	7.6	561.0	25.2	492.7	7.6
A-2_50	65	4.65	0.46880	0.02108	0.06189	0.00151	0.6532	16.1588	0.3944	0.0547	0.0019	390.4	14.5	387.1	9.2	400.0	75.3	387.1	9.2
A-2_51	427	3.14	0.20068	0.00532	0.02883	0.00052	0.7645	34.6915	0.6244	0.0503	0.0009	185.7	4.5	183.2	3.2	207.5	39.5	183.2	3.2
A-2_52	2,435	0.07	0.78575	0.01332	0.09688	0.00138	0.9195	10.3220	0.1474	0.0586	0.0004	588.8	7.5	596.1	8.1	551.0	14.7	596.1	8.1
A-2_53	330	2.97	0.37172	0.00825	0.05029	0.00071	0.7452	19.8859	0.2798	0.0534	0.0008	320.9	6.1	316.3	4.3	344.8	33.6	316.3	4.3
A-2_54	790	1.40	0.08610	0.00248	0.01234	0.00022	0.7151	81.0615	1.4339	0.0504	0.0010	83.9	2.3	79.0	1.4	213.4	46.5	79.0	1.4
A-2_55	1,642	2.16	0.69518	0.01183	0.08497	0.00117	0.8955	11.7689	0.1625	0.0591	0.0005	535.9	7.1	525.7	7.0	569.9	16.7	525.7	7.0
A-2_56	509	2.69	0.17183	0.00500	0.02354	0.00038	0.6797	42.4792	0.6918	0.0527	0.0011	161.0	4.3	150.0	2.4	316.1	48.4	150.0	2.4
A-2_57	847	2.13	0.32094	0.00666	0.04368	0.00065	0.8057	22.8924	0.3387	0.0531	0.0007	282.6	5.1	275.6	4.0	331.0	28.0	275.6	4.0
A-2_58	913	0.68	2.27318	0.04040	0.20234	0.00303	0.9141	4.9422	0.0740	0.0811	0.0006	1204.0	12.5	1187.9	16.2	1224.4	14.3	1224.4	14.3
A-2_59	2,052	0.26	0.31136	0.00551	0.04332	0.00062	0.8867	23.0825	0.3286	0.0519	0.0004	275.2	4.3	273.4	3.8	280.8	18.9	273.4	3.8
A-2_60	990	2.41	0.27884	0.00572	0.03962	0.00060	0.8291	25.2377	0.3851	0.0508	0.0006	249.7	4.5	250.5	3.7	232.5	26.5	250.5	3.7
A-2_61	1,415	3.93	0.20749	0.00387	0.02924	0.00044	0.8880	34.1996	0.5187	0.0512	0.0004	191.4	3.2	185.8	2.8	251.6	19.9	185.8	2.8
A-2_62	661	2.58	0.29107	0.00610	0.04042	0.00062	0.8188	24.7389	0.3801	0.0520	0.0006	259.4	4.8	255.4	3.8	285.2	27.6	255.4	3.8
A-2_63	593	1.91	0.36915	0.00769	0.04981	0.00077	0.8252	20.0764	0.3100	0.0535	0.0006	319.0	5.7	313.4	4.7	350.7	26.7	313.4	4.7
A-2_64	777	1.20	0.49708	0.00975	0.06637	0.00099	0.8440	15.0675	0.2246	0.0541	0.0006	409.7	6.6	414.2	6.0	374.4	23.8	414.2	6.0
A-2_65	915	1.60	0.33186	0.00620	0.04535	0.00061	0.8212	22.0530	0.2974	0.0528	0.0006	291.0	4.7	285.9	3.8	322.1	24.4	285.9	3.8
A-2_66	749	2.06	0.47208	0.00888	0.06116	0.00082	0.8168	16.3499	0.2203	0.0557	0.0006	392.6	6.1	382.7	5.0	441.8	24.3	382.7	5.0
A-2_67	312	2.19	0.09789	0.00365	0.01479	0.00029	0.6455	67.6084	1.3146	0.0478	0.0014	94.8	3.4	94.7	1.8	88.9	66.9	94.7	1.8
A-2_68	1,213	0.45	0.96015	0.01548	0.10891	0.00144	0.9090	9.1816	0.1216	0.0637	0.0004	683.4	8.0	666.4	8.4	730.2	14.5	666.4	8.4
A-2_69	899	1.56	0.32791	0.00657	0.04365	0.00062	0.8030	22.9096	0.3235	0.0542	0.0007	288.0	5.0	275.4	3.8	381.2	27.0	275.4	3.8
A-2_70	1,791	1.17	0.31882	0.00552	0.04390	0.00060	0.8780	22.7797	0.3115	0.0524	0.0004	281.0	4.2	277.0	3.7	304.7	19.1	277.0	3.7
A-2_71	1,643	1.67	0.46636	0.00792	0.06161	0.00084	0.8875	16.2305	0.2204	0.0547	0.0004	388.7	5.5	385.4	5.1	398.2	17.8	385.4	5.1
A-2_72	230	6.53	0.33870	0.01061	0.04054	0.00069	0.6667	24.6696	0.4212	0.0603	0.0014	296.2	8.0	256.2	4.3	615.6	50.3	256.2	4.3
A-2_73	621	1.61	0.45571	0.00919	0.06067	0.00090	0.8261	16.4818	0.2452	0.0542	0.0006	381.3	6.4	379.7	5.5	380.8	25.6	379.7	5.5
A-2_74	200	2.73	0.43336	0.01177	0.05728	0.00090	0.6974	17.4582	0.2758	0.0546	0.0011	365.6	8.3	359.1	5.5	397.1	43.6	359.1	5.5
A-2_75	306	1.32	1.89696	0.03368	0.17999	0.00257	0.8851	5.5559	0.0792	0.0761	0.0006	1080.0	11.7	1066.9	14.0	1097.8	16.7	1097.8	16.7
A-2_76	2,687	0.46	0.45657	0.00815	0.05850	0.00089	0.9234	17.0940	0.2607	0.0564	0.0004	381.9	5.7	366.5	5.4	466.4	15.3	366.5	5.4
A-2_77	1,450	0.24	0.42980	0.00763	0.05764	0.00080	0.8702	17.3502	0.2411	0.0538	0.0005	363.0	5.4	361.2	4.9	364.6	19.9	361.2	4.9
A-2_78	532	4.50	0.27913	0.00600	0.03864	0.00057	0.7865	25.8781	0.3840	0.0522	0.0007	250.0	4.8	244.4	3.6	292.4	30.4	244.4	3.6
A-2_79	394	1.19	0.07250	0.00330	0.01051	0.00025	0.6433	95.1484	2.2857	0.0498	0.0018	71.1	3.1	67.4	1.6	186.3	80.1	67.4	1.6
A-2_80	1,783	0.17	0.45780	0.00742	0.05972	0.00080	0.9124	16.7442	0.2244	0.0554	0.0004	382.7	5.2	373.9	4.9	426.4	15.0	373.9	4.9
A-2_81	154	3.96	0.22420	0.01076	0.03029	0.00073	0.6255	33.0145	0.7930	0.0534	0.0020	205.4	8.9	192.4	4.6	347.9	83.6	192.4	4.6
A-2_82	929	0.49	1.81001	0.03005	0.17773	0.00245	0.9120	5.6265	0.0775	0.0735	0.0005	1049.1	10.8	1054.6	13.4	1028.8	14.0	1028.8	14.0

TABLE A1
(continued)

Sample Name	U ppm	U Th	Isotopic Ratios $^{207}Pb/^{235}U$	2 SE	$^{206}Pb/^{238}U$	2SE	Corr. Coef.	$^{238}U/^{206}Pb$	2SE	$^{207}Pb/^{206}Pb$	2SE	Ages $^{207}Pb/^{235}U$ Ma	2 SE Ma	$^{206}Pb/^{238}U$	2SE Ma	$^{207}Pb/^{206}Pb$ Ma	2SE Ma	Best Age Ma	2SE Ma
Washington State University data																			
A-2_83	434	2.54	0.40683	0.00892	0.05464	0.00086	0.8040	18.3025	0.2877	0.0538	0.0007	346.6	6.4	342.9	5.2	361.2	29.5	342.9	5.2
A-2_84	638	3.82	0.08432	0.00272	0.01213	0.00019	0.6290	82.4161	1.2853	0.0502	0.0013	82.2	2.5	77.7	1.2	203.4	58.2	77.7	1.2
A-2_85	252	4.41	0.21609	0.00708	0.03106	0.00056	0.6654	32.1977	0.5767	0.0502	0.0012	198.6	5.9	197.2	3.5	206.0	56.5	197.2	3.5
A-2_86	277	0.89	0.49172	0.01270	0.06103	0.00100	0.7348	16.3862	0.2681	0.0582	0.0010	406.1	8.6	381.9	6.1	536.6	38.3	381.9	6.1
A-2_87	168	1.92	0.38777	0.01262	0.05065	0.00087	0.6556	19.7422	0.3404	0.0553	0.0014	332.7	9.2	318.5	5.4	423.5	54.6	318.5	5.4
A-2_88	260	2.22	0.43373	0.01120	0.05709	0.00087	0.7049	17.5173	0.2663	0.0549	0.0010	365.8	7.9	357.9	5.3	406.6	41.0	357.9	5.3
A-2_89	811	3.53	0.29433	0.00625	0.04089	0.00061	0.7999	24.4531	0.3675	0.0520	0.0007	262.0	4.9	258.4	3.8	284.1	29.2	258.4	3.8
A-2_90	84	1.82	0.44772	0.01867	0.05679	0.00109	0.6058	17.6082	0.3367	0.0569	0.0019	375.7	13.0	356.1	6.6	488.6	72.8	356.1	6.6
A-2_91	2,009	1.29	0.47264	0.00823	0.06294	0.00086	0.8771	15.8890	0.2183	0.0542	0.0005	393.0	5.7	393.5	5.2	380.5	19.0	393.5	5.2
A-2_92	2,864	0.21	0.41155	0.00794	0.05306	0.00084	0.8916	18.8479	0.2986	0.0560	0.0005	350.0	5.7	333.3	5.1	452.8	19.5	333.3	5.1
A-2_93	409	1.54	0.58049	0.01205	0.07376	0.00113	0.8224	13.5566	0.2072	0.0568	0.0007	464.8	7.7	458.8	6.8	484.7	26.2	458.8	6.8
A-2_94	1,073	1.14	0.89618	0.01516	0.10567	0.00146	0.8992	9.4632	0.1305	0.0612	0.0005	649.7	8.1	647.6	8.5	647.6	16.1	647.6	8.5
A-2_95	188	4.21	0.20744	0.00813	0.02869	0.00054	0.6214	34.8607	0.6608	0.0522	0.0016	191.4	6.8	182.3	3.4	294.9	69.7	182.3	3.4
A-2_96	850	0.06	0.45213	0.00902	0.06004	0.00091	0.8437	16.6553	0.2530	0.0544	0.0006	378.8	6.3	375.9	5.5	386.6	24.2	375.9	5.5
A-2_97	30	1.63	0.35860	0.02448	0.04672	0.00139	0.5846	21.4039	0.6384	0.0554	0.0031	311.2	18.1	294.4	8.6	429.3	120.8	294.4	8.6
A-2_98	286	1.82	0.41813	0.01063	0.05699	0.00097	0.7629	17.5472	0.3000	0.0530	0.0009	354.7	7.6	357.3	5.9	327.9	37.2	357.3	5.9
A-2_99	1,141	2.24	0.52143	0.00990	0.06745	0.00104	0.8855	14.8261	0.2286	0.0558	0.0005	426.1	6.6	420.8	6.3	445.3	19.7	420.8	6.3
A-2_100	155	2.40	0.36121	0.01131	0.04985	0.00103	0.7458	20.0621	0.4161	0.0523	0.0011	313.1	8.4	313.6	6.3	299.7	47.2	313.6	6.3
A-2_101	555	1.39	0.83086	0.01590	0.09893	0.00141	0.8358	10.1085	0.1442	0.0606	0.0006	614.1	8.8	608.1	8.3	626.7	22.8	608.1	8.3
A-2_102	572	0.49	0.98527	0.01782	0.11350	0.00162	0.8716	8.8103	0.1254	0.0627	0.0006	696.3	9.1	693.1	9.3	697.4	19.1	693.1	9.3
A-2_103	126	3.08	0.35884	0.01169	0.05080	0.00109	0.7416	19.6868	0.4224	0.0510	0.0011	311.4	8.7	319.4	6.7	241.3	50.0	319.4	6.7
A-2_104	554	1.20	0.40242	0.00854	0.05273	0.00082	0.8166	18.9630	0.2940	0.0551	0.0007	343.4	6.2	331.3	5.0	416.4	27.4	331.3	5.0
A-2_105	593	1.80	0.35914	0.00716	0.04822	0.00067	0.8006	20.7365	0.2899	0.0538	0.0007	311.6	5.3	303.6	4.1	361.6	27.1	303.6	4.1
A-2_106	1,464	3.22	0.29272	0.00496	0.04016	0.00054	0.8784	24.8991	0.3324	0.0526	0.0004	260.7	3.9	253.8	3.3	312.8	18.7	253.8	3.3
A-2_107	2,766	3.35	0.07651	0.00160	0.01112	0.00015	0.7722	89.9015	1.2497	0.0497	0.0007	74.9	1.5	71.3	1.0	179.4	31.1	71.3	1.0
A-2_108	373	3.19	0.43554	0.00945	0.05756	0.00092	0.8201	17.3741	0.2781	0.0546	0.0007	367.1	6.7	360.8	5.6	397.5	27.9	360.8	5.6
A-2_109	1,492	3.32	0.19735	0.00399	0.02830	0.00045	0.8673	35.3305	0.5671	0.0503	0.0005	182.9	3.4	179.9	2.8	211.0	23.4	179.9	2.8
A-2_110	228	2.07	0.10870	0.00493	0.01468	0.00032	0.6126	68.1316	1.4693	0.0535	0.0019	104.8	4.5	93.9	2.0	349.1	80.2	93.9	2.0
A-2_111	531	3.44	0.18093	0.00467	0.02675	0.00045	0.7433	37.3887	0.6232	0.0488	0.0009	168.9	4.0	170.2	2.8	140.5	40.4	170.2	2.8
A-2_112	82	5.55	0.45690	0.01760	0.05988	0.00122	0.6489	16.6999	0.3406	0.0551	0.0016	382.1	12.2	374.9	7.4	416.1	65.0	374.9	7.4
A-2_113	1,175	1.77	0.41478	0.00796	0.05655	0.00087	0.8734	17.6823	0.2706	0.0530	0.0005	352.3	5.7	354.6	5.3	327.0	21.3	354.6	5.3
A-2_114	748	1.43	0.19268	0.00481	0.02827	0.00051	0.7980	35.3693	0.6352	0.0492	0.0007	178.9	4.1	179.7	3.2	157.8	35.1	179.7	3.2
A-2_115	930	0.31	0.38437	0.00743	0.05208	0.00074	0.8281	19.2018	0.2732	0.0533	0.0006	330.2	5.4	327.3	4.5	341.3	24.7	327.3	4.5
A-2_116	1,434	1.03	0.06888	0.00184	0.01040	0.00017	0.7296	96.1403	1.6156	0.0478	0.0009	67.6	1.7	66.7	1.1	90.1	43.2	66.7	1.1
A-2_117	62	1.53	0.53213	0.02220	0.06499	0.00147	0.6536	15.3861	0.3471	0.0591	0.0019	433.2	14.6	405.9	8.9	571.5	68.0	405.9	8.9
A-2_118	1,519	2.15	0.13247	0.00288	0.01811	0.00026	0.7695	55.2238	0.7992	0.0528	0.0007	126.3	2.6	115.7	1.7	321.2	31.6	115.7	1.7
A-2_119	516	0.98	0.73071	0.01310	0.08650	0.00112	0.8282	11.5610	0.1504	0.0610	0.0006	557.0	7.7	534.8	6.7	639.2	21.8	534.8	6.7
A-2_120	107	2.86	0.41491	0.01342	0.05529	0.00098	0.6670	18.0881	0.3205	0.0542	0.0013	352.4	9.6	346.9	6.0	379.0	54.0	346.9	6.0
A-2_121	2,000	1.29	0.77224	0.01314	0.09381	0.00131	0.9027	10.6598	0.1489	0.0594	0.0004	581.0	7.5	578.0	7.7	583.3	16.1	578.0	7.7
A-2_122	301	2.56	0.34018	0.00827	0.04705	0.00080	0.7832	21.2551	0.3605	0.0522	0.0008	297.3	6.2	296.4	4.9	294.6	34.5	296.4	4.9
A-2_123	1,082	0.78	0.29020	0.00634	0.03953	0.00066	0.8433	25.2958	0.4253	0.0530	0.0006	258.7	5.0	249.9	4.1	329.0	26.7	249.9	4.1

TABLE A1
(continued)

Sample Name	U ppm	U Th	Isotopic Ratios $^{207}Pb/^{235}U$	2 SE	$^{206}Pb/^{238}U$	2SE	Corr. Coef.	$^{238}U/^{206}Pb$	2SE	$^{207}Pb/^{206}Pb$	2SE	Ages $^{207}Pb/^{235}U$ Ma	2 SE Ma	$^{206}Pb/^{238}U$	2SE Ma	$^{207}Pb/^{206}Pb$ Ma	2SE Ma	Best Age Ma	2SE Ma
Washington State University data																			
A-2_124	919	1.60	0.10064	0.00256	0.01498	0.00024	0.7373	66.7493	1.0808	0.0485	0.0008	97.4	2.4	95.9	1.5	124.0	40.4	95.9	1.5
A-2_125	449	3.82	0.20223	0.00529	0.02808	0.00044	0.7123	35.6109	0.5602	0.0520	0.0010	187.0	4.5	178.5	2.8	285.4	42.0	178.5	2.8
A-2_126	86	3.23	0.58914	0.01702	0.07385	0.00132	0.7189	13.5409	0.2422	0.0576	0.0012	470.3	10.8	459.3	7.9	514.7	43.9	459.3	7.9
A-2_127	636	3.84	0.20739	0.00493	0.03010	0.00048	0.7670	33.2268	0.5312	0.0498	0.0008	191.4	4.1	191.2	3.0	183.7	35.5	191.2	3.0
A-2_128	1,156	1.83	0.58743	0.00996	0.07333	0.00100	0.8894	13.6363	0.1856	0.0578	0.0005	469.2	6.4	456.2	6.0	523.8	17.2	456.2	6.0
A-2_129	1,471	0.12	0.79894	0.01737	0.09306	0.00165	0.8768	10.7454	0.1901	0.0620	0.0007	596.2	9.8	573.6	9.7	673.8	22.4	573.6	9.7
A-2_130	1,255	1.20	0.07137	0.00201	0.01042	0.00017	0.6967	95.9358	1.5813	0.0494	0.0010	70.0	1.9	66.8	1.1	168.8	47.2	66.8	1.1
A-2_131	1,941	1.39	0.31941	0.00562	0.04335	0.00060	0.8688	23.0678	0.3167	0.0532	0.0005	281.4	4.3	273.6	3.7	337.5	19.9	273.6	3.7
A-2_132	337	2.24	0.10817	0.00463	0.01558	0.00029	0.5956	64.1876	1.2087	0.0501	0.0018	104.3	4.2	99.7	1.9	201.3	79.3	99.7	1.9
A-2_133	400	1.31	0.36201	0.00829	0.04779	0.00068	0.7371	20.9258	0.2996	0.0547	0.0009	313.7	6.2	300.9	4.2	400.0	34.8	300.9	4.2
A-2_134	147	0.67	0.43780	0.01218	0.05813	0.00101	0.7240	17.2038	0.2988	0.0544	0.0011	368.7	8.6	364.2	6.1	387.0	43.0	364.2	6.1
A-2_135	1,779	0.33	0.45135	0.00791	0.06107	0.00087	0.8910	16.3756	0.2322	0.0534	0.0004	378.2	5.5	382.1	5.3	344.5	18.2	382.1	5.3
A-2_136	992	0.80	0.31915	0.00570	0.04378	0.00061	0.8724	22.8403	0.3207	0.0526	0.0005	281.2	4.4	276.2	3.8	313.1	20.0	276.2	3.8
A-2_137	936	1.20	0.32996	0.00615	0.04542	0.00059	0.8005	22.0176	0.2837	0.0525	0.0006	289.5	4.7	286.3	3.6	305.5	25.7	286.3	3.6
A-2_138	1,210	0.32	0.67890	0.01164	0.08433	0.00114	0.8802	11.8582	0.1609	0.0581	0.0005	526.1	7.0	521.9	6.8	534.7	18.0	521.9	6.8
A-2_139	475	1.80	0.34789	0.00756	0.04738	0.00066	0.7536	21.1067	0.2951	0.0530	0.0008	303.1	5.7	298.4	4.1	329.7	32.5	298.4	4.1
A-2_140	2,599	3.58	0.19172	0.00348	0.02763	0.00037	0.8413	36.1905	0.4907	0.0501	0.0005	178.1	3.0	175.7	2.3	199.7	23.0	175.7	2.3
A-2_141	1,641	0.45	0.49059	0.00862	0.06396	0.00092	0.8972	15.6352	0.2247	0.0554	0.0004	405.3	5.9	399.7	5.6	427.9	17.5	399.7	5.6
A-2_142	408	4.91	0.27700	0.00667	0.03892	0.00057	0.7257	25.6929	0.3794	0.0514	0.0009	248.3	5.3	246.1	3.6	258.4	38.1	246.1	3.6
A-2_143	612	1.36	0.07070	0.00233	0.01040	0.00021	0.7020	96.1241	1.9101	0.0491	0.0012	69.4	2.2	66.7	1.3	151.4	54.6	66.7	1.3
A-2_144	138	2.70	0.38881	0.01188	0.04775	0.00088	0.7034	20.9425	0.3841	0.0588	0.0013	333.5	8.7	300.7	5.4	559.5	47.1	300.7	5.4
A-2_145	1,683	1.87	1.81786	0.02802	0.17554	0.00222	0.9150	5.6966	0.0722	0.0748	0.0005	1051.9	10.0	1042.6	12.2	1062.5	12.8	1062.5	12.8
A-2_146	845	2.93	2.14997	0.03350	0.19012	0.00243	0.9128	5.2598	0.0673	0.0817	0.0005	1165.0	10.7	1122.0	13.2	1237.3	12.7	1237.3	12.7
A-2_147	503	4.17	0.27941	0.00673	0.03892	0.00059	0.7376	25.6950	0.3908	0.0518	0.0009	250.2	5.3	246.1	3.7	278.4	37.3	246.1	3.7
A-2_148	1,408	1.55	0.35379	0.00586	0.04742	0.00060	0.8599	21.0879	0.2647	0.0539	0.0005	307.6	4.4	298.7	3.7	365.7	19.3	298.7	3.7
A-2_149	797	2.82	0.28046	0.00540	0.03886	0.00054	0.8160	25.7312	0.3561	0.0521	0.0006	251.0	4.3	245.8	3.3	290.2	25.6	245.8	3.3
A-2_150	734	2.17	0.30872	0.00603	0.04313	0.00061	0.8219	23.1871	0.3302	0.0517	0.0006	273.2	4.7	272.2	3.8	271.7	25.6	272.2	3.8
A-2_151	127	2.30	0.39080	0.01152	0.05167	0.00096	0.7237	19.3531	0.3579	0.0546	0.0011	335.0	8.4	324.8	5.9	396.3	45.4	324.8	5.9
A-2_152	364	7.88	0.30233	0.00735	0.04091	0.00057	0.6990	24.4422	0.3403	0.0534	0.0009	268.2	5.7	258.5	3.5	344.1	39.4	258.5	3.5
A-2_153	1,585	2.61	0.27798	0.00493	0.03924	0.00051	0.8397	25.4825	0.3342	0.0511	0.0005	249.1	3.9	248.1	3.2	247.5	22.4	248.1	3.2
A-2_154	190	5.67	0.29984	0.01119	0.04022	0.00069	0.6097	24.8629	0.4255	0.0538	0.0016	266.3	8.7	254.2	4.3	363.9	66.5	254.2	4.3
A-2_155	737	1.08	0.57748	0.01047	0.07390	0.00100	0.8442	13.5325	0.1839	0.0564	0.0006	462.8	6.7	459.6	6.0	469.3	21.7	459.6	6.0

U concentration uncertainty is ~20%.
Data not corrected for common-Pb.
Individual errors are given as 2 sigma standard deviation and only reflect the internal error, Systematic errors are $^{206}Pb/^{238}U = 1.2\%$, $^{207}Pb/^{206}Pb = 1.0\%$ (2s).
Data from WSU was analyzed with 30 microns spot beam and UCSC with 20 microns spot beam.

REFERENCES

Aguirre Urreta, B., Tunik, M., Naipauer, M., Pazos, P., Ottone, G., Fanning, M., and Ramos, V. A., 2011, Malargüe Group (Maastrichtian-Danian) deposits in the Neuquén Andes, Argentina: Implications for the onset of the first Atlantic transgression related to Western Gondwana break-up: Gondwana Research, v. 19, n. 2, p. 482–494, https://doi.org/10.1016/j.gr.2010.06.008

Allmendinger, R. W., 1986, Tectonic development, southeastern border of the Puna Plateau, northwestern Argentine Andes: Geological Society of America Bulletin, v. 97, n. 9, p. 1070–1082, https://doi.org/10.1130/0016-7606(1986)97<1070:TDSBOT>2.0.CO;2

Allmendinger, R. W., Strecker, M., Eremchuk, J. E., and Francis, P., 1989, Neotectonic deformation of the southern Puna Plateau, northwestern Argentina: Journal of South American Earth Sciences, v. 2, n. 2, p. 111–130, https://doi.org/10.1016/0895-9811(89)90040-0

Álvarez Cerimedo, J. M. , Orts, D. L., Rojas Vera, E. A., Folguera, A., Bottesi, G., and Ramos, V. A., 2013, Mechanisms and deformational stages at the easter Andean front (36°S, Argentina) [Mecanismos y fases de construcción orogénicos del frente oriental andino (36°S, Argentina]: Andean Geology, v. 40, n. 3, p. 504–520, https://doi.org/10.5027/andgeoV40n3-a06

Applegate, J. D. R., Walker, J. D., and Hodges, K. V., 1992, Late Cretaceous extensional unroofing in the Funeral Mountains metamorphic core complex, California: Geology, v. 20, n. 6, p. 519–522, https://doi.org/10.1130/0091-7613(1992)020<0519:LCEUIT>2.3.CO;2

Aragón, E., D'Eramo, F., Castro, A., Pinotti, L., Brunelli, D., Rabbia, O., Rivalenti, G., Varela, R., Spakman, W., Demartis, M., Cavarozzi, C. E., Aguilera, Y. E., Mazzucchelli, M., and Ribot, A., 2011, Tectonomagmatic response to major convergence changes in the North Patagonian suprasubduction system; the Paleogene subduction-transcurrent plate margin transition: Tectonophysics, v. 509, n. 3–4, p. 218–237, https://doi.org/10.1016/j.tecto.2011.06.012

Arévalo, C, Rivera, O., Iriarte, S., and Mpodozis, C., 1994, Cuencas extensionales y campos de calderas del Cretácico superior-Terciario inferior en la precordillera de Copiapo (27°-28°S), Chile: Concepción, Chile, Actas VII° Congreso Geológico Chileno, v. 2, n. 7, p. 1288–1292.

Balgord, E. A., 2017, Triassic to Neogene evolution of the south-central Andean arc determined by betrital zircon U-Pb and Hf analysis of Neuquén Basin strata, central Argentina (34°S-40°S): Lithosphere, v. 9, n. 3, p. 453–462, https://doi.org/10.1130/L546.1

Balgord, E. A., and Carrapa, B., 2016, Basin evolution of Upper Cretaceous–Lower Cenozoic strata in the Malargüe fold-and-thrust belt: northern Neuquén Basin, Argentina: Basin Research, v. 28, n. 2, p. 183–206, https://doi.org/10.1111/bre.12106

Barrio, C. A., 1990, Paleogeographic control of the Upper Cretaceous tidal deposits, Neuquén Basin, Argentina: Journal of South American Earth Sciences, v. 3, n. 1, p. 31–49, https://doi.org/10.1016/0895-9811(90)90016-T

Bascuñán, S., Arriagada, C., Le Roux, J., and Deckart, K., 2015, Unraveling the Peruvian phase of the Central Andes: Stratigraphy, sedimentology and geochronology of the Salar de Atacama basin (22°30'-23°S), northern Chile: Basin Research, v. 28, n. 3, p. 365–392, https://doi.org/10.1111/bre.12114

Bechis, F., Cristallini, E. O., Giambiagi, L. B., Yagupsky, D. L., Guzmán, C. G., and García, V. H., 2014, Transtensional tectonics induced by oblique reactivations of previous lithospheric anisotropies during the Late Triassic to Early Jurassic rifting in the Neuquén basin: Insights from analog models: Journal of Geodynamics, v. 79, p. 1–17, https://doi.org/10.1016/j.jog.2014.04.010

Boll, A., Alonso, J., Fuentes, F., Vergara, M., Laffitte, G., and Villar, H. J., 2014, Factores controlantes de las acumulaciones de hidrocarburos en el sector norte de la cuenca neuquina, entre los ríos Diamante y Salado, provincia de Mendoza, Argentina: Actas IX Congreso de Exploración y Desarrollo de Hidrocarburos: Trabajos Técnicos, v. 1, p. 3–44.

Bradley, D. C., Kusky, T. M., Haeussler, P. J., Goldfarb, R. J., Miller, M. L., Dumoulin, J. A., Nelson, S. W., and Karl, S. M., 2003, Geologic signature of early Tertiary ridge subduction in Alaska, *in* Sisson, V. B., Roeske, S. M.. and Pavlis, T. L., editors, Geology of a transpressional orogen developed during ridge-trench interactions along the North pacific margin: Geological Society of America Special Paper 371, p. 19–49, https://doi.org/10.1130/0-8137-2371-X.19

Branellec, M., Nivière, B., Callot, J. P., and Ringenbach, J. C., 2016, Mechanisms of basin contraction and reactivation in the basement-involved Malargüe fold-and-thrust belt, Central Andes (34–36° S): Geological Magazine, v. 153, n. 5–6, p. 926–944, https://doi.org/10.1017/S0016756816000315

Breitsprecher, K., and Thorkelson, D. J., 2009, Neogene kinematic history of Nazca-Antarctic-Phoenix slab windows beneath Patagonia and the Antarctic Peninsula: Tectonophysics, v. 464, n. 1–4, p. 10–20, https://doi.org/10.1016/j.tecto.2008.02.013

Buatois, L. A., and Encinas, A., 2011, Ichnology, sequence stratigraphy and depositional evolution of an Upper Cretaceous rocky shoreline in central Chile: Bioerosion structures in a transgressed metamorphic basement: Cretaceous Research, v. 32, n. 2, p. 203–212, https://doi.org/10.1016/j.cretres.2010.12.003

Burns, W. M., Jordan, T. E., Copeland, P., and Kelley, S. A., 2006, The case for extensional tectonics in the Oligocene-Miocene Southern Andes as recorded in the Cura Mallín basin (36–38 S), *in* Kay, S. M., and Ramos, V. A., editors, Evolution of an Andean Margin: a tectonic and magmatic view from the Andes to the Neuquén Basin (35-39°S): Special Papers of the Geological Society of America Special, v. 407, p. 163–184, https://doi.org/10.1130/2006.2407(08)

Cande, S. C., and Leslie, R. B., 1986, Late Cenozoic tectonics of the Southern Chile trench: Journal of Geophysical Research-Solid Earth, v. 91, n. B1, p. 471–496, https://doi.org/10.1029/JB091iB01p00471

Capitanio, F. A., Faccenna, C., Zlotnik, S., and Stegman, D. R., 2011, Subduction dynamics and the origin of Andean orogeny and the Bolivian orocline: Nature, v. 480, p. 83–86, https://doi.org/10.1038/nature10596

Carbone, O., Franzese, J., Limeres, M., Delpino, D., and Martínez, R. 2011, El Ciclo Precuyano (Triásico Tardío-Jurásico Temprano) en la Cuenca Neuquina, *in* Leanza, H. A., Arregui, O., Carbone, O., Danieli, J. C., and Vallés, J. M., editors, Geología y recursos naturales de la Provincia del Neuquén: Relatorio del VXIII Congreso Geológico Argentino, p. 63–76.

Chang, Z., Vervoort, J. D., McClelland, W. C., and Knaack, C., 2006, U-Pb dating of zircon by LA-ICP-MS: Geochemistry, Geophysics, Geosystems, v. 7, n. 5, Q05009, https://doi.org/10.1029/2005GC001100

Charrier, R., Wyss, A. R., Flynn, J. J., Swisher III, C. C., Norell, M. A., Zapatta, F., McKenna, M. C., and Novacek, M. J., 1996, New evidence for Late Mesozoic-Early Cenozoic evolution of the Chilean Andes in the Upper Tinguiririca Valley (35° S), Central Chile: Journal of South American Earth Sciences, v. 9, n. 5–6, p. 393–422, https://doi.org/10.1016/S0895-9811(96)00035-1

Charrier, R., Baeza, O., Elgueta, S., Flynn, J. J., Gans, P., Kay, S. M., Muñoz, N., Wyss, A. R., and Zurita, E., 2002, Evidence for Cenozoic extensional basin development and tectonic inversion south of the flat-slab segment, southern Central Andes, Chile (33–36 SL): Journal of South American Earth Sciences, v. 15, n. 1, p. 117–139, https://doi.org/10.1016/S0895-9811(02)00009-3

Charrier, R., Pinto, L., and Rodriguez, M. P., 2007, Tectonostratigraphic evolution of the Andean Orogen in Chile, *in,* Moreno, T., and Gibbons, W., editors, The Geology of Chile: Geological Society, London, p. 21–114, https://doi.org/10.1144/GOCH.3

Charrier, R., Ramos, V. A., Tapia, F., and Sagripanti, L., 2015, Tectono-stratigraphic evolution of the Andean Orogen between 31 and 37°S (Chile and Western Argentina), *in* Sepúlveda, S. A., Giambiagi, L. B., Moreiras, S. M., Pinto, L., Tunik, M., Hoke, G. D., and Farías, M., editors, Geodynamic Processes in the Andes of Central Chile and Argentina: Geological Society, London, Special Publications, v. 399, p. 13–61, https://doi.org/10.1144/SP399.20

Chase, C. G., Sussman, A. J., and Coblentz, D. D., 2009, Curved Andes: Geoid, forebulge, and flexure: Lithosphere, v. 1, n. 6, p. 358–363, https://doi.org/10.1130/L67.1

Cingolani, C. A., and Ramos, V. A., 2017, Pre-Carboniferous tectonic evolution of the San Rafael Block, Mendoza Province, *in* Cingolani, C. A., editor, Pre-Carboniferous evolution of the San Rafael Block, Argentina: Cham, Switzerland, Springer Earth System Sciences, p. 239–255, https://doi.org/10.1007/978-3-319-50153-6_13

Cladouhos, T. T., Allmendinger, R. W., Coira, B., and Farrar, E., 1994, Late Cenozoic deformation in the Central Andes: Fault kinematics from the northern Puna, northwestern Argentina and southwestern Bolivia: Journal of South American Earth Sciences, v. 7, n. 2, p. 209–228, https://doi.org/10.1016/0895-9811(94)90008-6

Cobbold, P. R., and Rosello, E. A., 2003, Aptian to recent compressional deformation, foothills of the Neuquén Basin, Argentina: Marine and Petroleum Geology, v. 20, n. 5, p. 429–443, https://doi.org/10.1016/S0264-8172(03)00077-1

Comínguez, A. H., and Ramos, V. A., 1995, Geometry and seismic expression of the Cretaceous Salta Rift of northwestern Argentina, *in* Tankard, A. J., Suárez, R., and Welsink, H. J., editors, Petroleum Basins of South America: American Association of Petroleum Geologists, Memoir 62, p. 325–340, https://doi.org/10.1306/M62593C15

Coney, P. J., and Harms, T. A., 1984, Cordilleran metamorphic core complexes: Cenozoic extensional relics of Mesozoic compression: Geology, v. 12, n. 9, p. 550–554, https://doi.org/10.1130/0091-7613(1984)12<550:CMCCCE>2.0.CO;2

Corfu, F., Hanchar, J. M., Hoskin, P. W. O., and Kinny, P., 2003, Atlas of zircon textures: Reviews in Mineralogy and Geochemistry, v. 53, n. 1, p. 469–500, https://doi.org/10.2113/0530469

Dalmayrac, B., and Molnar, P., 1981, Parallel thrust and normal faulting in Peru and constraints on the state of stress: Earth and Planetary Science Letters, v. 55, n. 3, p. 473–481, https://doi.org/10.1016/0012-821X(81)90174-6

DeCelles, P., 2004, Late Jurassic to Eocene evolution of the Cordilleran thrust belt and foreland basin system, western U.S.A.: American Journal of Science, v. 304, n. 2, p. 105–168, https://doi.org/10.2475/ajs.304.2.105

DeCelles, P. G., and Giles, K. A., 1996, Foreland basin systems: Basin Research, v. 8, n. 2, p. 105–123, https://doi.org/10.1046/j.1365-2117.1996.01491.x

DeCelles, P., Ducea, M. N., Kapp, P., and Zandt, G., 2009, Cyclicity in Cordilleran orogenic systems: Nature Geoscience, v. 2, p. 251–257, https://doi.org/10.1038/ngeo469

Dewey, J. F., 1988, Extensional collapse of orogens: Tectonics, v. 7, n. 6, p. 1123–1139, https://doi.org/10.1029/TC007i006p01123

Di Giulio, A., Ronchi, A., Sanfilippo, A., Tiepolo, M., Pimentel, M., and Ramos, V. A., 2012, Detrital zircon provenance from the Neuquén Basin (south-central Andes): Cretaceous geodynamic evolution and sedimentary response in a retroarc-foreland Basin: Geology, v. 40, n. 6, p. 559–562, https://doi.org/10.1130/G33052.1

Dicarlo, D. J., and Cristallini, E., 2007, Estructura de la margen Norte del Río Grande, Bardas Blancas, Provincia de Mendoza: Revista de la Asociación Geológica Argentina, v. 62, n. 2, p. 187–199.

Dimieri, L. V., 1997, Tectonic wedge geometry at Bardas Blancas, southern Andes (36°S), Argentina: Journal of Structural Geology, v. 19, n. 11, p. 1419–1422, https://doi.org/10.1016/S0191-8141(97)00055-2

Dumitru, T. A., Ernst, W. G., Hourigan, J. K., and McLaughlin, R. J., 2015, Detrital zircon U-Pb reconnaissance of the Franciscan subduction complex in northwestern California: International Geology Review, v. 57, n. 5–8, p. 767–800, https://doi.org/10.1080/00206814.2015.1008060

Dyhr, C. T., Holm, P. M., and Llambías, E. J., 2013a, Geochemical constraints on the relationship between the Miocene–Pliocene volcanism and tectonics in the Palaoco and Fortunoso volcanic fields, Mendoza Region, Argentina: New insights from $^{40}Ar/^{39}Ar$ dating, Sr–Nd–Pb isotopes and trace elements: Journal of Volcanology and Geothermal Research, v. 266, p. 50–68, https://doi.org/10.1016/j.jvolgeores.2013.08.005

Dyhr, C. T., Holm, P. M., Llambías, E. J., and Scherstén, A., 2013b, Subduction controls on Miocene back-arc lavas from Sierra de Huantraico and La Matancilla and new $^{40}Ar/^{39}Ar$ dating from the Mendoza Region, Argentina: Lithos, v. 179, p. 67–83, https://doi.org/10.1016/j.lithos.2013.08.007

Echaurren, A., Folguera, A., Gianni, G., Orts, D., Tassara, A., Encinas, A., Giménez, M., and Valencia, V., 2016, Tectonic evolution of the North Patagonian Andes (41°–44°S) through recognition of syntectonic strata: Tectonophysics, v. 677–678, p. 99–114, https://doi.org/10.1016/j.tecto.2016.04.009

Egan, S., Buddin, T., Kane, S. J., and Williams, G. D., 1997, Three-dimensional modeling and visualization in structural geology: New techniques for the restoration and balancing of volumes, British Geologyical Survey, Proceedings of the 1996 Geoscience Information Group Conference on Geological Visualisation: Electronic Geology, v. 1, p. 67–82.

Encinas, A., Stinnesbeck, W., and Valencia, V. A., 2014, First radiometric age (U-Pb, LA-ICP-MS, on detrital zircons) from the Punta Topocalma Formation: Insights on Late Cretaceous marine deposition in central Chile: Andean Geology, v. 41, n. 2, p. 436–445, https://doi.org/10.5027/andgeoV41n2-a08

Encinas, A., Folguera, A., Oliveros, V., Del Mauro, L. D. G., Tapia, F., Riffo, R., Hervé, F., Finger, K. L., Valencia, V. A., Gianni, G., and Álvarez, O., 2016, Late Oligocene–early Miocene submarine volcanism and deep-marine sedimentation in an extensional basin of southern Chile: Implications for the tectonic development of the North Patagonian Andes: Geological Society of America Bulletin, v. 128, n. 5–6, p. 807–823, https://doi.org/10.1130/B31303.1

Espinoza, F., Morata, D., Pelleter, E., Maury, R.C., Suárez, M., Lagabrielle, Y., Polvé, M., Bellon, H., Cotton, J., De la Cruz, R., and Guivel, C., 2005, Petrogenesis of the Eocene and Mio-Pliocene alkaline basaltic magmatism in Meseta Chile Chico, southern Patagonia, Chile: Evidence for the participation of two slab windows: Lithos, v. 82, n. 3–4, p. 315–343, https://doi.org/10.1016/j.lithos.2004.09.024

Espurt, N., Funiciello, F., Martinod, J., Guillaume, B., Regard, V., Faccenna, C., and Brusset, S., 2008, Flat subduction dynamics and deformation in the South American plate: Insights from analog modeling: Tectonics, v. 27, n. 3, TC3011, https://doi.org/10.1029/2007TC002175

Fennell, L. M., Folguera, A., Naipauer, M., Gianni, G., Rojas Vera, E. A., Bottesi, G., and Ramos, V. A., 2017, Cretaceous deformation of the southern Central Andes: Synorogenic growth strata in the Neuquén Group (35°30'–37°S): Basin Research, v. 29, n. S1, p. 51–72, https://doi.org/10.1111/bre.12135

Fennell, L. M., Quinteros, J., Iannelli, S. B., Litvak, V. D., and Folguera, A., 2018, The role of the slab pull force in the late Oligocene to early Miocene extension in the Southern Central Andes (27°–46°S): Insights from numerical modeling: Journal of South American Earth Sciences, v. 87, p. 174–187, https://doi.org/10.1016/j.jsames.2017.12.012

Flynn, J. J., Charrier, R., Croft, D. A., Gans, P. B., Herriott, T. M., Wertheim, J. A., and Wyss, A. R., 2008, Chronologic implications of new Miocene mammals from the Cura-Mallín and Trapa Trapa formations, Laguna del Laja area, south central Chile: Journal of South American Earth Sciences, v. 26, n. 4, p. 412–423, https://doi.org/10.1016/j.jsames.2008.05.006

Folguera, A., and Ramos, V. A., 2011, Repeated eastward shifts of arc magmatism in the Southern Andes: A revision to the long-term pattern of Andean uplift and magmatism: Journal of South American Earth Sciences, v. 32, n. 4, p. 531–546, https://doi.org/10.1016/j.jsames.2011.04.003

Folguera, A., Rojas Vera, E. A., Bottesi, G., Zamora Valcarce, G., and Ramos, V. A., 2010, The Loncopué Trough: A Cenozoic basin produced by extension in the southern Central Andes: Journal of Geodynamics, v. 49, n. 5, p. 287–295, https://doi.org/10.1016/j.jog.2010.01.009

Folguera, A., Bottesi, G., Duddy, I., Martín-González, F., Orts, D., Sagripanti, L., Rojas Vera, E. A., and Ramos, V. A., 2015a, Exhumation of the Neuquén Basin in the southern Central Andes (Malargüe fold and thrust belt) from field data and low-temperature thermochronology: Journal of South American Earth Sciences, v. 64, Part 2, p. 381–398, https://doi.org/10.1016/j.jsames.2015.08.003

Folguera, A., Zárate, M., Tedesco, A., Dávila, F., and Ramos, V. A., 2015b, Evolution of the Neogene Andean foreland basins of the Southern Pampas and northern Patagonia (34°–41°S), Argentina: Journal of South American Earth Sciences, v. 64, Part 2, p. 452–466, https://doi.org/10.1016/j.jsames.2015.05.010

Folguera, A., Naipauer, M., Sagripanti, L., Ghiglione, M., Orts, D. L., and Giambiagi, L., 2016, Growth of the Southern Andes: Switzerland, Springer Earth System Sciences, 276 p., https://doi.org/10.1007/978-3-319-23060-3

Fosdick, J. C., Reat, E. J., Carrapa, B., Ortiz, G., and Alvarado, P. M., 2017, Retroarc basin reorganization and aridification during Paleogene uplift of the southern central Andes: Tectonics, v. 36, n. 3, p. 493–514, https://doi.org/10.1002/2016TC004400

Fuentes, F., Horton, B. K., Starck, D., and Boll, A., 2016, Structure and tectonic evolution of hybrid thick- and thin-skinned systems in the Malargüe fold –thrust belt, Neuquén basin, Argentina: Geological Magazine, v. 153, n. 5–6, p. 1066–1084, https://doi.org/10.1017/S0016756816000583

Gana, P., and Wall, R., 1997, Evidencias geocronológicas $^{40}Ar/^{39}Ar$ y K-Ar de un *hiatus* Cretácico Superior-Eoceno en Chile Central (33–33°30'S): Andean Geology, v. 24, n. 2, p. 145–163.

Gansser, A., 1973, Facts and theories on the Andes: Journal of the Geological Society, v. 129, p. 93–131, https://doi.org/10.1144/gsjgs.129.2.0093

García Morabito, E., and Ramos, V. A., 2012, Andean evolution of the Aluminé fold and thrust belt, Northern Patagonian Andes (38°30'–40°30'S): Journal of South American Earth Sciences, v. 38, p. 13–30, https://doi.org/10.1016/j.jsames.2012.03.005

Garrett, S. W., and Storey, B. C., 1987, Lithospheric extension on the Antarctic Peninsula during Cenozoic subduction, *in* Coward, M. P., Dewey, J. F., and Hancock P. L, editors, Continental Extensional Tectonics, Geological Society, London, Special Publications, v. 28, n. 1, p. 419–431, https://doi.org/10.1144/GSL.SP.1987.028.01.26

Gaschnig, R. M., Vervoort, J. D., Lewis, R. S., and McClelland, W. C., 2010, Migrating magmatism in the northern US Cordillera: *In situ* U-Pb geochronology of the Idaho batholith: Contributions to Mineralogy and Petrology, v. 159, n. 6, p. 863–883, https://doi.org/10.1007/s00410-009-0459-5

Georgieva, V., Melnick, D., Schildgen, T. F., Ehlers, T. A., Lagabrielle, Y., Enkelmann, E., and Strecker, M. R., 2016, Tectonic control on rock uplift, exhumation, and topography above an oceanic ridge collision: Southern Patagonian Andes (47°S), Chile: Tectonics, v. 35, n. 6, p. 1317–1341, https://doi.org/10.1002/2016TC004120

Giambiagi, L., Bechis, F., Garcia, V., and Clark, A. H., 2008, Temporal and spatial relationships of thick- and thin-skinned deformation: A case study from the Malargüe fold-and-thrust belt, southern Central Andes: Tectonophysics, v. 459, n. 1–4, p. 123–139, https://doi.org/10.1016/j.tecto.2007.11.069

Giambiagi, L., Ghiglione, M., Cristallini, E., and Bottesi, G., 2009, Kinematic models of basement/cover interaction: Insights from the Malargüe fold and thrust belt, Mendoza, Argentina: Journal of Structural Geology, v. 31, n. 12, p. 1443–1457, https://doi.org/10.1016/j.jsg.2009.10.006

Giambiagi, L., Mescua, J., Bechis, F., Tassara, A., and Hoke, G., 2012, Thrust belts of the southern Central Andes: Along-strike variations in shortening, topography, crustal geometry, and denudation: Geological Society of America Bulletin, v. 124, n. 7–8, p. 1339–1351, https://doi.org/10.1130/B30609.1

Giambiagi, L., Alvarez, P., and Spagnotto, S., 2016, Temporal variation of the stress field during the construction of the central Andes: Constraints from the volcanic arc region (22–26°S), Western Cordillera, Chile, during the last 20 Ma: Tectonics, v. 35, n. 9, p. 2014–2033, https://doi.org/10.1002/2016TC004201

Gianni, G. M., Navarrete, C. G., and Folguera, A., 2015, Synorogenic foreland rifts and transtensional basins: A review of Andean imprints on the evolution of the San Jorge Gulf, Salta Group and Taubaté basins: Journal of South American Earth Sciences, v. 64, Part 2, p. 288–306, https://doi.org/10.1016/j.jsames.2015.08.004

Gianni, G. M., Echaurren, A., Folguera, A., Likerman, J., Encinas, A., García, H. P. A., Dal Molin, C., and Valencia, V. A., 2017, Cenozoic intraplate tectonics in Central Patagonia: Record of main Andean phases in a weak upper plate: Tectonophysics, v. 721, p. 151–166, https://doi.org/10.1016/j.tecto.2017.10.005

Gianni, G. M., Dávila, F. M., Echaurren, A., Fennell, L., Tobal, J., Navarrete, C., Quezada, P., Folguera, A., and Giménez, M., 2018a, A geodynamic model linking Cretaceous orogeny, arc migration, foreland dynamic subsidence and marine ingression in southern South America: Earth-Science Reviews, v. 185, p. 437–462, https://doi.org/10.1016/j.earscirev.2018.06.016

Gianni, G. M., Pesce, A., and Soler, S. R., 2018b, Transient plate contraction between two simultaneous slab windows: Insights from Paleogene tectonics of the Patagonian Andes: Journal of Geodynamics, v. 121, p. 64–75, https://doi.org/10.1016/j.jog.2018.07.008

Giovanni, M. K., Horton, B. K., Garzione, C. N., McNulty, B., and Grove, M., 2010, Extensional basin evolution in the Cordillera Blanca, Perú: Stratigraphic and isotopic records of detachment faulting and orogenic collapse in the Andean hinterland: Tectonics, v. 29, n. 6, TC6007, https://doi.org/10.1029/2010TC002666

Godoy, E., Yáñez, G., and Vera, E., 1999, Inversion of an Oligocene volcano-tectonic basin and uplifting of its superimposed Miocene magmatic arc in the Chilean Central Andes: First seismic and gravity evidences: Tectonophysics, v. 306, n. 2, p. 217–236, https://doi.org/10.1016/S0040-1951(99)00046-3

González, E., 1989, Hydrocarbon resources in the coastal zone of Chile, *in* Ericksen, G. E., Cañas Pinochet, M. T., and Reinemund, J. A., editors, Geology of the Andes and its relation to hydrocarbon and mineral resources: Circum-Pacific Council for Energy and Mineral Resources Earth Science Series, v. 11, p. 383–404.

González, O., and Vergara, M., 1962, Reconocimiento geológico de la Cordillera de los Andes entre los paralelos 35° y 38°S: Instituto de Geología, v. 24, 70 p.

González Díaz, E. F., 1979, Descripción geológica a escala 1:200.000 de la hoja 31d, La Matancilla: Boletín de la Dirección Nacional de Geología y Minería, Carta Geológico-Económica de la República Argentina 173, 96 p.

Gripp, A. E., and Gordon, R. G., 2002, Young tracks of hotspots and current plate velocities: Geophysical Journal International, v. 150, n. 2, p. 321–361, https://doi.org/10.1046/j.1365-246X.2002.01627.x

Groeber, P., 1946, Observaciones Geológicas a lo largo del meridiano 70: 1. Hoja Chos Malal: Revista de la Sociedad Geológica Argentina, v. 1, n. 3, p. 117–208. Reprinted by Asociación Geológica Argentina, Serie C Reimpresiones 1980, v. 1, p. 5–36.

——— 1947, Observaciones geológicas a lo largo del meridiano 70: 3, Hojas Domuyo, Mari Mahuida, Huarhuar-co y parte de Epu Lauken, 4, Hojas Bardas Blancas y Los Molles: Revista de la Sociedad Geológica Argentina, v. 2, no. 4, p. 347–433. Reprinted by Asociación Geológica Argentina, Serie C Reimpresiones 1980, v. 1, p. 75–161.

Gulisano, C. A., and Gutiérrez Pleimling, A. R., 1994, The Jurassic of the Neuquén Basin: Field Guide: Asociacion Geologica Argentina, Series E, 111 p.

Hayward, A. B., and Graham, R. H., 1989, Some geometrical characteristics of inversion, *in* Cooper, M. A., and Williams, G. D., editors, Inversion Tectonics: Geological Society, London, Special Publications, v. 44, n. 1, p. 17–39, https://doi.org/10.1144/GSL.SP.1989.044.01.03

Hervé, F., Pankhurst, R. J., Drake, R., and Beck, M. E., 1995, Pillow metabasalts in a mid-Tertiary extensional basin adjacent to the Liquiñe-Ofqui fault zone: The Isla Magdalena area, Aysén, Chile: Journal of South American Earth Sciences, v. 8, n. 1, p. 33–46, https://doi.org/10.1016/0895-9811(94)00039-5

Heuret, A., and Lallemand, S., 2005, Plate motions, slab dynamics and back-arc deformation: Physics of the Earth and Planetary Interiors, v. 149, n. 1–2, p. 31–51, https://doi.org/10.1016/j.pepi.2004.08.022

Hodges, K. V., and Walker, J. D., 1992, Extension in the Cretaceous Sevier orogen, North American Cordillera: Geological Society of America Bulletin, v. 104, n. 5, p. 560–569, https://doi.org/10.1130/0016-7606(1992)104<0560:EITCSO>2.3.CO;2

Horton, B. K., 2018, Tectonic regimes of the Central and Southern Andes: Responses to variations in plate coupling during subduction: Tectonics, v. 37, n. 2, p. 402–429, https://doi.org/10.1002/2017TC004624

Horton, B. K., and Fuentes, F., 2016, Sedimentary record of plate coupling and decoupling during growth of the Andes: Geology, v. 44, n. 8, p. 647–650, https://doi.org/10.1130/G37918.1

Horton, B. K., Fuentes, F., Boll, A., Starck, D., Ramírez, S. G., and Stockli, D. F., 2016, Andean stratigraphic record of the transition from backarc extension to orogenic shortening: A case study from the northern Neuquén Basin, Argentina: Journal of South American Earth Sciences, v. 71, p. 17–40, https://doi.org/10.1016/j.jsames.2016.06.003

Iannelli, S. B., Fennell, L. M., Litvak, V. D. , Fernández Paz, L., Encinas, A., and Folguera, A., 2018, Geochemical and tectonic evolution of Late Cretaceous to early Paleocene magmatism along the Southern Central Andes (35-36°S): Journal of South American Earth Sciences, v. 87, p. 139–156, https://doi.org/10.1016/j.jsames.2017.12.008

Jordan, T. E., Burns, W. M., Veiga, R., Pángaro, F., Copeland, P., Kelley, S., and Mpodozis, C., 2001, Extension and basin formation in the southern Andes caused by increased convergence rate: A mid-Cenozoic trigger for the Andes: Tectonics, v. 20, n. 3, p. 308–324, https://doi.org/10.1029/1999TC001181

Kane, S., Williams, G., and Buddin, T., 1997, Flexural-slip based restoration in 3D, a new approach, *in* 1997 AAPG Annual Convention Official Program, Bakersfield, California.

Kay, S. M., and Copeland, P., 2006, Early to middle Miocene backarc magmas of the Neuquén Basin: Geochemical consequences of slab shallowing and the westward drift of South America, *in* Kay, S. M., and Ramos, V. A., editors, Evolution of an Andean Margin: A tectonic and magmatic view from the Andes to the Neuquén Basin (35-39°S): Geological Society of America Special Paper 407, p. 185–213, https://doi.org/10.1130/2006.2407(09)

Kay, S. M., Coira, B., and Viramonte, J., 1994, Young mafic back arc volcanic rocks as indicators of continental lithospheric delamination beneath the Argentine Puna plateau, central Andes: Journal of Geophysical Research–Solid Earth, v. 99, n. B12, p. 24323–24339, https://doi.org/10.1029/94JB00896

Kay, S. M., Godoy, E., and Kurtz, A., 2005, Episodic arc migration, crustal thickening, subduction erosion, and magmatism in the south-central Andes: Geological Society of America Bulletin, v. 117, n. 1–2, p. 67–88, https://doi.org/10.1130/B25431.1

Kay, S. M., Burns, W. M., Copeland, P., and Mancilla, O., 2006, Upper Cretaceous to Holocene magmatism and evidence for transient Miocene shallowing of the Andean subduction zone under the northern Neuquén Basin, *in* Kay, S. M., and Ramos, V. A., editors, Evolution of an Andean Margin: A tectonic and magmatic view from the Andes to the Neuquén Basin (35-39°S): Geological Society of America Special Paper 407, p. 19–60, https://doi.org/10.1130/2006.2407(02)

Kay, S. M., Ardolino, A. A., Gorring, M. L., and Ramos, V. A., 2007, The Somuncura Large Igneous Province in Patagonia: Interaction of a transient mantle thermal anomaly with a subducting slab: Journal of Petrology, v. 48, n. 1, p. 43–77, https://doi.org/10.1093/petrology/egl053

Kozlowski, E., Manceda, R., and Ramos, V. A., 1993, Estructura, *in* Ramos, V. A., editor, Geología y Recursos Naturales de Mendoza: Relatorio del XII Congreso Geológico Argentino y II Congreso de Exploración de Hidrocarburos, p. 235–256.

Lagabrielle, Y., Suárez, M., Rossello, E. A., Hérail, G., Martinod, J., Régnier, M., and de la Cruz, R., 2004, Neogene to Quaternary tectonic evolution of the Patagonian Andes at the latitude of the Chile Triple Junction: Tectonophysics, v. 385, n. 1–4, p. 211–241, https://doi.org/10.1016/j.tecto.2004.04.023

Lagabrielle, Y., Suarez, M., Malavieille, J., Morata, D., Espinoza, F., Maury, R. C., Scalabrino, B., Barbero, L., de la Cruz, R., Rossello, E. A., and Bellon, H., 2007, Pliocene extensional tectonics in the Eastern Central Patagonian Cordillera: Geochronological constraints and new field evidence: Terra Nova, v. 19, n. 6, p. 413–424, https://doi.org/10.1111/j.1365-3121.2007.00766.x

Lallemand, S., Heuret, A., and Boutellier, D., 2005, On the relationships between slab dip, back-arc stress, upper plate absolute motion, and crustal nature in subduction zones: Geochemistry, Geophysics, Geosystems, v. 6, n. 9, Q09006, https://doi.org/10.1029/2005GC000917

Lamb, S., and Davis, P., 2003, Cenozoic climate change as a possible cause for the rise of the Andes: Nature, v. 425, p. 792–797, https://doi.org/10.1038/nature02049

Legarreta, L., and Gulisano, C. A., 1989, Análisis estratigráfico secuencial de la Cuenca Neuquina (Triásico Superior–Terciario inferior), *in* Chebli, G., and Spalletti, L., editors, Cuencas Sedimentarias Argentinas: Serie Correlación Geológica, v. 6, p. 221–243.

Legarreta, L., and Uliana, M. A., 1991, Jurassic-Cretaceous marine oscillations and geometry of back-arc basin fill, central Argentine Andes, *in* McDonald, D. I. M., editor, Sedimentation, Tectonics and Eustasy: Sea-Level changes at Active Margins: IAS Special Publication, v. 12, p. 429–450, https://doi.org/10.1002/9781444303896.ch23

——— 1996, The Jurassic succession in west-central Argentina: Stratal patterns, sequences and paleogeographic evolution: Palaeogeography, Palaeoclimatology, Palaeoecology, v. 120, n. 3–4, p. 303–330, https://doi.org/10.1016/0031-0182(95)00042-9

Litvak, V. D., Spagnuolo, M. G., Folguera, A., Poma, S., Jones, R. E., and Ramos, V. A., 2015, Late Cenozoic calc-alkaline volcanism over the Payenia shallow subduction zone, South-Central Andean back-arc (34° 30′–37° S), Argentina: Journal of South American Earth Sciences, v. 64, Part 2, p. 365–380, https://doi.org/10.1016/j.jsames.2015.09.010

Llambías, E. J., and Aragón, E., 2011, Volcanismo Paleógeno, *in* Leanza, H.A., Arregui, O., Carbone, O., Danieli, J. C., and Vallés, J. M., Geología y recursos naturales de la Provincia del Neuquén: Relatorio del XVIII Congreso Geológico Argentino, p. 265–274.

Llambías, E. J., and Rapela, C. W., 1989, Las vulcanitas de Collipilli, Neuquén, y su relación con otras unidades paleógenas de la Cordillera: Revista de la Asociación Geológica Argentina, v.44, p. 224–236.

Long, S. P., Thomson, S. N., Reiners, P. W., and Di Fiori, R. V., 2015, Synorogenic extension localized by upper-crustal thickening: An example from the Late Cretaceous Nevadaplano: Geology, v. 43, n. 4, p. 351–354, https://doi.org/10.1130/G36431.1

López-Escobar, L., and Vergara, M., 1997, Eocene-Miocene longitudinal depression and Quaternary volcanism in the Southern Andes, Chile (33-42.5°S): A geochemical comparison: Revista Geológica de Chile, v. 24, n. 2, p. 227–244.

Lossada, A. C., Giambiagi, L., Hoke, G. D., Fitzgerald, P. G., Creixell, C., Murillo, I., Mardonez, D., Velásquez, R., and Suriano, J., 2017, Thermochronological evidence for late Eocene Andean mountain building at 30°S: Tectonics, v. 36, n. 11, p. 2693–2713, https://doi.org/10.1002/2017TC004674

Ludwig, K. J., 2003, Isoplot 3.00: Berkeley, California, Special Publication of the Berkeley Geochronology Center, v. 4, 70 p.

Maloney, K. T., Clarke, G. L., Klepeis, K. A., and Quevedo, L., 2013, The Late Jurassic to present evolution of the Andean margin: Drivers and the geological record: Tectonics, v. 32, n. 5, p. 1049–1065, https://doi.org/10.1002/tect.20067

Manceda, R., and Figueroa, D., 1995, Inversion of the Mesozoic Neuquén rift in the Malargüe fold and thrust belt, Mendoza, Argentina, *in* Tankard, A.J., Suárez, R., and Welsink, H. J., editors, Petroleum Basins of South America: American Association of Petroleum Geologists, Memoir 62, p. 369 – 382.

Manceda, R., Bolatti, N. D., and Manoni, R., 1992, Modelo estructural para la zona de Bardas Blancas: Boletin de información Petrolera, Tercera Época, v. 9, n. 3, p. 32–103.

Marrett, R. A., Allmendinger, R. W., Alonso, R. N., and Drake, R. E., 1994, Late Cenozoic tectonic evolution of the Puna Plateau and adjacent foreland, northwestern Argentine Andes: Journal of South American Earth Sciences, v. 7, n. 2, p. 179–207, https://doi.org/10.1016/0895-9811(94)90007-8

Martinod, J., Husson, L., Roperch, P., Guillaume, B., and Espurt, N., 2010, Horizontal subduction zones, convergence velocity and the building of the Andes: Earth and Planetary Science Letters, v. 299, n. 3–4, p. 299–309, https://doi.org/10.1016/j.epsl.2010.09.010

McClay, K. R., and Buchanan, P. G., 1992, Thrust faults in inverted extensional basins, *in* McClay, K. R., editor, Thrust tectonics: Dordretch, Springer, p. 93–104, https://doi.org/10.1007/978-94-011-3066-0_8

McNulty, B., and Farber, D., 2002, Active detachment faulting above the Peruvian flat slab: Geology, v. 30, n. 6, p. 567–570, https://doi.org/10.1130/0091-7613(2002)030<0567:ADFATP>2.0.CO;2

Mercier, J. L., Sebrier, M., Lavenu, A., Cabrera, J., Bellier, O., Dumont, J., and Machare, J., 1992, Changes in the tectonic regime above a subduction zone of Andean type: The Andes of Perú and Bolivia during the Pliocene-Pleistocene: Journal of Geophysical Research-Solid Earth, v. 97, n. B8, p. 11945–11982, https://doi.org/10.1029/90JB02473

Mescua, J. F., and Giambiagi, L. B., 2012, Fault inversion vs. new thrust generation: A case study in the Malargüe fold-and-thrust belt, Andes of Argentina: Journal of Structural Geology, v. 35, p. 51–63, https://doi.org/10.1016/j.jsg.2011.11.011

Mescua, J. F., Giambiagi, L. B., and Ramos, V. A., 2013, Late Cretaceous Uplift in the Malargüe fold-and-thrust belt (35°S), southern Central Andes of Argentina and Chile: Andean Geology, v. 40, n. 1, p. 102–116, https://doi.org/10.5027/andgeoV40n1-a05

Mescua, J. F., Giambiagi, L. B., Tassara, A., Gimenez, M., and Ramos, V. A., 2014, Influence of pre-Andean history over Cenozoic foreland deformation: Structural styles in the Malargüe fold-and-thrust belt at 35°S, Andes of Argentina: Geosphere, v. 10, n. 3, p. 585–609, https://doi.org/10.1130/GES00939.1

Mosolf, J. G., Gans, P. B., Wyss, A. R., Cottle, J. M., and Flynn, J. J., 2018, Late Cretaceous to Miocene volcanism, sedimentation, and upper-crustal faulting and folding in the Principal Cordillera, central Chile: Field and geochronological evidence for protracted arc volcanism and transpressive deformation: Geological Society of America Bulletin, v. 131, n. 1–2, p. 252–273, https://doi.org/10.1130/B31998.1

Mpodozis, C., and Allmendinger, R. W., 1993, Extensional tectonics, Cretaceous Andes, northern Chile (27° S): Geological Society of America Bulletin, v. 105, n. 11, p. 1462–1477, https://doi.org/10.1130/0016-7606(1993)105<1462:ETCANC>2.3.CO;2

Müller, R. D., Seton, M., Zahirovic, S., Williams, S. E., Matthews, K. J., Wright, N. M., Shephard, G. E., Maloney, K. T., Barnett-Moore, N., Hosseinpour, M., Bower, D. J. and Cannon, J., 2016, Ocean basin evolution and global-scale plate reorganization events since Pangea breakup: Annual Review of Earth and Planetary Sciences, v. 44, n. 1, p. 107–138, https://doi.org/10.1146/annurev-earth-060115-012211

Muñoz, J., and Niemeyer, H., 1984, Hoja Laguna del Maule, Regiones del Maule y Biobío: Servicio Nacional de Geología y Minería: Carta Geológica de Chile, v. 64, p. 1–98.

Muñoz, J., Troncoso, R., Duhart, P., Crignola, P., Farmer, L., and Stern, C. R., 2000, The relation of the mid-Tertiary Coastal magmatic belt in south-central Chile to the late Oligocene increase in plate convergence rate: Revista Geológica de Chile, v. 27, n. 2, p. 177–203, https://doi.org/10.4067/S0716-02082000000200003

Muñoz, M., Tapia, F., Persico, M., Benoit, M., Charrier, R., Farías, M., and Rojas, A., 2018, Extensional tectonics during Late Cretaceous evolution of the Southern Central Andes: Evidence from the Chilean main range at ~35°S: Tectonophysics, v. 744, p. 93–117, https://doi.org/10.1016/j.tecto.2018.06.009

Naipauer, M., and Ramos, V. A., 2016, Changes in Source Areas at Neuquén Basin: Mesozoic Evolution and Tectonic Setting Based on U–Pb Ages on Zircons, *in* Folguera, A., Naipauer, M., Sagripanti, L., Ghiglione, M., Orts, D. L., and Giambiagi, L., editors, Growth of the Southern Andes: Cham, Switzerland, Springer International Publishing, p. 33–61, https://doi.org/10.1007/978-3-319-23060-3_3

Naipauer, M., Tapia, F., Mescua, J., Farías, M., Pimentel, M. M., and Ramos, V. A., 2015, Detrital and volcanic zircon U–Pb ages from southern Mendoza (Argentina): An insight on the source regions in the northern part of the Neuquén Basin: Journal of South American Earth Sciences, v. 64, Part 2, p. 434–451, https://doi.org/10.1016/j.jsames.2015.09.013

Niemeyer, H., and Muñoz, J., 1983, Hoja Laguna de la Laja, Región del Bio Bio: Servicio Nacional de Geología y Minería, Carta Geológica de Chile 57, p. 1–52.

Niviere, B., Messager, G., Carretier, S., and Lacan, P., 2013, Geomorphic expression of the southern Central

Andes forebulge (37°S, Argentina): Terra Nova, v. 25, n. 5, p. 361–367, https://doi.org/10.1111/ter.12044
Nullo, F. E., Stephens, G., Otamendi, J., and Baldauf, P., 2002, El volcanismo del Terciario superior del sur de Mendoza: Revista de la Asociación Geológica Argentina, v. 57, n. 2, p. 119–132.
Nullo, F. E., Stephens, G., Combina, A., Dimieri, L., Baldauf, P., Bouza, P., and Zanettini, J.C., 2005, Hoja Geológica 3569-III Malargüe: Programa Nacional de Cartas Geológicas de la República Argentina a escala 1:250.000, Boletín del SEGEMAR 346, p. 1–85.
Oncken, O., Hindle, D., Kley, J., Elger, K., Victor, P., and Schemmann, K., 2006, Deformation of the Central Andean upper plate system - Facts, fiction, and constraints for plateau models, *in* Oncken, O., Chong, G., Franz, G., Giese, P., Götze, H. J., Ramos, V. A., Strecker, M. R., and Wigger, P., editors, The Andes: Berlin, Heidelberg, Springer, Frontiers in Earth Sciences, p. 3–27, https://doi.org/10.1007/978-3-540-48684-8_1
Onnis, L., Violante, R. A., Osella, A., de la Vega, M., Tassone, A., and López, E., 2018, Neogene-Quaternary seismic stratigraphy of the Llancanelo Lake Basin, Mendoza, Argentina: Andean Geology, v. 45, n. 1, p. 35–46, https://doi.org/10.5027/andgeoV45n1-3026
Orts, D. L., Folguera, A., Giménez, M., and Ramos, V. A., 2012, Variable structural controls through time in the Southern Central Andes (~36°S): Andean Geology, v. 39, n. 2, p. 220–241, https://doi.org/10.5027/andgeoV39n2-a02
Paces, J. B., and Miller Jr., J. D., 1993, Precise U-Pb ages of Duluth Complex and related mafic intrusions, northeastern Minnesota: Geochronological insights to physical, petrogenetic, paleomagnetic, and tectonomagmatic processes associated with the 1.1 Ga midcontinental rift system: Journal Geophysical Research-Solid Earth, v. 98, n. B8, p. 13997–14013, https://doi.org/10.1029/93JB01159
Pardo-Casas, F., and Molnar, P., 1987, Relative motion of the Nazca (Farallon) and South American plates since Late Cretaceous time: Tectonics, v. 6, n. 3, p. 233–248, https://doi.org/10.1029/TC006i003p00233
Parras, A., and Griffin, M., 2013, Late Cretaceous (Campanian/Maastrichtian) freshwater to restricted marine mollusk fauna from the Loncoche Formation, Neuquén Basin, west-central Argentina: Cretaceous Research, v. 40, p. 190–206, https://doi.org/10.1016/j.cretres.2012.07.002
Parras, A. M., Casadío, S., and Pires, M., 1998, Secuencias Depositacionales del Grupo Malargüe y el Límite Cretácico-Paleógeno, en el sur de la Provincia de Mendoza, Argentina: Asociación Paleontológica Argentina, Publicación Especial 5, p. 61–69.
Piquer, J., Castelli, J. C., Charrier, R., and Yáñez, G., 2010, The Cenozoic of the upper Teno River, cordillera principal, central Chile: Stratigraphy, plutonism and their relation with deep structures (El Cenozoico del alto río Teno, Cordillera Principal, Chile central: Estratigrafía, plutonismo y su relación con estructuras profundas): Andean Geology, v. 37, n. 1, p. 32–53, https://doi.org/10.4067/S0718-71062010000100002
Radic, J. P., 2010, Cenozoic basins and their control on volcanism of Nevados de Chillan and Copahue-Callaqui complexes (36-39° S, Southern Andes) [Las cuencas cenozoicas y su control en el volcanismo de los Complejos Nevados de Chillán y Copahue-Callaqui (Andes del Sur, 36-39° S)]: Andean Geology, v. 37, n. 1, p. 220–246, https://doi.org/10.4067/S0718-71062010000100009
Radic, J. P., Alvarez, P., and Rojas, L., 2005, Tectonostratigraphic evolution of the Arauco-Itata fore-arc basin, central Chile: 6th International Symposium of Andean Geodynamics (ISAG) Extended Abstracts, p. 586–587.
Radic, J. P., Alvarez, P., Rojas, L., Czollak, C., Parada, R., and Ortiz, V., 2009, La Cuenca de Valdivia como parte del sistema de antearco de la plataforma continental de Chile central entre los 36° y 40°S: Actas XII° Congreso Geológico Chileno, S10-032.
Ramos, V. A., 1999, Plate tectonic setting of the Andean Cordillera: Episodes, v. 22, n. 3, p. 183–190.
——— 2009, Anatomy and global context of the Andes: Main geologic features and the Andean orogenic cycle, *in* Kay, S. M., Ramos, V. A., and Dickinson, W. R., editors, Backbone of the Americas: Shallow Subduction, Plateau Uplift, and Ridge and Terrane Collision: Geological Society of America Memoirs, v. 204, p. 31–65, https://doi.org/10.1130/2009.1204(02)
——— 2010, The tectonic regime along the Andes: Present-day and Mesozoic regimes: Geological Journal, v. 45, n. 1, p. 2–25, https://doi.org/10.1002/gj.1193
Ramos, V. A., and Barbieri, M., 1988, El volcanismo Cenozoico de Huantraico: Edad y relaciones isotópicas iniciales, Provincia de Neuquén: Revista de la Asociación Geológica Argentina, v. 43, n. 2, p. 210–223.
Ramos, V. A., and Folguera, A., 2005, Tectonic evolution of the Andes of Neuquén: Constraints derived from the magmatic arc and foreland deformation, i*n* Veiga, G. D., Spalletti, L. A., Howell, J. A., and Schwarz, E., editors, The Neuquén Basin, Argentina: A case Study in Sequence Stratigraphy and Basin Dynamics: Geological Society, London, Special Publications, v. 252, p. 15–35, https://doi.org/10.1144/GSL.SP.2005.252.01.02
——— 2009, Andean flat-slab subduction through time, *in* Murphy, J. B., Keppie, J. D., and Hynes, A. J., editors, Ancient orogens and Modern Analogues: Geological Society, London, Special Publications, v. 327, p. 31–54, https://doi.org/10.1144/SP327.3
Ramos, V. A., and Kay, S. M., 1992, Southern Patagonian plateau basalts and deformation; back-arc testimony of ridge collisions: Tectonophysics, v. 205, n. 1–3, p. 261–282, https://doi.org/10.1016/0040-1951(92)90430-E
Ramos, M. E., Folguera, A., Fennell, L. M., Giménez, M., Litvak, V. D., Dzierma, Y., and Ramos, V. A., 2014a, Tectonic evolution of the North Patagonian Andes from field and gravity data (39–40° S): Journal of South American Earth Sciences, v. 51, p. 59–75, https://doi.org/10.1016/j.jsames.2013.12.010
Ramos, V. A., Litvak, V. D., Folguera, A., and Spagnuolo, M., 2014b, An Andean tectonic cycle: From crustal thickening to extension in a thin crust (34°-37°SL): Geoscience Frontiers, v. 5, n. 3, p. 351–367, https://doi.org/10.1016/j.gsf.2013.12.009
Rodríguez, M. P., Charrier, R., Brichau, S., Carretier, S., Farías, M., Parseval, P., and Ketcham, R. A., 2018,

Latitudinal and longitudinal patterns of exhumation in the Andes of north-central Chile: Tectonics, v. 37, n. 9, p. 2863–2886, https://doi.org/10.1029/2018TC004997
Rojas Vera, E. A., Folguera, A., Zamora Valcarce, G., Giménez, M., Ruiz, F., Martínez, P., Bottesi, G., and Ramos, V. A., 2010, Neogene to Quaternary extensional reactivation of a fold and thrust belt: The Agrio belt in the Southern Central Andes and its relation to the Loncopué trough (38°–39°S): Tectonophysics, v. 492, n. 1–4, p. 279–294, https://doi.org/10.1016/j.tecto.2010.06.019
Rojas Vera, E. A., Folguera, A., Zamora Valcarce, G., Bottesi, G. L., and Ramos, V. A., 2014, Structure and development of the Andean system between 36° and 39°S: Journal of Geodynamics, v. 73, p. 34–52, https://doi.org/10.1016/j.jog.2013.09.001
Sagripanti, L., Bottesi, G., Naipauer, M., Folguera, A., and Ramos, V. A., 2011, U/Pb ages on detrital zircons in the southern central Andes Neogene foreland (36°-37°S): Constraints on Andean exhumation: Journal of South American Earth Sciences, v. 32, n. 4, p. 555–566, https://doi.org/10.1016/j.jsames.2011.03.010
Sagripanti, L., Bottesi, G., Kietzmann, D., Folguera, A., and Ramos, V. A., 2012, Mountain building processes at the orogenic front. A study of the unroofing in Neogene foreland sequence (37°S): Andean Geology, v. 39, n. 2, p. 201–219, https://doi.org/10.5027/andgeoV39n2-a01
Salazar, C., Stinnesbeck, W., and Quinzio-Sinn, L. A., 2010, Ammonites from the Maastrichtian (Upper Cretaceous) Quiriquina Formation in central Chile: Neues Jahrbuch für Geologie und Paläontologie-Abhandlungen, v. 257, n. 2, p. 181–236, https://doi.org/10.1127/0077-7749/2010/0072
Sato, A. M., Llambías, E. J., Basei, M. A. S., and Castro, C. E., 2015, Three stages in the Late Paleozoic to Triassic magmatism of southwestern Gondwana, and the relationships with the volcanogenic events in coeval basins: Journal of South American Earth Sciences, v. 63, p. 48–69, https://doi.org/10.1016/j.jsames.2015.07.005
Scalabrino, B., Lagabrielle, Y., De la Rupelle, A., Malavieille, J., Polvé, M., Espinoza, F., Morata, D., and Suarez, M., 2009, Subduction of an active spreading ridge beneath southern South America: A review of the Cenozoic geological records from the Andean foreland, central Patagonia (46–47°S), *in* Lallemand, S., and Funiciello, F., editors, Subduction Zone Geodynamics: Berlin, Heidelberg, Springer-Verlag, p. 227–246, https://doi.org/10.1007/978-3-540-87974-9_12
Scalabrino, B., Ritz, J. F., and Lagabrielle, Y., 2011, Relief inversion triggered by subduction of an active spreading ridge: Evidence from glacial morphology in Central Patagonia: Terra Nova, v. 23, n. 2, p. 63–69, https://doi.org/10.1111/j.1365-3121.2010.00981.x
Schellart, W. P., 2008, Overriding plate shortening and extension above subduction zones: A parametric study to explain formation of the Andes Mountains: Geological Society of America Bulletin, v. 120, n. 11–12, p. 1441–1454, https://doi.org/10.1130/B26360.1
Schellart, W. P., and Moresi, L., 2013, A new driving mechanism for backarc extension and backarc shortening through slab sinking induced toroidal and poloidal mantle flow: Results from dynamic subduction models with an overriding plate: Journal of Geophysical Research-Solid Earth, v. 118, n. 6, p. 3221–3248, https://doi.org/10.1002/jgrb.50173
Schoenbohm, L. M., and Strecker, M. R., 2009, Normal faulting along the southern margin of the Puna Plateau, northwest Argentina: Tectonics, v. 28, n. 5, TC5008, https://doi.org/10.1029/2008TC002341
Schwartz, D. P., 1988, Paleoseismicity and Neotectonics of the Cordillera Blanca fault zone, northern Peruvian Andes: Journal of Geophysical Research-Solid Earth, v. 93, n. B5, p. 4712–4730, https://doi.org/10.1029/JB093iB05p04712
Sébrier, M., Mercier, J. L., Mégard, F., Laubacher, G., and Carey–Gailhardis, E., 1985, Quaternary normal and reverse faulting and the state of stress in the central Andes of south Peru: Tectonics, v. 4, n. 7, p. 739–780, https://doi.org/10.1029/TC004i007p00739
Sébrier, M., Mercier, J. L., Macharé, J., Bonnot, D., Cabrera, J., and Blanc, J. L., 1988, The state of stress in an overriding plate plate situated above a flat slab: The Andes of Central Peru: Tectonics, v. 7, n. 4, p. 895–928, https://doi.org/10.1029/TC007i004p00895
SERNAGEOMIN, 2003, Mapa Geológico de Chile: versión digital: Servicio Nacional de Geología y Minería, Publicación Geológica Digital 4.
Shockey, B. J., Flynn, J. J., Croft, D. A., Gans, P., and Wyss, A. R., 2012, New leontiniid Notoungulata (Mammalia) from Chile and Argentina: Comparative anatomy, character analysis, and phylogenetic hypotheses: American Museum Novitates, v. 3737, p. 1–64, https://doi.org/10.1206/3737.2
Silvestro, J., and Atencio, M., 2009, La cuenca Cenozoica del Río Grande y Palauco: Edad, evolución y control estructural, faja plegada de Malargüe (36°S): Revista de la Asociación Geológica Argentina, v. 65, n. 1, p. 154–169.
Silvestro, J., Kraemer, P., Achilli, F., and Brinkworth, W., 2005, Evolución de las cuencas sinorogéncias de la Cordillera Principal entre 35° - 36° S, Malargüe: Revista de la Asociación Geológica Argentina, v. 60, n. 4, p. 627–643.
Sláma, J., Kosler, J., Condon, D. J., Crowley, J. L., Gerdes, A., Hanchar, J. M., Horstwood, M. S. A., Morris, G. A., Nasdala, L., Norberg, N., Schaltegger, U., Schoene, B., Tubrett, M. N., and Whitehouse, M. J., 2008, Plesovice zircon – A new natural reference material for U-Pb and Hf isotopic microanalysis: Chemical Geology, v. 249, n. 1–2, p. 1–35, https://doi.org/10.1016/j.chemgeo.2007.11.005
Sobolev, S. V., and Babeyko, A. Y., 2005, What drives orogeny in the Andes?: Geology, v. 33, n. 8, p. 617–620, https://doi.org/10.1130/G21557AR.1
Somoza, R., and Ghidella, M. E., 2012, Late Cretaceous to recent plate motions in western South America revisited: Earth and Planetary Science Letters, v. 331–332, p. 152–163, https://doi.org/10.1016/j.epsl.2012.03.003
Somoza, R., and Zaffarana, C. B., 2008, Mid-Cretaceous polar standstill of South America, motion of the Atlantic hotspots and the birth of the Andean Cordillera: Earth and Planetary Science Letters, v. 271, n. 1–4, p. 267–277, https://doi.org/10.1016/j.epsl.2008.04.004

Spagnuolo, M. G., Folguera, A., Litvak, V. D., Rojas Vera, E. A., and Ramos, V. A., 2012a, Late Cretaceous arc rocks in the Andean retroarc region at 36.5°S: Evidence supporting a Late Cretaceous slab shallowing: Journal of South American Earth Sciences, v. 38, p. 44–56, https://doi.org/10.1016/j.jsames.2012.05.002

Spagnuolo, M. G., Litvak, V. D., Folguera, A., Bottesi, G., and Ramos, V. A., 2012b, Neogene magmatic expansion and mountain building processes in the southern Central Andes, 36–37°S, Argentina: Journal of Geodynamics, v. 53, p. 81–94, https://doi.org/10.1016/j.jog.2011.07.004

Suárez, M., and Emparan, C., 1995, The stratigraphy, geochronology and paleophysiography of a Miocene fresh-water interarc basin, southern Chile: Journal of South American Earth Sciences, v. 8, n. 1, p. 17–31, https://doi.org/10.1016/0895-9811(94)00038-4

Suárez, G., Molnar, P., and Burchfiel, B. C., 1983, Seismicity, fault plane solutions, depth of faulting, and active tectonics of the Andes of Peru, Ecuador and southern Colombia: Journal of Geophysical Research-Solid Earth, v. 88, n. B12, p. 10403–10428, https://doi.org/10.1029/JB088iB12p10403

Tapia, F., Farías, M., Naipauer, M., and Puratich, J., 2015, Late Cenozoic contractional evolution of the current arc-volcanic region along the southern Central Andes (35° 20′ S): Journal of Geodynamics, v. 88, p. 36–51, https://doi.org/10.1016/j.jog.2015.01.001

Thorkelson, D. J., 1996, Subduction of diverging plates and the principles of slab window formation: Tectonophysics, v. 255, n. 1–2, p. 47–63, https://doi.org/10.1016/0040-1951(95)00106-9

Tunik, M. A., 2003, Interpretación paleoambiental de los depósitos de la Formación Saldeño (Cretácico superior), en la alta Cordillera de Mendoza, Argentina: Revista de la Asociación Geológica Argentina, v. 58, n. 3, p. 417–433.

Tunik, M., Folguera, A., Naipauer, M., Pimentel, M., and Ramos, V. A., 2010, Early uplift and orogenic deformation in the Neuquén Basin: Constraints on the Andean uplift from U-Pb and Hf isotopic data of detrital zircons: Tectonophysics, v. 489, n. 1–4, p. 258–273, https://doi.org/10.1016/j.tecto.2010.04.017

Turienzo, M., Dimieri, L., Frisicale, C., Araujo, V., and Sánchez, N., 2012, Cenozoic structural evolution of the Argentinean Andes at 34°40'S: A close relationship between thick and thin-skinned deformation: Andean Geology, v. 39, n. 2, p. 317–357, https://doi.org/10.5027/andgeoV39n2-a07

Uliana, M. A., Biddle, K. T., and Cerdan, J., 1989, Mesozoic extension and the formation of argentine sedimentary basins: American Association of Petroleum Geologists, Memoir 46, p. 599–614.

Utgé, S., Folguera, A., Litvak, V. D., and Ramos, V. A., 2009, Geología del sector norte de la Cuenca de Cura Mallín en las Lagunas de Epulaufquen, Neuquén: Revista de la Asociación Geológica Argentina, v. 64, n. 3, p. 231–248.

van Dinther, Y., Morra, G., Funiciello, F., and Faccenna, C., 2010, Role of the overriding plate in the subduction process: Insights from numerical models: Tectonophysics, v. 484, n. 1–4, p. 74–86, https://doi.org/10.1016/j.tecto.2009.08.038

Vergani, G. D., Tankard, J., Belotti, J., and Welsink, J., 1995, Tectonic evolution and paleogeography of the Neuquén basin, Argentina, *in* Tankard, A. J., Suárez, R., and Welsink, H. J., editors, Petroleum Basins of South America: American Association of Petroleum Geologists, Memoir 62, p. 383–402.

Villar, H. J., Legarreta, L., Laffitte, G. A., Haring, C., and Varedé, R., 2014, Facies orgánicas no marinas de la cuenca Neuquina: Ambiente geológico y caracterización geoquímica de petróleos y rocas generadores: Actas IX° Congreso de Exploración y Desarrollo de Hidrocarburos: trabajos técnicos, v. 1, p. 45–70.

Wells, M. L., 1997, Alternating contraction and extension in the hinterlands of orogenic belts: An example from the Raft River Mountains, Utah: Geological Society of America Bulletin, v. 109, n. 1, p. 107–126, https://doi.org/10.1130/0016-7606(1997)109<0107:ACAEIT>2.3.CO;2

Wells, M. L., Dallmayer, R. D., and Allmendinger, R. W., 1990, Late Cretaceous extension in the hinterland of the Sevier thrust belt, northwestern Utah and southern Idaho: Geology, v. 18, n. 10, p. 929–933, https://doi.org/10.1130/0091-7613(1990)018<0929:LCEITH>2.3.CO;2

Wells, M. L., Hoisch, T. D., Cruz-Uribe, A. M., and Vervoort, J. D., 2012, Geodynamics of synconvergent extension and tectonic mode switching: Constraints from the Sevier-Laramide orogen: Tectonics, v. 31, n. 1, TC1002, https://doi.org/10.1029/2011TC002913

Winocur, D. A., Litvak, V. D., and Ramos, V. A., 2015, Magmatic and tectonic evolution of the Oligocene Valle del Cura basin, main Andes of Argentina and Chile: Evidence for generalized extension, *in* Sepúlveda, S. A., Giambiagi, L. B., Moreiras, S. M., Pinto, L., Tunik, M., Hoke, G. D., and Farías, M., editors, Geodynamic Processes in the Andes of Central Chile and Argentina: Geological Society, London, Special Publications, v. 399, p. 109–130, https://doi.org/10.1144/SP399.2

Wyss, A. R., Flynn, J. J., Norell, M. A., Swisher III, C. C., Novacek, M. J., McKenna, M. C., and Charrier, R., 1994, Paleogene mammals from the Andes of central Chile: a preliminary taxonomic, biostratigraphic and geochronologic assessment: American Museum Novitates, v. 3098, p. 1–31.

Zhou, R., Schoenbohm, L. M., and Cosca, M., 2013, Recent, slow normal and strike-slip faulting in the Pasto Ventura region of the southern Puna Plateau, NW Argentina: Tectonics, v. 32, n. 1, p. 19–33, https://doi.org/10.1029/2012TC003189